NEURAL RESPONSES TO INJURY: PREVENTION, PROTECTION, AND REPAIR
Annual Technical Report
1996-1997

Submitted by

Nicolas G. Bazan, M.D., Ph.D.
Project Director

Period Covered: 20 September, 1996 through 19 September, 1997

Cooperative Agreement DAMD17-93-V-3013

between

United States Army Medical Research and Development Command
(Walter Reed Army Institute of Research)

and

Louisiana State University Medical Center
Neuroscience Center of Excellence

Volume 7 of 9

Role of Growth Factors and Cell Signaling in the Response of Brain and Retina to Injury

Project Directors:
Prescott Deininger, Ph.D.
Nicolas G. Bazan, M.D., Ph.D.

Volume 7 Role of Growth Factors and Cell Signaling in the Response of Brain and Retina to Injury

Project Directors: Prescott Deininger, Ph.D.
Nicolas G. Bazan, M.D., Ph.D.

Participating Scientists: Julia Cook, Ph.D.
Haydee E. P. Bazan, Ph.D.
William C. Gordon, Ph.D.
Elena Rodriguez De Turco, Ph.D.
Victor Marcheselli, Ph.D.

Research Report

Temporal Changes In Gene Expression Following Cryogenic Rat Brain Injury

Julia L. Cook[*#%&], Victor Marcheselli[&], Jawed Alam[#%], Prescott L. Deininger[# %], Nicolas G. Bazan[&]

[#]Ochsner Medical Foundation, Division of Research, New Orleans, LA
[&]Ophthalmology and Neuroscience Center, LSUMC, New Orleans, LA
[%]Biochemistry and Molecular Biology, LSUMC, New Orleans, LA

text length: 44 pages
figures: 4 pages

*Corresponding author Fax: (504) 842-3381. E-mail: jcook@ochsner.org

Abstract

Expression of eighteen genes was examined at eight different time points between 1 h and 28 days following cryogenic rat brain injury. The genes include thymidine kinase (TK), p53 tumor suppressor, c-Fos, renin, myelin basic protein (MBP), proteolipid protein (PLP), transferrin, transferrin receptor, platelet-derived growth factor A (PDGF A), platelet-derived growth factor B (PDGF B), platelet-derived growth factor receptor α (PDGF α receptor), platelet-derived growth factor receptor β (PDGF β receptor), glial fibrillary acidic protein (GFAP), transforming growth factor-β1 (TGF-β1), basic fibroblast growth factor (bFGF), fibroblast growth factor receptor-1 (FGF-R1), insulin-like growth factor-1(IGF-1), and somatostatin.

Time courses of gene expression were determined for RNAs derived from hippocampus and cortex. Genes were divided into categories based upon those in which statistically significant changes in expression were first observed at or before 24 hours (early genes) and those in which changes were first observed at or after 72 hours (late genes). In the present model, many genes demonstrate elevated RNA levels in the cortex prior to hippocampus, following injury. RNAs transcribed from late genes tend to be elevated concurrently in cortex and hippocampus.

Theme: Cellular and Molecular Biology
Topic: Gene structure and function: general
Keywords: injury, cryogenic, growth factors

1. Introduction

A number of studies have addressed the expression of neural factors (growth, differentiation, and trophic factors) following brain injury. These studies have generally examined the corresponding protein and/or mRNA of a single gene and variably employ ischemia, trauma, or cryogenic wounds. Since the nature of the wound may itself influence the time course of expression and the maximum expression of a given gene, it is difficult to consolidate these studies in order to determine the relative time course of expression of multiple genes during wound healing.

In the present study, we simultaneously examined the expression of 18 genes at 8 different time points following injury. A modification of the method of Chalifour [9] was employed. Double-stranded, radiolabeled cDNAs, transcribed from RNAs collected at each time point, were hybridized to filter-bound plasmids possessing inserted mammalian DNAs of interest.

Both cortical and hippocampal RNAs were examined following cryogenic brain injury. All RNAs examined demonstrate changes following brain injury. Most exhibit elevated steady-state levels in both cortical and hippocampal tissues. Expression of all genes examined in cortex except three (IGF-1, PDGF β receptor and GFAP) returns to control levels by 28 days post-injury. Only PDGF β receptor RNA remains elevated at 28 days post-injury in hippocampus.

This study furnishes insight into the sequence of genetic events that follow brain injury, many of which may contribute to the wound-healing process.

2. Materials and methods

2.1. Rat brain cryogenic injury

Winstar rats weighing 250-275 g were ether anesthetized and a 9 mm diameter probe cooled in liquid nitrogen was place on the right parietal region of the rat skull for 1 min. The animals were then euthanized and the brains dissected at the specified times.

All studies involving experimental animals conformed to the guiding principles of the American Physiological Society and were approved in advance by the Ochsner Animal Care and Use Committee and the Ochsner Institutional Biosafety Committee.

2.2. Analysis of gene expression patterns

RNAs from rat brain were collected by the method of Chomczynski and Sacchi [11]. Double-stranded radiolabeled cDNAs were synthesized from rat cortex and hippocampus RNAs isolated at various time points following brain injury. Panels of nitrocellulose filter-fixed cDNA clones were then screened according to the method of Chalifour et al. [9]. Modifications included the use of 50 μg of RNA, 2000 u M-MLV reverse transcriptase (Gibco/BRL), 120 μCi ^{32}P-dCTP (3000 Ci/mM), and 2 u of klenow per sample. Nitrocellulose filters were hybridized to 2 x 10^6 cpm/ml of brain cDNA in 10 ml of hybridization solution.

2.3. Plasmids

Human somatostatin (ATCC 65122), human TK (ATCC 79803), mouse IGF-1 (ATCC 63070), mouse c-Fos (ATCC 41041), FGF-R1 (ATCC 102714), transferrin (ATCC 57228), and p53 (ATCC 57254) were obtained from the American Type Culture Collection (Rockville, MD).

The mouse GFAP clone in BSSK+ was a gift of Nancy Nichols (USC, Los Angeles, CA.). The human transferrin receptor was obtained from Frank Ruddle (Yale University, New Haven, CT). The mouse Ren-2 cDNA is from Ken Gross (Roswell Park Mem. Inst., NY). The full-length human bFGF cDNA is from A. Seddon (American Cyanamide Co., NY). TGF-β1 is from Rik Derynck (Genentech Inc., San Francisco, CA.). The mouse PDGF β receptor is from Y. Yarden (Genentech Inc., San Francisco, CA.). The PDGF α receptor was provided by L. Claesson-Welsch (University Hospital, Uppsala Sweden).

The filter-fixed MBP and PLP plasmids were pMBP-1 [[68] a 1.45 kb rat myelin basic protein cDNA] and p27 [[50], a 3019 bp cDNA clone of rat PLP in pUC18].

Controls were pUC19 and pBR322 (New England Biolabs, Beverly MA).

2.4. Statistics

Statistical analyses were performed using a one-way Analysis of Variance (ANOVA) followed by a Dunnett Multiple Comparisons post-hoc test.

3. Results

The present study reports the *on-set and time-course* of expression of various mRNAs following injury and their *relative expressions in cortex and hippocampus*. Nitrocellulose filter-fixed probes were hybridized to radiolabeled cDNAs generated from cortical (Fig. 1) and hippocampal (Fig. 2) RNAs. RNAs were collected at 0, 1, 6, 12, 24, and 72 h; and 1, 2 and 4 wk following cryogenic injury. For each time point, RNAs from 3 rats were collected and analyzed. Each panel within Figures 1 and 2 represents one of three independent experiments. Figures 3 and 4 are graphical presentations of the hybridization signals (mean $\pm$ standard deviation) obtained from the three independent experiments for each time point. The positions of each of the graphs within the array of 18 corresponds to the position of the corresponding filter-fixed probe in the dot blots of Figures 1 and 2. Since significant hybridization signals were not obtained for pUC19 (1A) and pBR322 (1B), and somatostatin in hippocampus (Fig. 4, 1C) they are not graphically represented.

Table 1 indicates those probes for which the hybridization signal significantly increases by 24 h (early genes), or at or after 72 h (late genes). For none of these genes is expression activated in hippocampus prior to cortex. However, the expression of many mRNAs is delayed in hippocampus relative to cortex. Table 2 indicates the relative onset of increased mRNA expression in cortex and hippocampus.

We feel it prudent to caution the reader about comparing the *absolute values* of hybridization signals obtained from *different* filter-fixed probes. The absolute densitometric value (hybridization signal) for a given filter-fixed DNA is dependent upon the length of

the homology, the extent of the homology (species-specificity of the filter-fixed DNA), and the hybridization conditions.

4. Discussion

Neurotrophic factor expression in the adult mammalian central nervous system (CNS) is largely neuronal. However, upon traumatic injury, "reactive astrocytes" express a number of neurotrophic factors [69]. Since astrocytes occupy one-third of the cerebral cortex and outnumber neurons ten to one [57], their contribution to the wound-healing process is not trivial. For instance, during gliosis, the most frequent neurocellular reaction to occur in diseases ranging from AIDS to infarction [14], the reactive astrocyte population seals the wound site and forms a scar which prevents infections. Reactive astrocytes may also express neurotrophic factors that facilitate axon regeneration. A more thorough understanding of the properties of reactive astrocytes may permit optimization of advantageous and reduction of detrimental properties.

GFAP

Conventionally, gliosis has referred to increases in size, number, and GFAP immunoreactivity, and altered morphology of astrocytes. Following mechanical brain injury, GFAP immunoreactivity generally increases within 1 to 3 days [40]. Mucke and colleagues observe changes in GFAP mRNA as early as 2 h following penetrating focal injury [54]. Expression peaks between 7 and 10 days (10-fold increases) post-injury and levels remain elevated at 21 days (4-5-fold). Other laboratories have found similar profiles of GFAP expression albeit with a reduced maximum fold-activation [8,35,36]. We observe significant mRNA increases by 24 h, and a 3-fold maximum activation with peak mRNA

levels occurring at 1 wk. GFAP mRNA remains above control levels at 4 wk in cortex, but returns to baseline in hippocampus by 2 wk. The time course of our observations in cortex are very similar to that of other investigators. However, our maximum activation appears to be more modest (perhaps a reflection of this particular injury model). Expression in hippocampus is more temperate and is attenuated much earlier than in cortex. This suggests a difference in the astrocyte population (number and/or properties) between these two regions.

bFGF

bFGF likely plays a role in glia development and differentiation *in vivo* [7,27]. It is believed, in addition, to have a significant role in the wound-healing response to CNS injury. FGFs are thought to be functional *in vivo* but, as they are not secreted via normal Golgi pathways, it is not clear how they function in an extracellular capacity [1]. It has been proposed that such growth factors may be released from plasma membrane disruptions such as those incurred upon cellular injury [55].

bFGF is one of a few genes which have been thoroughly studied with respect to brain injury. Intralesion (cortex, hippocampus, corpus callosum) bFGF injection has been shown to increase astrocyte hypertrophy and microglial proliferation [49]. It may also stimulate, in an autocrine cascade, local production of bFGF and the corresponding receptor [29]. bFGF has been shown to serve a protective role following mechanical damage to neuronal pathways. Intraventricular infusion of bFGF following fimbria-fornix transection

reduces loss of cholinergic neurons in the septum [2]. bFGF has further been shown to attenuate loss of neurons in adult rat retinal ganglion cells after optic nerve section [71] and adult dorsal root ganglion neurons following sciatic nerve transection [60].

aFGF and bFGF also have neurotrophic effects and promote differentiation and cell survival of many types of PNS and CNS neurons *in vitro*. Enokido and colleagues [18] have shown that bFGF can rescue twenty day rat embryonic basal forebrain, neocortical and hippocampal neurons from oxygen-induced cell death. The authors propose that bFGF plays an important role in rescuing neuronal cells from oxidative stress *in vivo* during their long post-mitotic life. bFGF also promotes survival and neurite extension of hippocampal, cortical, spinal cord, and mesencephalic neurons *in vitro* [3,52,73,76]. In addition, bFGF may modify production of other growth and neurotrophic factors. For instance, bFGF treatment of cultured neonatal rat cortical, striatal, hippocampal, septal and cerebellar astrocytes increases NGF mRNA and NGF protein secretion. These changes apparently originate at the level of NGF transcription [25,75,81].

Most importantly with regard to the present study, bFGF has been found to increase in the brain following ischemic or traumatic injury. *In situ* bFGF immunoreactivity has been shown to dramatically increase in hippocampus and caudate putamen following adult rat forebrain ischemia, suggesting a role for bFGF in healing [38]. The predominant cellular source of bFGF is controversial. Kiyota and colleagues, and others [22,38,63] suggest that bFGF and the corresponding mRNA are expressed predominately in neurons under normal *in vivo* conditions. However, they find that the increase in bFGF immunoreactivity upon injury occurs primarily in astroglia. Other studies indicate that

bFGF in normal brain is localized predominantly to astrocytes [16,28,29]. These differences may reflect specific antibodies employed (cross-reactivity with aFGF) or animal age. Most investigators are in agreement that the increases in bFGF expression following injury occur predominantly in reactive astrocytes and macrophages [23,24,51].

A few abbreviated time course profiles for bFGF following injury have been reported. Frautschy and colleagues [24] report that the distribution of bFGF mRNA (by *in situ* hybridization) at or near aspirate-induced lesions increases detectably by 4 h, peaks at 3 days and persists for 14 days. The increases in bFGF mRNA and protein were detected predominantly in astroglia. Follesa [23] report a 3-fold increase in bFGF mRNA in injured spinal cord tissue (using RNase protection) by 6 h post-injury. Increases are sustained for at least 7 days in this model.

We find statistically significant increases in bFGF mRNA in cortex and hippocampus by 72 h in the present injury model. High levels are sustained for at least 2 wk and return to control levels by 4 wk. While we do not detect bFGF mRNA as rapidly following injury as has been reported in other studies, this may reflect our injury model. In the Frautschy study, the investigators specifically report changes in the expression of FGF mRNA in cells adjacent to the lesion [24]. Our mRNA levels reflect expression in the entire injured brain ipsilateral cortex or hippocampus.

FGF-R1 receptor

A number of cell types including neurons, endothelia, glia and fibroblasts possess FGF receptors. Expression of FGF receptors type 1-4 have all been demonstrated in the rat brain [4,77] and each show some cellular-specificity. Astrocytic FGF-R has been found (by immunofluorescence) to increase by day 2 in tissue adjacent to scalpel blade wound cavities [67]. In this model, staining increases further through day 10 and decreases to control levels by day 28.

We find that FGF-R1 expression closely parallels that of bFGF and is similar to that described above. Using a FGF-R1 probe (which may detect other FGF receptor mRNAs) RNA levels are significantly elevated by 72 h and sustained for at least 2 wk. mRNA levels return to control by 4 wk post-injury. Basal hippocampal FGF-R mRNA levels are about one-half that of cortex. However, the relative increase in mRNA and the duration that the increase is sustained is very similar between the two tissues.

The parallel expression of FGF-R and bFGF mRNAs, in our injury model, is consistent with the hypothesis that bFGF is involved in an autocrine cascade that promotes astrocytic reactivity and/or proliferation following injury [29].

PDGF A and B, PDGF α *and* β *receptors*

During development, astrocytes produce PDGF A. Astrocyte-derived PDGF A is believed to be mitogenic for O-2A cells, progenitors of oligodendrocytes. However, PDGF is also present in blood and neurons, probably in endothelia and microglia [31], and the

relative contribution from each source to the CNS extracellular PDGF pool is unknown. Damage to astrocytes and oligodendrocytes, that accompanies brain injury, results in demyelination. In the present study, the increase in PDGF A observed following injury may promote proliferation of adult O-2A cells. An increase in the progenitor O-2A pool may, in turn, increase numbers of mature myelinating oligodendrocytes, and thus enhance remyelination. Therefore, while there are no direct studies addressing the role of PDGF in remyelination following injury *in vivo* or *in vitro*, one can speculate that it may modulate glial proliferation and differentiation.

Takayama and colleagues examined PDGF B chain immunoreactivity in rat brain following penetrating injury [72]. They found enhanced immunoreactivity in neurons and macrophages in the vicinity of the wound between 1 and 4 days post-injury. (In their model, wound healing is complete by day 10). In the present model (cryogenic injury), the increase in PDGF B chain is delayed compared to that observed in the penetrating injury model. The increases are also sustained to at least 2 weeks. The PDGF B chain expression profile that we observe is more similar to that following facial nerve axotomy, in which B chain mRNA increases 2-fold by day 6 and returns to control levels by 26 days [34]. In the latter model, PDGF A chain mRNA exhibits a similar expression profile but with a greater magnitude of induction whereas PDGF receptor α mRNA increases 2-fold by day 12 and returns to background by day 26.

We find that control PDGF A levels in the hippocampus are approximately 3-fold less than that of cortex and the magnitude of the induction is less. This may reflect cell

population distribution between these two regions of brain (perhaps neuron:glia ratio). The PDGF A and B mRNAs increase significantly by 1 wk in the cortex and hippocampus, and elevated levels are maintained through at least 2 wk. By 4 wk, PDGF A and B mRNAs return to control levels. We find that the PDGF β receptor mRNA is not detectable until 3 days and that it remains detectable at 4 wk. Therefore, PDGF β receptor (one of merely three surveyed messages not detected in control tissue), is one of three mRNAs, in this study, still significantly enhanced at 4 wk.

In addition to a speculative role in remyelination, PDGFs and corresponding receptors may have neuroprotective functions. PDGF AA and PDGF BB have been shown to protect cultured hippocampal neurons from glucose deprivation and oxidative stress [10]. Some of the neuroprotective action of the PDGF's may result from induction of catalase, SOD and glutathione peroxidase activities. PDGF BB may also exercise some of its neuroprotective function through inhibition of N-methyl-D-aspartate (NMDA) receptors [74] and consequent NMDA-dependent excitotoxicity.

PDGF levels are elevated in a number of CNS conditions including trauma, stroke, meningitis, cerebral abscesses, and glial and meningeal cysts [74]. Valenzuela and associates suggest that PDGF elevations may contribute to the tissue repair processes that accompany these diseases.

Somatostatin

Somatostatin is a hypothalamic/pituitary regulatory peptide and a neuromodulator in the CNS. While it is believed to be primarily neuronal, it is expressed by glia in early development and can be present in glial cell cultures depending upon the culture conditions [15]. Davidson and Gillies suggest that glial production of somatostatin is likely to be important in injury and repair processes within the CNS. To our collective knowledge, no injury-related time courses for somatostatin mRNA or protein production have been reported. However, somatostatin protein levels increase 2-fold in cerebral cortex epileptic foci and almost 3-fold in cerebral scar tissue of posttraumatic epilepsy [41]. In the present study we observe approximately a 2-fold increase in somatostatin mRNA in the cortex following injury. No mRNA is detectable in hippocampus. Significant increases occur by 24 h in cortex and levels return to control by 4 wk.

Somatostatin can cause vasoconstriction and subsequent increased vascular permeability in the rat CNS [47]. It is possible that localized breakdown of the blood-brain barrier could increase local brain levels of selective growth factors and thus contribute to the wound-healing process. Glial cells have been reported to internalize plasma proteins and retain them long-term suggesting that extravasated plasma proteins may serve physiological functions in wound healing [44].

c-Fos

A number of studies indicate that c-Fos mRNA and protein levels increase following brain injury [39,56,65]. c-Fos has been previously shown, in a cold-injury model, to localize to regenerating endothelium within the lesion site, and to astrocytes, endothelium and neurons in the perilesional area. c-Fos may regulate the long-term expression of preproenkephalin, nerve growth factor, dynorphin, vasoactive intestinal polypeptide, tyrosine hydroxylase and other genes with AP-1 sites in their promoters (reviewed in [82]). Increases are transient and generally decline to control levels by 6 h post-injury. Both IGF-1 [20] and platelet-activating factor [5] have been implicated in c-Fos gene expression. In our model, IGF-1 mRNA elevations do not precede c-Fos mRNA elevations. Consequently, increased IGF-1 is not likely responsible for c-Fos up-regulation. However, IGF-1 baseline protein levels may be involved in c-Fos regulation.

In the present model, c-Fos mRNA is not detectable in uninjured brain. It is detectable 1 h after injury but returns to control levels by 6 h post-injury.

PLP and MBP

Proteolipid protein (PLP) is produced by oligodendrocytes and is the major protein constituent of CNS myelin membranes. PLP, together with myelin basic protein (MBP), comprise approximately 80% of the protein present in the CNS myelin sheath [17,30,58]. Few studies have addressed physical and biochemical changes in oligodendrocytes following injury. Following ischemic injury, pathological changes in oligodendrocytes

include swelling, vacuolation and interlamellar space formation [61]. Pathological changes appear early and many glia are lethally injured.

We speculate that the increases that we observe in PLP (up to 4.7-fold) and MBP (up to 2-fold) mRNAs reflect compensatory changes in viable oligodendrocytes. Remyelination may also require proliferation of adult O-2a cells, differentiation and maturation (myelin production). Reports from other laboratories suggest that stab wound injuries result in numerical increases in immature oligodendrocytes [79]. MBP and PLP mRNAs appear to significantly increase following injury later in the hippocampus compared to the cortex. MBP mRNA is significantly elevated at 24 h in the cortex and 72 h in the hippocampus. PLP mRNA is significantly elevated at 12 h in the cortex and 24 h in the hippocampus. MBP and PLP mRNA levels return to control by 4 wk in the cortex whereas the corresponding mRNAs return to control levels by 2 wk in the hippocampus. These differences may reflect both the injury model employed here and the cell-type distribution between the cortex and hippocampus.

Transferrin, Transferrin receptor

Iron is directly involved in myelin production as a required co-factor for cholesterol and lipid biosynthesis and indirectly because of its requirement for oxidative metabolism (which occurs at a high rate in oligodendrocytes) [12]. The predominant cell type containing ferritin, transferrin, and iron throughout the brain at all ages is the oligodendrocyte [6]. However, ferritin and iron are also present in microglial cells in all

brain regions, particularly the hippocampus. The relative roles of oligodendrocytes and microglial cells in the sequestration, utilization and detoxification of iron are unknown. A further complication is the reported manifestation of transferrin receptors on macrophages, endothelial cells and reactive astrocytes following brain injury [59]. It is speculated that these changes may play an important role in lesion repair.

Since disruptions in iron availability may affect oligodendrocyte viability and myelin production, elevated expression of transferrin and transferrin mRNA, as we observe in the present study, may serve to increase survival of oligodendrocytes and to accelerate remyelination. In the present model, increases in cortical transferrin and transferrin receptor mRNAs occur late (72 h) and rapidly decline (return to baseline by 2 wk). No changes in mRNA expression for these two proteins are observed in hippocampus.

p53

In the present injury model, p53 mRNA levels increase rapidly (by 6 h in the cortex and 12 h in the hippocampus) up to a maximum of 2-fold. Levels return to baseline by 1 wk in both regions of the brain. p53 expression is increased in models of ischemia and epilepsy and it is proposed to mediate seizure induced neuronal damage [13,53]. p53 mRNA has also been shown to increase within hours following kainate-mediated excitotoxicity [70]. It is suggested that p53 induction is a marker of irreversible injury in postmitotic cells of the CNS and that it could have functional significance in determining selective neuronal vulnerability. It appears that CNS neurons containing at least one copy of p53 are severely

damaged by exposure to kainate or glutamate. Morphologically, these cells appear to undergo apoptosis. However, neurons deficient in p53 exhibit little or no damage [78].

IGF-1 and TGF-β1

Both IGF-1 and TGF-β1 induce migration of scratch-wounded astrocytes in tissue culture, and consequent wound closure [19]. Increases in these growth factors following brain injury may serve similar purposes.

Focal elevation of immunoreactive TGF-β1 has been demonstrated in lesioned brain tissue. Following stereotactic rat brain incision, TGF-β1 mRNA and protein levels are found to be elevated in astrocytes, microglia, polymorphs, macrophages, neurons, ependymal cells and choroid plexus cells with peak expression around 3 days [37,46]. TGF-β1 may have an impact upon scar formation. Logan and colleagues suggest that TGF-β1 increases deposition of fibrous scar tissue following injury [45]. They show that TGF-β1 neutralizing antibodies reduce scar formation. In contrast, Lindholm et al. [42] report that TGF-β1 strongly inhibits astrocyte proliferation and suppresses the mitotic effects of FGF and EGF on astrocytes. They suggest that TGF-β1 may limit scar formation in vivo. TGF-β1 may also increase synthesis of fibronectin [62] and NGF [43], thus contributing to extracellular matrix deposition and nerve regeneration, respectively.

In the present study, TGF-β1 mRNA is not detectable in control animals but is consistently detectable between 6 h and 1 wk post-injury in cortex and 12 h and 1 wk in hippocampus.

IGF-1 expression is increased in astrocytes and microglia by 3 days following hypoxic-ischemic injury [26]. The increase may partially reflect IGF-1 movement from the CSF into the parenchyma [32]. However, other injury models suggest that IGF-1 is elevated by local production. IGF-1 mRNA increases by 3 days in astrocytes following demyelinating cryogenic spinal cord injury [80]. Levels peak between 21 and 28 days and decline to near control levels by 56 days post-injury. Since central administration of IGF-1 can rescue neurons in the cortex, striatum, hippocampus, dentate gyrus and thalamus following hypoxic injury [33], local production following injury is believed to be meaningful in the wound healing process.

In the present model, we find IGF-1 mRNAs to be significantly increased by 24 h in cortex and 72 h in hippocampus. Levels decline to baseline by 4 wk in the hippocampus but remain elevated in cortex. IGF-1, therefore, is one of three surveyed mRNAs which remains elevated above control levels at 4 wk.

Renin

All of the essential components of the renin-angiotensin system (RAS) are present in brain, and angiotensin II is produced and mediates effects locally [21,64,66]. Rat angiotensinogen mRNA has been shown to be insignificantly altered at 3 h or 24 h post-injury [48]. In apparent contrast, AII, AT1 and AT2 receptor mRNAs are reported to be significantly increased in rat brain following injury [48,84]. The present study indicates that renin mRNA significantly increases by 1 h post-injury in cortex and 6 h in hippocampus.

Maximum increases of 3.8-fold and 2.8-fold were obtained in cortex and hippocampus with returns to baseline by 2 wk and 1 wk post-injury, respectively.

To our collective knowledge, investigations of renin or renin mRNA modifications following injury have not been reported. A central local RAS is clearly involved in elevation of arterial pressure, and balance of fluids and electrolytes [66]. Since fluid imbalance may accompany brain injury, stimulation of production of components of the RAS may serve to regulate fluid exchange.

Summary

One of the most interesting observations from the present study is that a number of mRNAs upregulated early in cortex are increased between 5 and 48 h later in hippocampus. This could reflect the model, in which hippocampus lies at a distance from the epicenter of injury. It could also reflect variations in cell type distribution between these two brain regions. No mRNAs are up-regulated in hippocampus prior to cortex. Those genes expressed late in cortex tend to be expressed simultaneously in hippocampus.

Knowledge of the stepwise events controlling wounding healing following brain injury should contribute to the tailored treatment of affected patients. Administration of peptides or drugs which induce or repress peptide expression may optimize healing and minimize excessive scar tissue formation. Antisense oligonucleotides, for instance, can inhibit GFAP production by astrocytes and may be useful in modifying scar formation in vivo [83]. As gene therapy techniques become increasingly sophisticated and efficient,

expression plasmid, viral vector, or oligonucleotide administration may become commonplace strategies. Treatments may be most effective if tailored to specific forms of injury or to specific regions of the brain. Regardless, effective treatment of brain injuries with drugs, peptides or genes will require a thorough understanding of the complex cellular changes and inter-cellular interactions which occur following insult.

Acknowledgments

This work was supported by grant DAMD17-93-V-3013 from the Dept. of Defense.

References

1. Abraham, J.A., Mergia, A., Whang, J.L., Tumolo, A., Friedman, J., Hjenild, K.A., Gospodarowicz, D. and Fiddes, J.C., Nucleotide sequence of a bovine clone encoding the angiogenic protein, basic fibroblast growth factor, *Science*, 233(1986) 545-548.

2. Anderson, K.J., Dam, D., Lee, S. and Cotman, C.W., Basic fibroblast growth factor prevents death of lesioned cholinergic neurons *in vivo*, *Nature,* 332(6162) (1988) 360-361.

3. Araujo, D.M., Chabot, J. and Quirion, R., Potential neurotrophic factors in the mammalian central nervous system: functional significance in the developing and aging brain, *Intn. Rev. Neurol.*, 32(1990) 141-174.

4. Asai, T., Wanaka, A., Kato, H., Masana, Y., Seo, M. and Tohyama, M., Differential expression of two members of the FGF receptor gene family, FGFR-1 and FGFR-2, in the adult rat central nervous system, *Mol. Brain Res.,* 17(1993) 174-178.

5. Bazan, N.G. and Allan, G., Platelet-activating factor in the modulation of excitatory amino acid neurotransmitter release and of gene expression, *J. Lipid Mediat. Cell Signal*, 14(1-3)(1996) 321-330.

6. Benkovic, S.A. and Connor, J.R., Ferritin, transferrin, and iron in selected regions of the adult and aged rat brain, *J. Comp. Neurol.*, 338(1)(1993) 97-113.

7. Bogler, O., Wren, D., Barnett, S.C., Land, H. and Noble, M., Cooperation between two growth factors promotes extended self-renewal and inhibits differentiation of oligodendrocyte-type-2 astrocyte (O-2A) progenitor cells, *Proc. Natl. Acad. Sci.*, 87(1990) 6368-6372.

8. Cavicchioli, L., Flanigan, T.P., Polato, P., Vantini, G., Toffano, G. and Leon, A., Evidence for early glial activation in the CNS following mechanical injury, *J.Neurochem. Suppl.*, 52(1989) S114.

9. Chalifour, L.E., Fahmy, R., Holder, E.L., Hutchinson, E.W., Osterland, C.K., Schipper, H.M. and Wang, E., A method for analysis of gene expression patterns, *Anal. Biochem.*, 216(1994) 299-304.

10. Cheng, B. and Mattson, M.P., PGDFs protect hippocampal neurons against energy deprivation and oxidative injury: evidence for induction of antioxidant pathways, *J. Neurosci*, 15(11)(1995) 7095-7104.

11. Chomczynski, P. and Sacchi, N., Single-step method of RNA isolation by acid guanidinium thiocyanate-phenol-chloroform extraction, *Anal. Biochem.*, 162(1987) 156-159.

12. Connor, J.R. and Menzies, S.L., Relationship of iron to oligodendrocytes and myelination, *Glia*, 17(2)(1996) 83-93.

13. Crumrine, R.C., Thomas, A.L. and Morgan, P.F., Attenuation of p53 protects against focal ischemic damage in transgenic mice, *J. Cereb. Blood Flow Metab.*, 14(6)(1994) 887-891.

14. da Cunha, A., Jefferson, J.J., Tyor, W.R., Glass, J.D., Jannotta, F.S. and Vitkovic, L., Gliosis in human brain: relationship to size but not other properties of astrocytes, *Brain Res.*, 600(1993) 161-165.

15. Davidson, K. and Gillies, G.E., Neuronal vs. glial somatostatin in the hypothalamus: a cell culture study of the ontogenesis of cellular location, content and release, *Brain Res.*, 624(1-2)(1993) 75-84.

16. Eckenstein, F.P., Anderson, C., Kuzis, K. and Woodward, W.R., Distribution of acidic and basic fibroblast growth factors inthe mature, injured and developing rat nervous system, *Prog. Brain Res.*, 103(1994) 55-64.

17. Eng, L.F., Chao, T.C., Gerstl, B., Pratt, D. and Tavastastjerna, M.G., The maturation of human white matter myelin, fractionation of the myelin membrane proteins, *Biochemistry*, 7 (1968) 4455-4465.

18. Enokido, Y., Akaneya, Y., Niinobe, M., Mikoshiba, K. and Hatanaka, H., Basic fibroblast growth factor rescues CNS neurons from cell death caused by high oxygen atmosphere in culture, *Brain Res.*, 599(1992) 261-271.

19. Faber-Elman, A., Solomon, A., Abraham, J.A., Marikovsky, M. and Schwartz, M., Involvement of wound-associated factors in rat brain astrocyte migratory response to axonal injury: *in vitro* simulation, *J. Clin. Invest.*, 97(1)(1996) 162-171.

20. Fernandez, A.M., Garcia-Estrada, J., Garcia-Segura, L.M. and Torres-Aleman, I., Insulin-like growth factor I modulates c-Fos induction and astrocytosis in response to neurotoxic insult, *Neurosci.*, 76(1)(1997) 117-122.

21. Ferrario, C.M., Santos, R.A.S., Brosnihan, K.B., Block, C.H., Schiavone, M.T., Khosla, M.C. and Greene, L.J., A hypothesis regarding the function of angiotensin peptides in the brain, *Clin. and Exper. -Theory and Practice*, A10(Suppl.1)(1988) 107-121.

22. Finklestein, S.P., Apostolides, P.J., Caday, C.G., Prosser, J., Philips, M.F. and Klagsbrun, M., Increase basic fibroblast growth factor (bFGF) immunoreactivity at the site of focal brain wounds, *Brain Res.*, 460(1988) 253-259.

23. Follesa, P., Wrathall, J.R. and Mocchetti, I., Increased basic fibroblast growth factor mRNA following contusive spinal cord injury, *Mol. Brain Res.*, 22(1-4)(1994) 1-8.

24. Frautschy, S.A., Walicke, P.A. and Baird, A., Localization of basic fibroblast growth factor and its mRNA after CNS injury, *Brain Res.*, 553(1991) 291-299.

25. Fukumoto, H., Kakihana, M. and Suno, M., Recombinanat human basic fibroblast growth factor (rhbFGF) induces secretion of nerve growth factor (NGF) in cultured rat astroglial cells, *Neurosci. Lett.,* 122(1991) 221-224.

26. Gluckman, P.D., Klempt, N.D., Guan, J., Mallard, E.C., Sirimanne, E., Dragunow, M., Klempt, M., Singh, K., Williams, C.E. and Nikolics, K., A role for IGF-1 in the rescue of CNS neurons following hypoxic-ischemic injury, *Biochem. Biophys. Res. Comm.,* 182(1992) 593-599.

27. Goldman, J.E., Regulation of oligodendrocyte differentation, *TINS*, 15(10)(1992) 359-362.

28. Gomez-Pinilla, F. and Cotman, C.W., Transient lesion-induced increase of basic fibroblast growth factor and its receptor in layer VIb (subplate cells) of the adult rat cerebral cortex, *Neurosci.,* 49(4)(1992) 771-780.

29. Gomez-Pinilla, F., Vu, L. and Cotman, C.W., Regulation of astrocyte proliferation by FGF-2 and heparin sulfate *in vivo*, *J. Neurosci.,* 15(3)(1995) 2021-2029.

30. Gonzales-Sastre, F., The protein composition of isolated myelin, *J. Neurochem.,* 17 (1970) 1049-1056.

31. Grinspan, J.B., Stern, J.L., Pustilnik, S.M. and Pleasure, D., Cerebral white matter contains PDGF-responsive precursors to O2A cells, *J. Neurosci.*, 10(6)(1990) 1866-1873.

32. Guan, J., Williams, C.E., Skinner, S.J.M., Mallard, E.C. and Gluckman, P.D., The effects of insulin-like growth factor (IGF)-1, IGF-2, and des-IGF-1 on neuronal loss after hypoxic-ischemic brain injury in adult rats: evidence for a role for IGF binding proteins, *Endocrinology*, 137(3)(1996) 893-898.

33. Guan, J., Skinner, S.J.M., Beilharz, E.J., Hua, K.M., Hodgkinson, S., Gluckman, P.D. and Williams, C.E., The movement of IGF-I into the brain parenchyma after hypoxic-ischaemic injury, *Neuroreport*, 7(1996) 632-636.

34. Hermanson, M., Olsson, T., Westermark, B. and Funa, K., PDGF and its receptors following facial nerve axotomy in rats: expression in neurons and surrounding glia, *Exp. Brain. Res.*, 102(3)(1995) 415-422.

35. Hozumi, I., Chiu, F-C. and Norton, W.T., Biochemical and immunocytochemical changes in glial fibrillary acidic protein after stab wounds, *Brain Res.*, 524(1990) 64-71.

36. Hozumi, I., Aquino, D.A. and Norton, W.T., GFAP mRNA levels following stab wounds, *Brain Res.*, 534(1990) 291-294.

37. Kiefer, R., Streit, W.J., Toyka, K.V., Kreutzberg, G.W. and Hartung, H., Transforming growth factor-β1: a lesion-associated cytokine of the nervous system, *Intn. J. Devel. Neurosci.*, 13(3-4)(1995) 331-339.

38. Kiyota, Y., Takami, K., Iwane, M., Shino, A., Miyamoto, M., Tsukuda, R. and Nagaoka, A., Increase in basic fibroblast growth-like immunoreactivity in rat brain after forebrain ischemia, *Brain Res.*, 545(1991) 322-328.

39. Kohmura, E., Yuguchi, T., Yamada, K., Sakaguchi, T., Wanaka, A. and Hayakawa, T., Expression of c-fos mRNA after cortical ablation in rat brain is modulated by basic fibroblast growth factor (bFGF) and the NMDA receptor is involved in c-fos expression, *Mol. Brain Res.*, 28(1995) 117-121.

40. Landis, D.M.D., The early reactions of non-neuronal cells to brain injury, *Ann. Rev. Neurosci.*, 17(1994) 133-151.

41. Lang, S., Peigen, K., Liu, J., Zhang, F., Chen, X. and Liu, Z., Somatostatin concentrations in cerebrospinal fluid and brain tissue of patients with refractory epilepsy, *Mol. Chem. Neuropathol.*, 17(3)(1992) 239-247.

42. Lindholm, D., Castren, E., Kiefer, R., Zafra, F. and Thoenen, H., Transforming growth factor-beta 1 in the rat brain: increase after injury and inhibition of astrocyte proliferation, *J. Cell Biol.*, 117(2)(1992) 395-400.

43. Lindholm, D., Hengerer, B., Zafra, F. and Thoenen, H., Transforming growth factor-beta 1 stimulates expression of nerve growth factor in the rat CNS, *Neuroreport*, 1 (1)(1990) 9-12.

44. Liu, H.M. and Sturner, W.Q., Extravasation of plasma proteins in brain trauma, *Forensic. Sci. Intn.*, 38(3-4)(1988) 285-295.

45. Logan, A., Berry, M., Gonzalez, A.M., Frautschy, S.A., Sporn, M.B. and Baird, A., Effects of transforming growth factor β1 on scar production in the injured central nervous system of the rat, *Eur. J. Neurosci.*, 6(1994) 355-363.

46. Logan, A., Frautschy, S.A., Gonzalez, A.M., Sporn, M.B. and Baird, A., Enhanced expression of transforming growth factor beta 1 in the rat brain after a localized cerebral injury, *Brain Res.*, 587(2)(1992) 216-225.

47. Long, J.B., Rigamonti, D.D., Dosaka, K., Kraimer, J.M. and Martinez-Arizala, A., Somatostatin causes vasoconstriction, reduces blood flow and increases vascular permeability in the rat central nervous system, *J. Pharmacol. Exp. Ther.*, 260 (3)(1992) 1425-1432.

48. Makino, I., Shibata, K., Ohgami, Y., Fujiwara, M. and Furukawa, T., Transient upregulation of the AT2 receptor mRNA level after global ischemia in the rat brain, *Neuropeptides*, 30(6)(1996) 596-601.

49. Menon, V.K. and Landerholm, T.E., Intralesion injection of basic fibroblast growth factor alters glial reactivity to neural trauma, *Exp. Neurol.*, 129(1994) 142-154.

50. Milner, R.J., Lai, C., Nave, K.-A., Lenoir, D., Ogata, J. and Sutcliff, J.G., Nucleotide sequences of two mRNAs for rat brain myelin proteolipid protein, *Cell*, 42(1985) 931-939.

51. Mocchetti, I. and Wrathall, J.R., Neurotropic factors in central nervous system trauma, *J. Neurotrauma.,* 12(1995) 853-870.

52. Morrison, R.S., Sharma, A., DeVell, J. and Bradshaw, R.A., Basic fibroblast growth factor supports the survival of cerebral cortical neurons in primary culture, *Proc. Natl. Acad. Sci.,* 83(1986) 7537-7541.

53. Morrison, R.S., Wenzel, H.J., Kinoshita, Y., Robbins, C.A., Donehower, L.A. and Schwartzkroin, P.A., Loss of the p53 tumor suppressor gene protects neurons from kainate-induced cell death, *J. Neurosci.*, 16(4)(1996) 1337-1345.

54. Mucke, L., Oldstone, M.B.A., Morris, J.C. and Nerenberg, M.I., Rapid activation of astrocyte-specific expression of GFAP-lacZ transgene by focal injury, *The New Biologist.*, 3(5)(1991) 465-474.

55. Muthukrishnan, L., Warder, E. and McNeil, P.L., Basic fibroblast growth factor is efficiently released from a cytolsolic storage site through plasma membrane disruptions of endothelial cells, *J. Cell. Physiol.,* 148(1991) 1-16.

56. Nag, S., Cold-injury of the cerebral cortex: immunolocalization of cellular proteins and blood-brain barrier permeability studies, *J. Neuropathol. Exp. Neurol.*, 55 (8)(1996) 880-888.

57. Norenberg, M.D., Astrocyte responses to CNS injury, *J. Neuropath. and Exp. Neurol.*, 53(3)(1994) 213-220.

58. Norton, W.T. and Poduslo, S.E., Myelination in rat brain: Changes in myelin composition during brain maturation, *J. Neurochem.*, 21(1973) 759-773.

59. Orita, T., Akimura, T., Nishizaki, T., Kamiryo, T., Ikeyama, Y., Aoki, H. and Ito, H., Transferrin receptors in injured brain, *Acta. Neuropathol.*, 79(6)(1990) 686-688.

60. Otto, D., Unsicker, K. and Grothe, C., Pharmacological effects of nerve growth factor and fibroblast growth factor applied to the transectioned sciatic nerve on neuron death in adult rat dorsal root ganglia, *Neurosci. Lett.*, 83(1987) 156-160.

61. Pantoni, L., Garcia, J.H. and Gutierrez, J.A., Cerebral white matter is highly vulnerable to ischemia, *Stroke*, 27(9)(1996) 1641-1647.

62. Pasinetti, G.M., Nichols, N.R., Tocco, G., Morgan, T., Laping, N. and Finch, C.E., Transforming growth factor beta 1 and fibronectin messenger RNA in rat brain: responses to injury and cell-type localization, *Neuroscience*, 54(4)(1993) 893-907.

63. Pettmann, B., Labourdette, G., Weibel, M. and Sensenbrenner, M., The brain fibroblast growth factor (FGF) is localized in neurons, *Neurosci. Lett.*, 68(1986) 175-180.

64. Printz, M.P., Regulation of the brain angiotensin system: a thesis of multicellular involvement, *Clin. and Exper. Hyper. -Theory and Practice*, 10(1)(1988) 17-35.

65. Raghupathi, R., McIntosh, T.K. and Smith, D.H., Cellular responses to experimental brain injury, *Brain Pathol.*, 5(4)(1995) 437-442.

66. Reid, I.A., Actions of angiotensin II on the brain: mechanisms and physiologic role, *Am. J. Physiol.* 24(1984) F533-F543.

67. Reilly, J.F. and Kumari, V.G., Alterations in fibroblast growth factor receptor expression following brain injury, *Exp. Neurol.*, 140(1996) 139-150.

68. Roach, A., Boylan, K., Horvath, S., Prusiner, S.B. and Hood, L.E., Characterization of cloned cDNA representing rat myelin basic protein: Absence of expression in brain of shiverer mutant mice, *Cell*, 34(1983) 799-806.

69. Rudge, J.S., Pasnikowski, E.M., Holst, P. and Lindsay, R.M., Changes in neurotrophic factor expression and receptor activation following exposure of hippocampal neuron/astrocyte cocultures to kainic acid, *J. Neurosci.* 15(10)(1995) 6856-6867.

70. Sakhi, S., Bruce, A., Sun, N., Tocco, G., Baudry, M. and Schreiber, S.S., p53 induction is associated with neuronal damage in the central nervous system, *Proc. Natl. Acad. Sci.*, 91(1994) 7525-7529.

71. Sievers, J., Hausmann, B., Unsicker, K. and Berry, M., Fibroblast growth factors promote the survival of adult rat retinal ganglion cells after transection of the optic nerve, *Neurosci. Lett.*, 76(2) (1987) 157-162.

72. Takayama, S., Sasahara, M., Iihara, K., Handa, J. and Hazama, F., Platelet-derived growth factor B-chain-like immunoreactivity in injured rat brain, *Brain Res.* 653(1994) 131-140.

73. Unsicker, K., Reichert-Preibsh, H., Schmidt, R., Pettmann, B., Labourdette, G. and Sensenbrenner, M., Astroglial and fibroblast growth factors have neurotrophic functions for cultured peripheral and central nervous system neurons, *Proc. Natl. Acad. Sci.*, 84(15)(1997) 5459-5463.

74. Valenzuela, C.F., Xiong, Z., MacDonald, J.F., Weiner, J.L., Frazier, C.J., Dunwiddie, T.V., Kazlauskas, A., Whiting, P.J. and Harris, R.A., Platelet-derived growth factor induces a long-term inhibition of *N*-methyl-D-aspartate receptor function, *J. Biol. Chem.*, 271(27)(1996) 16151-16159.

75. Vige', X., Costa, E. and Wise, B.C., Mechanism of nerve growth factor mRNA regulation by interleukin-1 and basic fibroblast growth factor in primary cultures of rat astrocytes, *Mol. Pharm.*, 40(1991) 186-192.

76. Walicke, P., Cowan, W.M., Ueno, N., Baird, A. and Guillemin, R., Fibroblast growth factor promotes survival of dissociated hippocampal neurons and enhances neurite extention, *Proc. Natl. Acad. Sci.*, 83(1986) 3012-3016.

77. Wanaka, A., Johnson, Jr., E.M., and Milbrandt, J., Localization of FGF receptor mRNA in the adult rat central nervous system by *in situ* hybridization, *Neuron.*, 5 (1990) 267-281.

78. Xiang, H., Hochman, D.W., Saya, H., Fujiwara, T., Schwartzkroin, P.A. and Morrison, R.S., Evidence for p53-mediated modulation of neuronal viability, *J. Neurosci.*, 16(21)(1996) 6753-6765.

79. Xie, D., Schultz, R.L. and Whitter, E.F., The oligodendroglial reaction to brain stab wounds: an immunohistochemical study, *J. Neurocytol.*, 24(6)(1995) 435-448.

80. Yao, D.-L., West, N.R., Bondy, C.A., Brenner, M., Hudson, L.D., Zhou, J., Collins, G.H. and Webster, H.D., Cryogenic spinal cord injury induces astrocytic gene expression of insulin-like growth factor I and insulin-like growth factor binding protein 2 during myelin regeneration, *J. Neurosci. Res.*, 4(1995) 647-659.

81. Yoshida, K. and Gage, F.H., Fibroblast growth factors stimulate nerve growth factor synthesis and secretion by astrocytes, *Brain Res.*, 538(1991) 118-126.

82. Yu, A.C., Lee, Y.L., Fu, W.Y., and Eng, L.F., Gene expression in astrocytes during and after ischemia, *Prog. Brain Res.*, 105(1995) 245-253.

83. Yu, A.C.H., Lee, Y.L., and Eng, L.F., Astrogliosis in culture: I. The model and the effect of antisense oligonucleotides on glial fibrillary acidic protein synthesis, *J. Neurosci. Res.*, 34(1993) 295-303.

84. Zhang, Z.W., Yi, S.Y. and Zhang, X., Changes in and significance of atrial natriuretic peptide, angiotensin II after experimental brain injury, *Chung Hua I Hsueh Tsa Chih*, 74(9)(1994) 545-547,583.

Table 1. Gene Expression Post-Injury[1]

Early Genes			Late Genes		
(c) (h)	c-Fos	1h	(c) (h)	bFGF	72h
(c)	Renin	1h	(c) (h)	FGF-R1	72h
(h)	Renin	6h	(c) (h)	PDGF β receptor	72h
(c)	TK	6h	(c)	Transferrin receptor	72h
(c)	TGF-β1	6h	(c)	Transferrin	72h
(c)	p53	6h	(h)	Somatostatin	72h
(h)	TGF-β1	12h	(h)	MBP	72h
(h)	p53	12h	(h)	IGF-1	72h
(h)	TK	24h	(h)	GFAP	72h
(c) (h)	PLP	24h	(c) (h)	PDGF A	1wk
(c)	GFAP	24h	(c) (h)	PDGF B	1wk
(c)	IGF-1	24h	(c) (h)	PDGF α receptor	1wk
(c)	MBP	24h			
(c)	Somatostatin	24h			

[1]Time at which hybridization signal is first significantly expressed (above 0h control in cortex (c) and hippocampus (h). Categories indicate genes for which mRNA levels are first elevated at or before 24 h (Early Genes), and those elevated at or after 72h (Late Genes).

Table 2. Relative Temporal Changes in Gene Expression in Cortex and Hippocampus

Probe [1]	Cortex[2]	Hippocampus[2]	Δ[3]
c-Fos	1h	1h	0h
PLP	24h	24h	0h
Renin	1h	6h	5h
TGF-β1	6h	12h	6h
p53	6h	12h	6h
GFAP	24h	72h	48h
IGF-1	24h	72h	48h
MBP	24h	72h	48h
Somatostatin	24h	72h	48h
bFGF	72h	72h	0h
FGF-R1	72h	72h	0h
PDGF β receptor	72h	72h	0h
Transferrin receptor	72h	----	N/A
Transferrin	72h	----	N/A
PDGFA	1wk	1wk	0h
PDGF B	1wk	1wk	0h
PDGF α receptor	1wk	1wk	0h

[1]Probes listed in upper table are those for which cortical hybridization signals increase at or before 24h. Those in lower table increase at or after 72h.
[2]Time of onset of increased mRNA accumulation (compared to 0h control).
[2]Δ is the delay (in hours) in the expression of RNAs in hippocampus compared to cortex.

Figure Legend

Fig. 1. Dot-blots of radiolabeled cDNAs (generated from rat cortex RNAs following injury) hybridized to nitrocellulose filter-fixed clones. 1A, pUC19; 1B, pBR322; 1C, somatostatin; 1D, MBP; 1E, PLP; 2A, GFAP; 2B, TK; 2C, IGF-1; 2D, renin; 2E, c-Fos; 3A, bFGF; 3B, FGF-R1; 3C, transferrin; 3D, transferrin receptor; 3E, p53; 4A, PDGF α receptor; 4B, PDGF A; 4C, PDGF β receptor; 4D, PDGF B; 4E, TGF-β1.

Fig. 2. Dot-blots of radiolabeled cDNAs (generated from rat hippocampus RNAs following injury) hybridized to nitrocellulose filter-fixed clones. See Fig. 1 for identity of filter-fixed clones.

Fig. 3. Graphical illustrations of cortex-derived radiolabeled cDNAs bound to filter-fixed clones, as a function of time post-injury. Bars represent mean and standard deviation of three unrelated experiments. Asterisks indicate values significantly greater than 0 h control, $p< 0.05$. Positions of the graphs within the array correspond to positions of the dots within the dot-blot arrays in Fig. 1.

Fig. 4. Graphical illustrations of hippocampus-derived radiolabeled cDNAs bound to filter-fixed clones, as a function of time post-injury. Bars represent mean and standard deviation of three unrelated experiments. Asterisks indicate values significantly greater

than 0 h control, $p < 0.05$. Positions of the graphs within the array correspond to positions of the dots within the dot-blot arrays in Fig. 2.

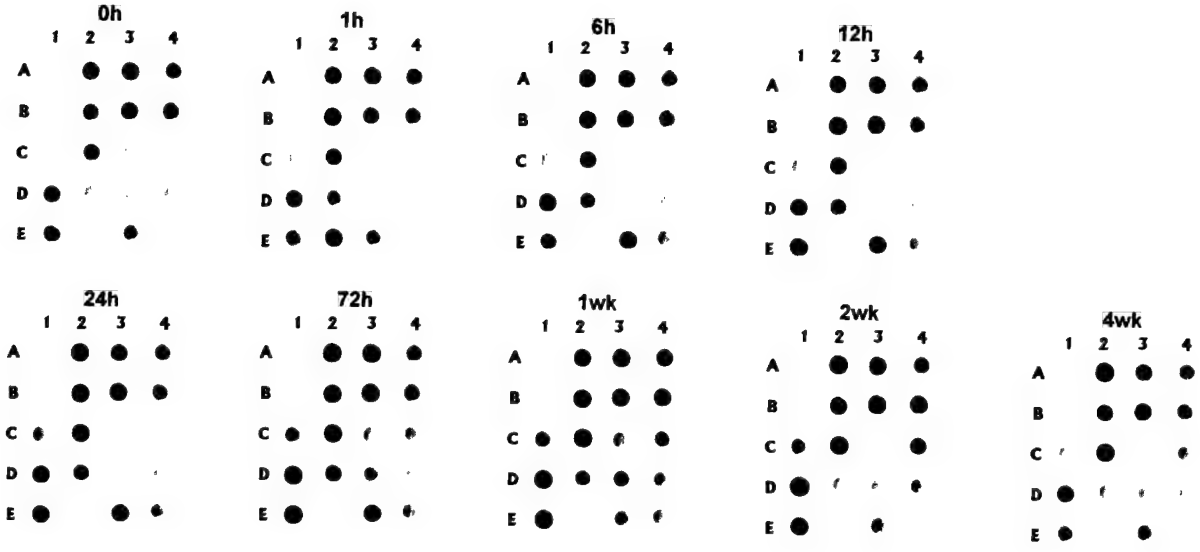
0h
1h
6h
12h
24h
72h
1wk
2wk
4wk
1 2 3 4
A
B
C
D
E

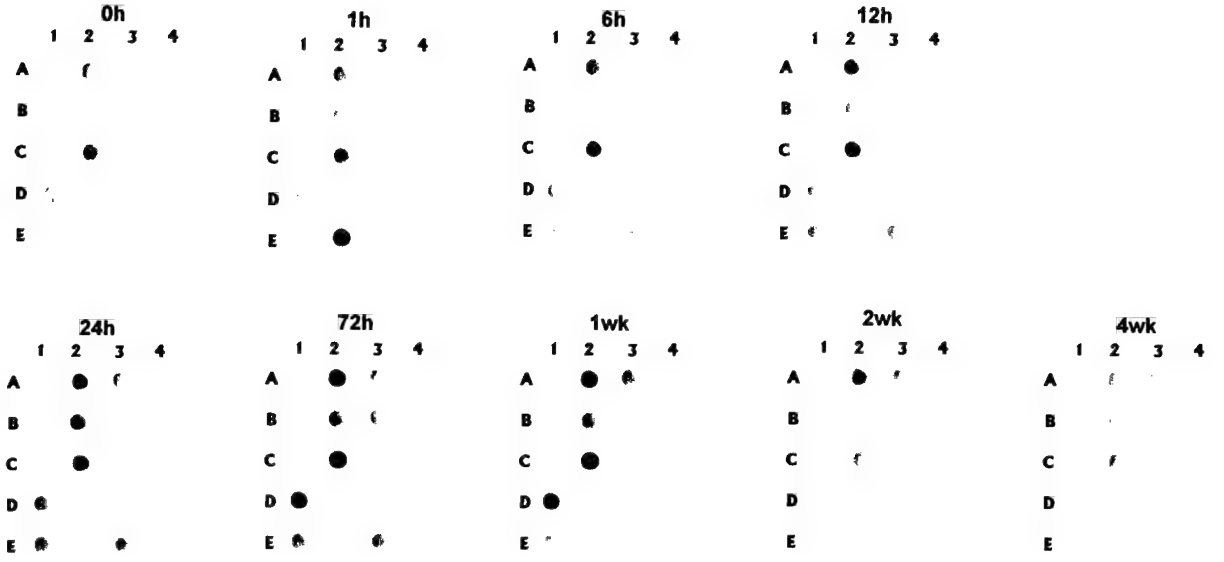
0h
1h
6h
12h
24h
72h
1wk
2wk
4wk
1 2 3 4
A
B
C
D
E

Relative Densitometric Units
Time Post-Injury
0h
1h
6h
12h
24h
72h
1wk
2wk
4wk
2A GFAP
2B Thymidine Kinase
2C IGF-1
2D Renin
2E c-Fos
3A bFGF
3B FGF-R1
3C Transferrin
3D Transferrin receptor
3E p53
4A PDGF α receptor
4B PDGF A
4C PDGF β receptor
4D PDGF B
4E TGF-β1
1C Somatostatin
1D MBP
1E PLP

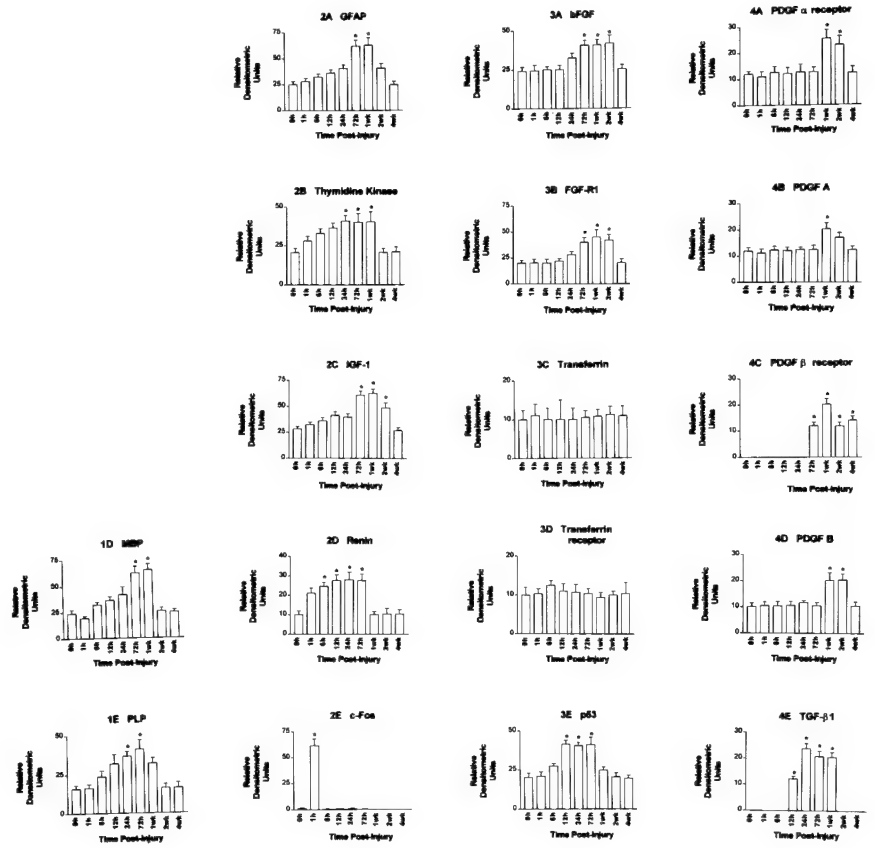
2A GFAP
3A bFGF
4A PDGF α receptor
2B Thymidine Kinase
3B FGF-R1
4B PDGF A
2C IGF-1
3C Transferrin
4C PDGF β receptor
1D MBP
2D Renin
3D Transferrin receptor
4D PDGF B
1E PLP
2E c-Fos
3E p53
4E TGF-β1
Relative Densitometric Units
Time Post-Injury

Aim 1: ROLE OF PDGF IN BRAIN DEVELOPMENT

The objective of this study was to determine the roles of PDGF in the brain by generating and studying mice deficient in brain PDGF A and B forms. We chose to use a dominant negative mutant cDNA of PDGF which has been shown to bind to and inactivate both PDGF A and B forms by heterodimerization (1). We had previously used this dominant negative mutant cDNA (1308) in transient expression assays of a cultured COS cell line and in stably transfected glial cell lines. We then established five strains of mice transgenic for the mutant PDGF cDNA in which expression was controlled by the glial-specific JC viral promoter/enhancer. Three of the strains demonstrated a proportional small size phenotype with variable expressivity and two strains exhibited a hydrocephalic phenotype in addition to small size. The transgene mRNA was expressed in brain but not liver, eye, spleen, muscle, heart or lung. However, as the mice were progressively bred, these distinctive phenotypes became less prevalent and finally disappeared completely. This was accompanied by a loss of transgene expression though the transgene DNA was still present. Despite our limited success with these initial constructs we felt it was worthwhile to try similar strategies using different promoters. Expression of viral promoters is frequently down-regulated in *in vivo* situations, presumably due to alterations in chromatin structure. Use of cellular promoters can potentially increase duration of transgene expression.

The following describes the method of approach.

Approach

A PDGF dominant negative mutant cDNA (1308) was expressed from the neuron-specific enolase promoter. This vector was modified from the pMT2 expression vector. The NSE promoter/enhancer region was ligated upstream of a chimeric set of SV40 donor/acceptor splice junctions that permit splicing of the expressed RNA. The full-length PDGF cDNA was inserted so that the initiator ATG represents the first ATG of the RNA produced. DHFR cDNA sequences have been left in the vector from the original pMT2 vector and generally provide some stabilization of otherwise short-lived mRNAs. The translation product will initiate at the first ATG in the PDGF A chain cDNA and terminate at the normal A chain termination signal and therefore will form normal PDGF (not a chimera with the DHFR). The poly(A) addition site is provided by the double SV40 poly(A) site. The VA RNA genes are irrelevant to this particular consturct. Cleavage with Bam HI and Ssp I permits removal of the relevant expression cassette from the plasmid sequences. The transgenic mice were generated using this cassette.

DNX, using our DNA construct, generated eight transgenic animals and sent those to us together with two control animals of the same genetic background. We first tested those animals to ensure that they were, indeed, transgenic by PCR analysis. We then bred the animals to generate homozygotes and analyzed these for expression of the transgene in mouse brain. Primers, designed to generate a fragment 300 bp in length, were used in RT/PCR reactions. Earlier progress reports submitted to the DOD showed that in several tested animals, the transgene was expressed in brain but not detectable in liver, testes,

lung, muscle, heart, spleen, and eye. Therefore, we had achieved specificity of expression using the NSE promoter.

Earlier progress reports have included photographs of PCR products generated from transgenic genomic DNAs and cDNAs.

Summary

Unfortunately, despite dominant negative mutant transgene expression in the brain, we observed no consistent detectable phenotype. It may be that blood-borne PDGF can cross the blood-brain barrier and compensate for low brain tissue levels. Alternatively, it may be that other growth factors can compensate for a deficiency in brain PDGF. Despite the fact that PDGFs have been hypothesized to have a pivotal role in brain glial cell development and differentiation, and are expressed in mature neurons our findings support the hypothesis that redundancy of brain growth factors may compensate for deficiences. It may be difficult to unravel the functions of growth factors in the CNS by reducing levels of those factors.

References

1) Mercola, M., Deininger, P.L., Shamah, S. M., Porter, J., Wang, C. and C. D. Stiles. 1990. Genes and Development 4:2333-2341.

Aim 2: CHANGES IN GENE EXPRESSION AS A FUNCTION OF BRAIN INJURY

The goal of this subproject was to utilize a rat brain cryogenic injury model to study the patterns of gene expression as a function of time following the injury. This would be useful in identifying the various gene expression responses as either the most immediate responses or more long-term responses. This would in turn provide some idea of whether therapies might be possible that then attempted to modify some of those gene expressions.

Approach.

We chose 18 different cDNA clones for mRNAs that either serve as controls in the experiment, or RNAs that might code for proteins that could play a role in response to injury. These included a number of transcription factors, as well as growth factors and their receptors, and structural proteins that might respond to injury. These cDNAs were utilized in a reverse dot blot assay developed by Chalifour et al (1994) that allowed us to simultaneously assay the expression of all of them in either the cortex or the hippocampus.

These studies are described in detail in the accompanying manuscript. Many of the genes chosen for study exhibited significant changes in expression levels in response to injury. In general we found that many genes responded earlier in the cortex compared to the hippocampus. This would suggest that therapies for injuries might vary depending on the timing after the trauma and the brain region to be treated. Immediate early genes, like fos, were found to respond rapidly and transiently as might be expected. Other genes such as thymidine kinase and renin responded at an intermediate rate and then declined after about a week. The thymidine kinase activity demonstrates that cell proliferation began early and continued at a significant rate for at least a week. Many of the growth factors and their receptors, as well as genes associated with remyelination following the injury responded after about 12 hours of treatment and stayed on for the first week. Only a few genes showed a slower response that was maintained for a number of weeks. The specific relevance of each of the genes is discussed in more detail in the manuscript.

Summary.

One of the particular benefits of this study is that it allowed the simultaneous measurement of gene expression from all of these genes from a single sample, thus minimizing experimental variation and allowing the most reliable comparison. This technique is becoming more widely used and there are now panels of cDNAs available for the studies that include thousands of known, and unknown, genes to allow a more thorough survey of gene expressions. It is now necessary for us to take the more interesting results, such as the late onset of PDGF receptor and TGF β expression and determine which cell types within the injured brain are showing this response. This will allow us to obtain a better picture of the cross-communication occurring between the different cell types and how they utilize these signals to respond to the injury.

References

Chalifour, L. E., Fahmy, R., Holder, E. L., Hutchinson, E. W., Osterland, C. K., Schipper, H. M., Wang, E. 1994. Analytical Biochem. 216:299-304.

PATHOPHYSIOLOGICAL EVENTS TRIGGERED DURING LIGHT-INDUCED DAMAGE TO THE RETINA.

INTRODUCTION

Photoreceptor cells in the retina are damaged by exposure to intense light, with the rod photoreceptors being particularly sensitive. As the damage progresses, sight is impaired and blindness can eventually result. Light-induced rod photoreceptor death has been shown to proceed via apoptosis (Rapp, 1995). Apoptosis is a process of programmed cell death in which a defined cascade of events results in the activation of specific endonucleases, fragmentation of nuclear DNA, and ultimately in the cessation of cellular function (White, 1996). Apoptosis is a normal component of development and tissue maintenance in the mature organism, but can be inappropriately triggered by pathophysiological stimuli. Apoptotic cells retain their membrane integrity, and thus are usually phagocytosed before cell lysis can occur. Hence the surrounding tissue is not damaged by the release of lytic enzymes, and an inflammatory response is not triggered. This contrasts with the other major form of cell death, necrosis. Necrotic cell death usually results from gross chemical or physical insults and death proceeds in a less well defined manner. Ultimately, membrane integrity is lost, fluid enters the cells and lysis occurs. An inflammatory response is triggered, with infiltration of neutrophils and ultimately the deposition of scar tissue. DNA fragmentation is a common motif of both forms of cell death. However, whereas necrotic DNA fragmentation is random, apoptotic DNA cleavage is ordered, firstly into large 50 and 300 kilobase pieces and then into multiples of ~180-200 base pairs (the length between intranucleosomal stretches) (Wyllie et al., 1980; Oberhammer et al, 1993).

Specific genes have been characterized that trigger and regulate the initiation, timing, and extent of apoptosis. As the mechanisms by which apoptosis is triggered and proceeds become defined in more detail, steps at which the apoptotic cascade can be controlled will

become apparent. The concept that this form of cell death may be preventable provides a potential route to thwart the progress of many degenerative disorders.

We have explored the possibility that a significant step in promotion of apoptosis in photoreceptors and other neuronal cells is the induction of prostaglandin G/H synthase-2 (COX 2). COX 2 is an isoform of the enzyme that catalyzes the rate-limiting step in the biosynthesis of prostagladins and thromboxanes, the conversion of arachidonic acid (AA) to prostglandin H_2. There are two isoforms of COX, COX 1 and COX 2. In most tissues, COX 1 is constitutively expressed, whereas COX 2 expression is stimulated by growth factors and cytokines, and displays a pattern of induction typical of the product of an immediate-early gene (Herschman, 1996).

The rationale behind having two isoforms of COX is not immediately apparent. One explanation is that COX 1 is responsible for the biosynthesis of constitutively required prostanoids, whereas COX 2 is responsible for prostanoid biosynthesis under stimulated conditions. However, the roles of COX 2 may be more complex. Upon stimulus, the activation of phospholipase A_2, the major enzyme responsible for the release of arachidonic acid, is rapidly activated (1-2 minutes), COX 2 protein levels are don not usually begin to be elevated until 1-2 hours later, and peak at 6-8 hours after stimulus. The AA initially released is probably utilized by COX 1. Additionally, whereas COX 1 protein expression is confined to the endoplasmic reticulum, COX 2 has also been found in both endoplasmic reticulum and nuclear membranes (Morita et al, 1995; Coffey et al, 1997), and, in neurons, in post-synaptic dendrite formations (Kaufmann et al, 1996). COX 2 may therefore utilize arachidonic acid pools distinct from those utilized by COX 1, and may also be responsible for the synthesis of prostanoids involved in

nuclear signalling events. It is important to note that nervous tissue there is a basal expression of COX 2, which is without precedent in almost every other tissue (DeWitt and Smith, 1995), and which may represent the result of ongoing synaptic stimulation (Yamagata et al, 1993). This may indicate that in the central nervous system COX 2 may play a specific metabolic role. However, under stress conditions an excess of COX 2 is generated, which represents a threshold between physiological processes and the turning on of pathophysiological processes.

We and others have shown that COX 2 is activated as a result of several forms of neurological insult (Marcheselli and Bazan, 1996; Bazan et al, 1996; Yamagata et al, 1993; Miettinen et al, 1997) and we have presented preliminary evidence that COX 2 is induced in our light damage model (year 3 report). In one type of neurotrauma, kainic acid-induced seizures, where neurons from distinct areas of the rat brain are subsequently lost through apoptosis (Pollard et al, 1994), COX 2 is most highly induced in those brain regions most prone to subsequent cell loss. Furthermore, COX 2 is more highly induced in damaging (kainic acid) than non-damaging (electroconvulsive shock) seizures (Marcheselli and Bazan, 1996), suggesting a correlation between COX 2 induction and neuronal apoptosis. We have shown, using the PAF receptor antagonist BN 50730, that PAF is an activator of COX 2 expression *in vitro* (Bazan et al, 1994) and *in vivo* (Marcheselli and Bazan, 1996), and have presented preliminary evidence that this compound inhibits light-induced COX 2 induction in the rat retina (Year 3 report). The aim of our studies, therefore, is to test the hypothesis that PAF produced during retinal light damage stimulates photoreceptor apoptosis through COX 2 overactivation.

BODY

Previous work

In previous years (years 1-3) we have used two models of light damage to rat retinas, long-term exposure to moderately-damaging light (300 lux, 6 days cycled light, or 1400 lux, 3 days of cycled light), and a short-term exposure to more intense light (7000 lux, 2 hours). In both models light was delivered from above the animals. We have performed detailed histological studies showing that our protocols induce rod photoreceptor apoptosis and cell loss with a temporal and spatial pattern characteristic of light delivered from above, with most damage occurring in the inferior-nasal quadrant of the retina. We also used western blotting and immunohistochemistry to demonstrate a light-damage induction, in the intense light model, of COX 2 and to show that the PAF antagonist BN 50730 blocked this induction.

Objectives, year 4

We aimed to expand on our previous year's work to establish a time course of light damage-induced apoptosis in the retina using the intense light model in order to define the time at which apoptosis was at its peak. Knowing this, we could then determine if BN 50730, in addition to its ability to block COX 2 induction, could also block apoptosis. In addition to TUNEL staining, we needed a second, more quantitative assessment of apoptosis to confirm our findings. For this we used an ELISA method based on the release of mono- and poly-oligosomes from nuclear chromatin to demonstrate apoptosis and the protective effects of BN 50730.

The light from above model produces a characteristic pattern of photoreceptor damage owing to the different levels of light exposure experienced by different quadrants of the retina.

Because the retina may have regional sensitivity levels to light damage (Rapp and Williams, 1980; Rapp and Smith, 1992), we wanted to compare our findings from the intense light from above model with those from retinas exposed to the same intensity of light, for the same time period, but delivered uniformly from 360°. For this we used a radial light device consisting of a horizontal stack of toroidal fluorescent tubes. Animals were inserted into the device in a transparent lucite cylinder and thus exposed to light coming from 360°. The two models were then to be used to compare data on light-induced COX 2 expression and photoreceptor apoptosis.

MATERIALS AND METHODS

Light-damage animal model:

Sprague Dawley rats, (175-200 g body weight) were kept in the LSUMC institutional animal facility for at least 24 hours after arrival from the animal nursery before experimental procedures. Animals were kept on a 12 hours light/12 hours dark cycles, with food and water *ad libitum*. When experiments were designed to test the protective effect of BN-50730 an antagonist to PAF receptors, an intra-vitreal injection of the drug or its vehicle (DMSO) in doses up to 30 μg, in 2 μl/eye.

Two light damage procedures were used in the following experiments:

- *Light from above model*: dark adapted rats, for at least 12 hours, were caged in individual compartments, and exposed to 7,000 lux of fluorescent light, for a two hours period. After light

treatment, rats were returned to cycled light (12/12 hours of dark/dim (50 lux) light). This model produces damage to a small area of the retina in the lower nasal region, allowing to use the opposite region as a control.

- *Circular light*: Under this model, animals were inserted into cylindrical cages made in acrylic , receiving light from toroidal fluorescent tubes, delivering 7,000 lux as measured at the center of the cages. Light stimulation was maintained for two hours, then rats were returned to cycled light (12/12 hours dark/dim light). This animal model is proposed to be more dramatic, producing extensive damage to the whole retina.

In experiments were designed to test the protective effect of BN-50730, the drug was dissolved in dimethyl sulfoxide (DMSO) delivered by intra-vitreal injection (Figure 3), in doses up to 30 μg, in 2 μl/eye. Controls were injected with DMSO alone. The ability of the drug to be delivered to the retina from the injection site was assessed using a small amount of blue tracer dye dissolved in DMSO (Figure 4).

At the specified times after light damage, animals were decapitated (after light ether anesthesia), the retinas were dissected from ocular tissues and either used for histology, or homogenized in the appropriate buffer for either Western blotting or apoptosis ELISA.

Western blotting:. Tissue samples were rapidly homogenized in 50 μl of lysis buffer (10 mM Tris-HCl, 10 mM EDTA, 5mM EGTA, 1 % Triton-X-100, pH 7.4. Protease inhibitors (0.1M phenyl methyl sulfonyl fluoride, 0.1TIU/ml aprotinin, and 0.1M leupeptin) were added just before use at room temperature. Homogenization was carried out with 2 ml glass/glass homogenizers until the tissue was completely disrupted. Protein concentration was measured

using a Bio-Rad assay kit and adjusted to 2 μg/μl with lysis buffer. An equal volume of 2 X concentrated electrophoresis sample buffer (250 mM Tris-HCl, pH 6.5, 2 % SDS, 10 % glycerol, 0.006 % bromophenol blue, and 10 μl/ml β-mercaptoethanol) was added to each sample, then boiled for 3 - 5 min, and loaded to a 10% SDS-polyacrylamide gel. Samples were run at 180 volts for about 40 min using Bio-Rad Protean II mini-cells. Proteins were transferred to nitrocellulose membranes (Hybond™ ECL™, Amersham, Arlington Heights, IL) using a semi-dry apparatus. Membranes were soaked overnight at 4°C with oscillation in blocking buffer (58 mM Na_2HPO_4, 17 mM NaH_2PO_4, 68 mM NaCl, 0.2% I-Block (Tropix, Bedford, MA), 0.1% Tween 20, pH 7.4), then incubated with primary antibody overnight at 25°C. Antibody dilutions were: COX 1 1/5000 (Peptide) Cat.# PG16 Oxford Biochemical Research. , or COX 2 1/2500 (Peptide) Cat.# PG26 Oxford Biochemical Research. Membranes were washed in 58 mM Na_2HPO_4, 17 mM NaH_2PO_4, 68 mM NaCl, 0.1% Tween 20, pH 7.4, and incubated with secondary antibody for 120 min at 25 °C, in a rotatory oven. Dilutions of secondary antibodies were: Anti-Mouse IgG, and Anti-Rabbit IgG, 1/10,000 dilution (IgG alkaline phosphatase conjugated) Tropix, Bedford, MA.

Enhanced chemiluminescence detection for Alkaline-phosphatase: Membranes were equilibrated in assay buffer (0.1 M diethanolamine, 1 mM $MgCl_2$, pH 10), twice for 2 min, then incubated in 5 ml of assay buffer containing 0.25 mM CSPD (Western-light™, Tropix, Bedford, MA), 1:20 Nitro-Block(Western-light™, Tropix), for 1 min then rapidly exposed to autoradiography film (Hyperfilm-ECL) or a phosphoimager plate.

Cell death detection ELISA: An ELISA assay for cell death, based on the detection of mono- and oligo-nucleosomes, was carried out using a commercially-available kit (Boehringer-Mannheim, Indianapolis, IL). Briefly, tissue samples were homogenized in a phosphate buffer containing a cocktail of protease inhibitors (0.5 mM phenylmethylsulfonyl fluoride, 2 μg/ml aprotinin, 2 μg/ml leupeptin, 2 μg/ml pepstatin (soy bean). The protein content of the samples was normalized, then samples were diluted 10 fold with a lysis buffer provided with the ELISA kit. 20μl aliquots were loaded in 96-well plates, and incubated for two hours with 80μl of incubation buffer containing the monoclonal antibodies directed against DNA and histones for detection of mono and oligo-nucleosomes. After washing away the unbound antibodies, the immunocomplex of DNA-histone-antibodies, remained bound to the streptavidin coated plates, and was detected using a horseradish peroxidase-linked secondary antibody. Quantitative analysis was performed in a Spectramax-250 96-well plate reader (Molecular Devices).

TUNEL staining: Retinas were collected, fixed in formaldehyde and embedded in paraffin. Sections (10μm thick) were then deparaffinized, processed through the TUNEL reaction with FITC-tagged dUTP using a commercially-available kit (Promega, Madison, WI) and counterstained with propidium iodide.

RESULTS

Time course of TUNEL staining in light-above model

Rats were dark adapted overnight, exposed for 2 hours to 7000 lux overhead fluorescent light, and then placed in a dark cabinet for varying times prior to sacrifice. It has been shown previously under these conditions that in a normally posturing animal the inferior-temporal quadrant of the retina demonstrates the first response to intense illumination (Figure 5). With time, damage can begin to spread towards the superior-nasal quadrant, although little or no structural damage is apparent in this region even after 8 days. Accordingly, retinas were sectioned to sample the superior-nasal quadrant (A) and portions of the inferior-temporal quadrant proximal (B) and distal (C) to the optic nerve (Figures 5 and 6). Retinas were collected 6, 12, 18, 24, 30, and 36 hours after the start of the light exposure (e.g. 6 hours = 2h light + 4h dark; 12 hours =2h light + 10h dark etc.) and sections from regions A, B, and C processed through the TUNEL staining method. Controls (0 hours) were from animals kept in the dark throughout the course of the experiment. The TUNEL (terminal deoxynucleotidyl transferase-mediated dUTP end labelling) method relies on the incorporation of FITC-tagged dUTP onto the 3' termini of nicked DNA strands. Thus the nuclei of cells undergoing the DNA fragmentation characteristic of apoptosis show as green when visualized by fluorescence microscopy. Counterstaining with propidium iodide shows all nuclei as red (Figures 2 and 3). A peak of TUNEL-stained apoptotic nuclei was observed at 18 - 24 hours and, as predicted, more damage was seen in the inferior-temporal quadrant (B and C) than in the superior-nasal quadrant (A) (Figures 7 - 29).

Inhibition of photoreceptor apoptosis by the PAF antagonist BN 50730

The peak time for the appearence of TUNEL-stained nuclei was used as a time point for testing the ability of the PAF antagonist BN 50730 to block photoreceptor apoptosis. The drug, dissolved in DMSO, was delivered intravitreally using a 36-gauge needle (Figure 3). An injection with blue dye was used to illustrate the region of drug delivery (Figure 4). Using the 24 hour time point (2 hours light + 22 hours dark), while the inferior-nasal section of the retina of light-treated animals showed many TUNEL-stained nuclei (Figure 30), retinas from drug-treated and dark-control animals showed virtually no stained nuclei (Figures 31 and 32). This showed that the drug was protective against light-induced nuclear DNA nicking, and implies a role for PAF in light-induced photoreceptor apoptosis.

In a number of experimental systems it has become apparent to ourselves and other investigators that not all cells that display one or more of the hallmarks of apoptosis (e.g. TUNEL staining, expression of nuclear "apoptotic" antigens) are genuinely apoptotic. For this reason, multiple criteria are often required to confirm the progression of the apoptotic cascade. We had previously shown that the light-damage model induces laddering of nuclear DNA (year 2). Since we carried out those investigations, an assay kit has become commercially available which detects and quantifies mono- and oligo-nucleosomes released from nuclear chromatin. This ELISA-based method complements DNA laddering in that both techniques are based on the specific cleavage of inter-nucleosomal stretches of DNA that is characteristic of apoptotic, but not necrotic cell death. The ELISA method showed a strong induction by bright light of apoptosis in the inferior-nasal quadrant of the retina, with a 170±28-fold increase in nucleosome release by

30 hours (Figure 33).

Comparison of light-above and circular light models: COX 2 induction and apoptosis.

In the light-above model, COX 2 is induced most dramatically in the inferior half of the retina (Figure 34a), correlating with the region that subsequently displays the greatest photoreceptor loss. This induction is inhibited by pretreatment via intravitreal injection with the PAF receptor antagonist BN 50730. Interestingly, another type of PAF receptor antagonist, BN 52021 does not inhibit (Figure 34b). In brain the two PAF antagonists have been shown to be selective for different PAF binding activities, BN 50730 for a microsomal site and BN 52021 for a synaptosomal site (Marcheselli et al, 1990, 1994). Furthermore, BN 50730 has been shown to inhibit COX 2 transcriptional activity induced by PAF *in vitro* (Bazan et al, 1994), and by experimental seizures *in vivo* (Marcheselli and Bazan, 1996).

Using the circular light model, which we had anticipated would produce more severe damage to the retina, we were surprised to find that COX 2 induction was less than in the light above model. Whereas the increase in COX 2 protein in the light-above model (lower half) of the retina was 4.51±1.76 fold (Figure 34a), in the circular light model this was only 1.63±0.27 fold (Figure 35). The difference in COX 2 induction was more than matched by a lower release of nucleosomes in the circular light model (3.7±1.5-fold versus 170±28-fold increase in the light above model) (Figure 36). BN 50730 was able to inhibit both COX 2 induction and nucleosome release in the circular light model.

CONCLUSIONS

- Damage to the rat retina using the light from above model produces a characteristic pattern of TUNEL-stained apoptotic nuclei, more intense in the inferior-nasal quadrant, and peaking at 18-24 hours after the start of a 2-hour 7000 lux light exposure. An ELISA assay for apoptosis, based on the release from chromatin of mono- and oligo-nucleosomes shows a steadily-increasing release of nucleosomes up to 30 hours after the light insult. BN 50730 was shown to be protective against light damage induced apoptosis in this model as assessed by TUNEL staining. These findings imply a role for PAF in light-induced photoreceptor apoptosis, and indicate that PAF antagonists may be useful in preventing or treating retinal damage resulting from exposure to bright light.

- Surprisingly, a model in which light of the same intensity and duration as used in the light from above model is delivered from 360° (circular light model) failed to induce as much photoreceptor apoptosis or COX 2 induction. We have yet to further determine, using histological studies, whether this is evidence of a topographic distribution of sensitive rod photoreceptors in the rat retina, as has been suggested in other studies (Rapp and Williams, 1980; Rapp and Smith, 1992). If this were the case, then by using whole retinas for Western blotting and ELISA, large inductions of either COX 2 protein or apoptosis in small regions of the retina might be diluted out by the relative unresponsiveness of the remainder of the tissue.

- We have provided evidence, based on the protective effects of the PAF receptor antagonist BN 50730, that PAF is involved in the light-induction of COX 2, and in light-induced photoreceptor

apoptosis. Further experiments are needed to establish if PAF-mediated COX 2 induction represents a step in the photoreceptor apoptotic cascade, and thus a potential target for light damage protective strategies.

REFERENCES.

Bazan NG, Fletcher BS, Herschman HR, Mukherjee PK. 1994. Platelet-activating factor and retinoic acid synergistically activate the inducible prostaglandin synthase gene. Proc. Natl. Acad. Sci. USA. 91: 5252-5256.

Bazan NG, Allan G, Marcheselli VL. 1996. in "Improved Non-steroid Anti-inflammatory Drugs; COX-2 Enzyme Inhibitors", Edited by Sir John Vane, L. Botting and R. Botting, pp. 145-166

Coffey RJ. Hawkey CJ. Damstrup L. Graves-Deal R. Daniel VC. Dempsey PJ. Chinery R. Kirkland SC. DuBois RN. Jetton TL. Morrow JD. 1997. Epidermal growth factor receptor activation induces nuclear targeting of cyclooxygenase-2, basolateral release of prostaglandins, and mitogenesis in polarizing colon cancer cells. Proc. Natl. Acad. Sci. USA. 94: 657-662.

DeWitt DS, Smith WL. 1995. But do they still get headaches? Cell. 83: 354-348

Herschman HR. 1996. Prostaglandin synthase 2. Biochimica et Biophysica Acta. 1299: 125-140.

Kaufmann WE, Worley PF, Pegg J, Bremer M, Isakson P. 1996. COX-2, a synaptically induced enzyme, is expressed by excitatory neurons at postsynaptic sites in rat cerebral cortex. Proc. Natl. Acad. Sci. USA. 93: 2317-2321.

Marcheselli VL, Rossowska MJ, Domingo MT, Braquet P, Bazan NG. 1990. Distinct platelet-activating factor binding sites in synaptic endings and in intracellular membranes of rat cerebral cortex. J. Biol. Chem. 265: 9140-9145.

Marcheselli VL, Bazan NG. 1994. Platelet-activating factor is a messenger in the electroconvulsive shock-induced transcriptional activation of c-fos and zif-268 in hippocampus. J. Neurosci. Res. 37: 54-61.

Marcheselli VL, Bazan NG. 1996. Sustained induction of prostaglandin endoperoxide synthase-2 by seizures in hippocampus. Inhibition by a platelet-activating factor antagonist. J. Biol. Chem. 271: 24794-24799.

Miettinen S, Fusco FR, Yrjanheikki J, Keinanen R, Hirvonen T, Roivainen R, Narhi M, Hokfelt T, Koistinaho J. 1997 Spreading depression and focal brain ischemia induce cyclooxygenase-2 in cortical neurons through N-methyl-D-aspartic acid-receptors and phospholipase A_2. Proc. Natl. Acad. Sci. USA. 94: 6500-6505.

Morita I, Schindler M, Regier MK, Otto JC, Hori T, DeWitt DL, Smith WL. 1995. Different intracellular locations for prostaglandin endoperoxide H synthase-1 and -2. J. Biol. Chem. 270: 10902-10908.

Oberhammer F, Wilson JW, Dive C, Morris ID, Wakeling AE, Walker PR. Sikorska M. 1993

Apoptotic death in epithelial cells: cleavage of DNA to 300 and/or 50 kb fragments prior to or in the absence of internucleosomal fragmentation. EMBO J. 12: 3679-3684.

Pollard H, Charriaut-Marlangue C, Cantagrel S, Represa A, Robain O, Moreau J, Ben-Ari Y. 1994. Kainate-induced apoptotic cell death in hippocampal neurons. Neuroscience. 63: 7-18.

Rapp LM, Williams TP. 1980. A parametric study of retinal light damage in albino and pigmented rats. In: The Effects of Constant Light on Visual Processes (Eds. Williams TP, Baker BN.) Plenum, New York, NY. pp 135-159.

Rapp LM, Smith SC. 1992. Morphologic comparisons between rhodopsin-mediated and short wavelenght classes of retinal light damage. Inv. Ophth. Vis. Sci. 33: 3367-3377.

Rapp LM. 1995. Retinal phototoxicity. In: Handbook of Neurotoxicology. (Chang LW, Dyer RS eds) Marcel Dekker: New York, NY. pp 963-1003

White E 1996 Life, death, and the pursuit of apoptosis. Genes & Dev. 10: 1-15.

Wyllie AH, Kerr JFR, Currie AR. Cell death: the significance of apoptosis. Int. Rev. Cytol. 68: 251-306.

Yamagata K, Andreasson KI, Kaufmann WE, Barnes CA, Worley PF. 1993 Expression of a

mitogen-inducible cyclooxygenase in brain neurons: regulation by synaptic activity and glucocorticoids. Neuron. 11: 371-386.

Figure 1

Diagram of the light from above light damage apparatus.

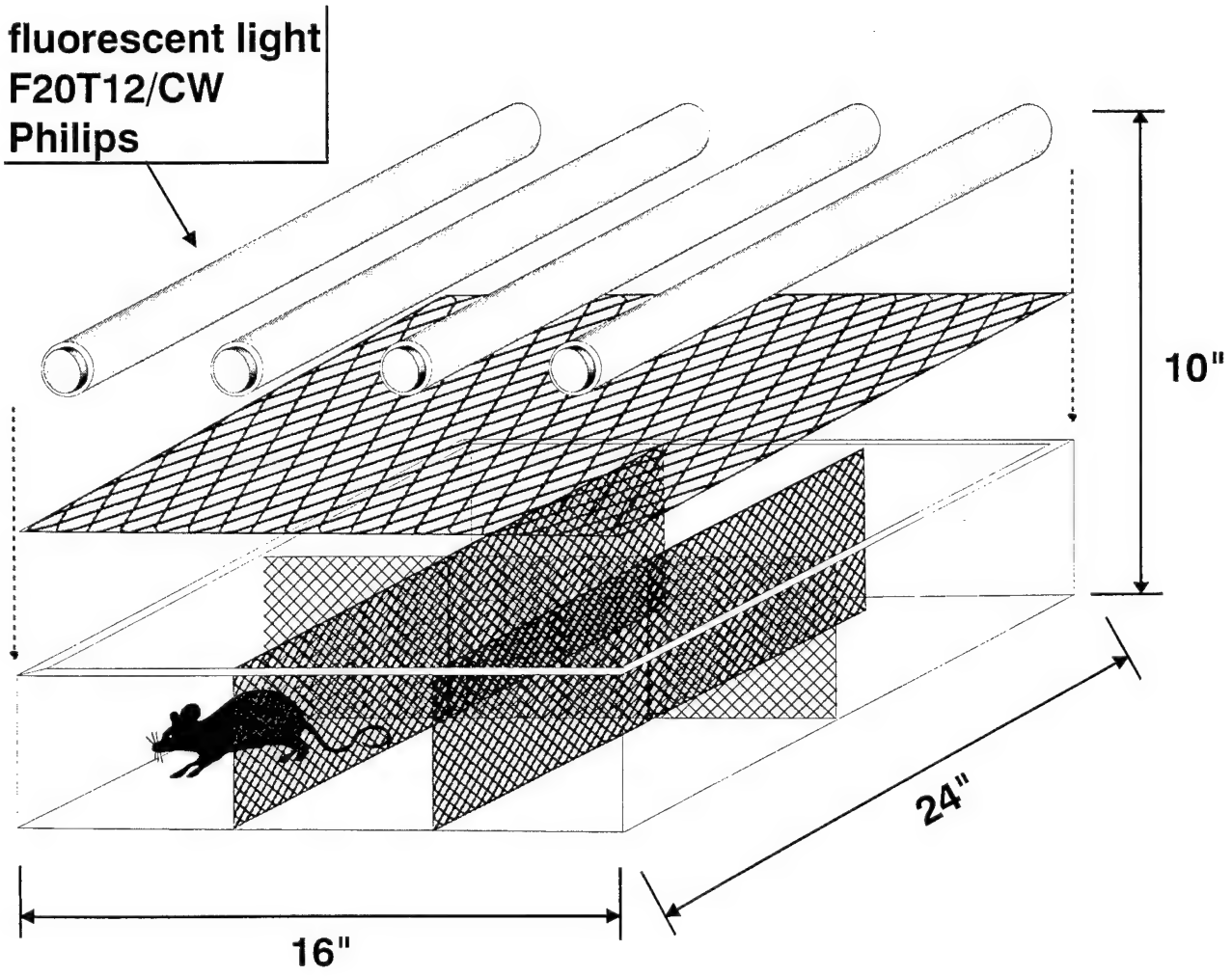
fluorescent light
F20T12/CW
Philips
10"
24"
16"

Figure 2

Diagram of the circular light light damage apparatus.

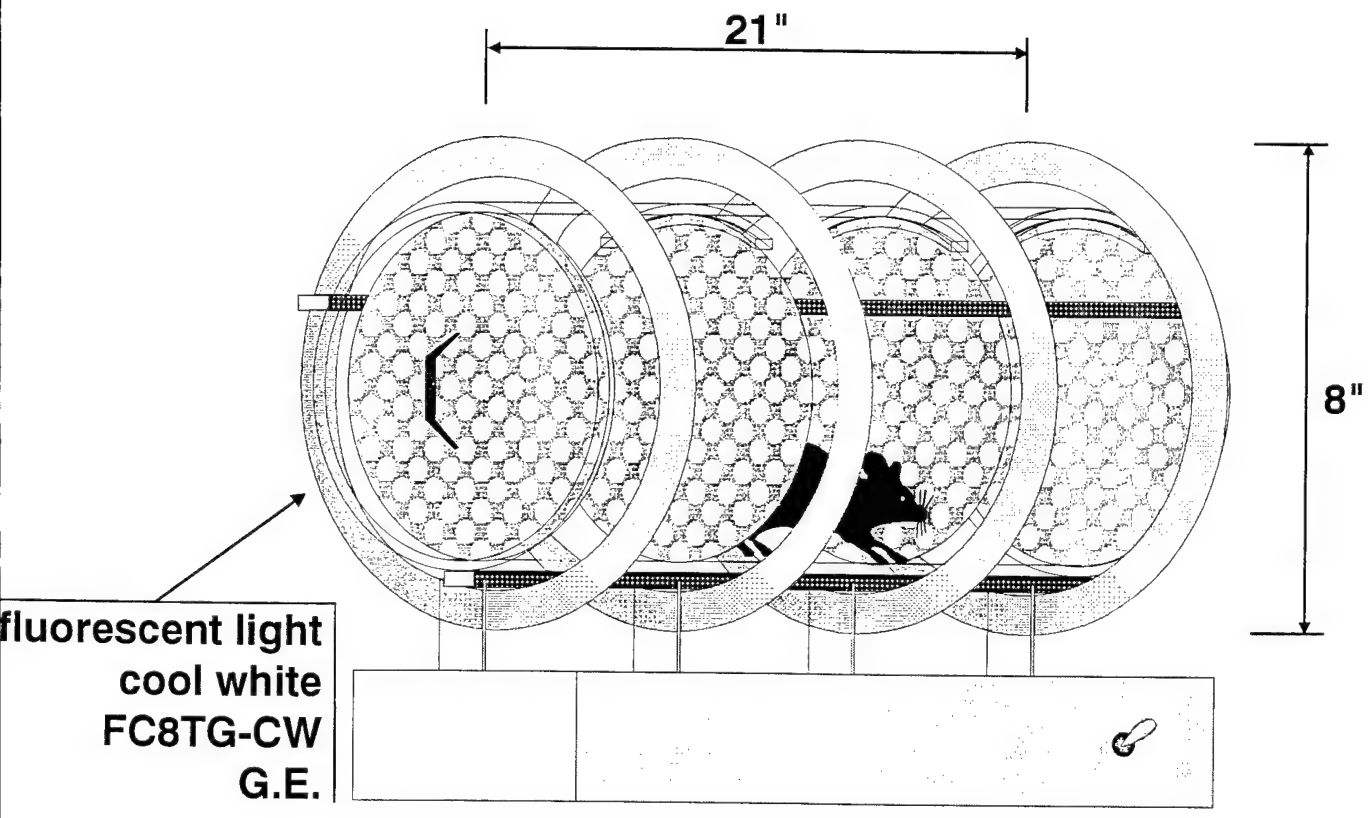
21"
8"
fluorescent light
cool white
FC8TG-CW
G.E.

Figure 3

This hemisected eye shows the method of delivering the drug and the carrier compound. A fine needle (36 gauge) was fitted with a tube that would act as a stop to insure that the depth of the injection was constant. Cornea is up, nasal edge of eye is to the right.

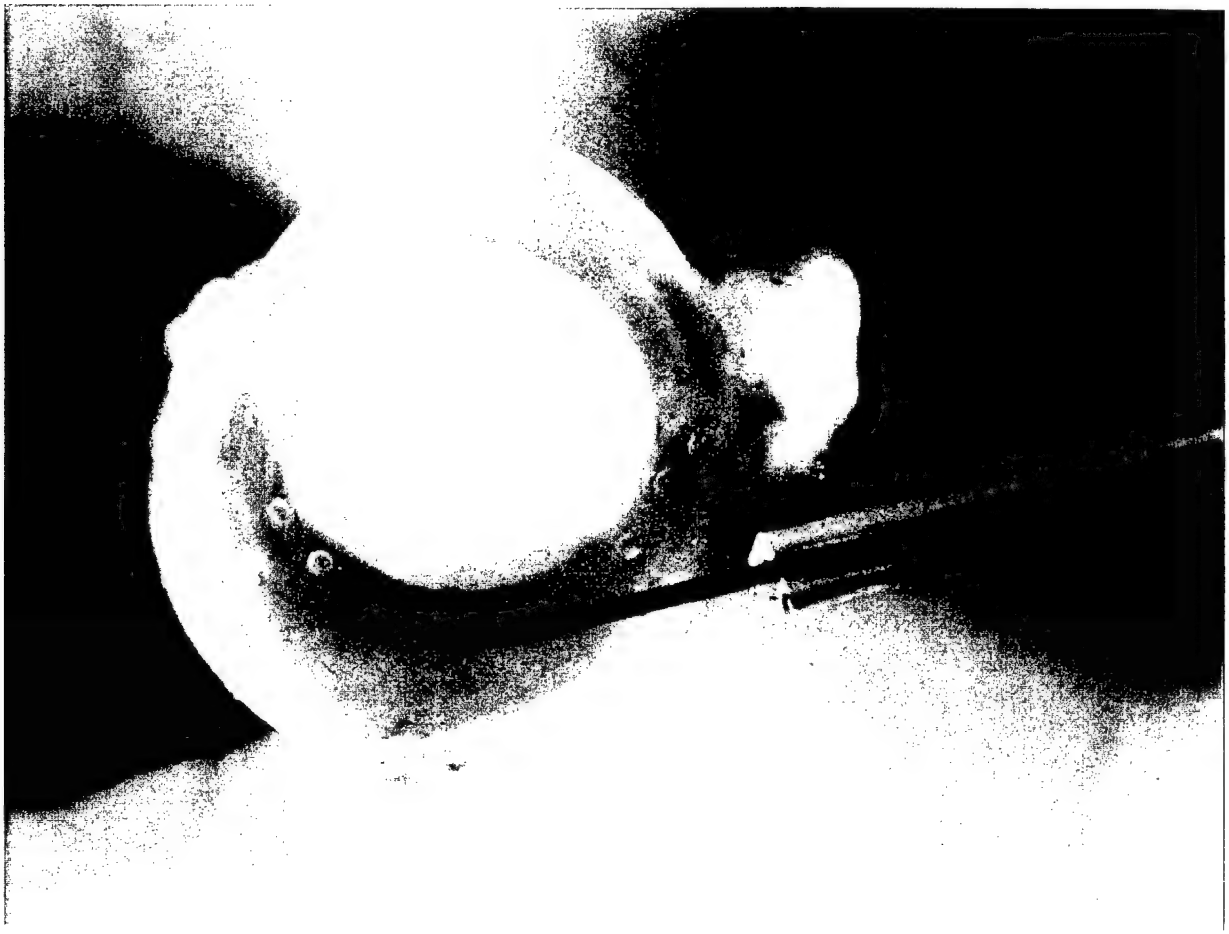

Figure 4

This hemisected eye illustrates the region of drug delivery within the eye during injection. To illustrate, a small amount of blue dye was injected into the eye prior to removal and dissection.

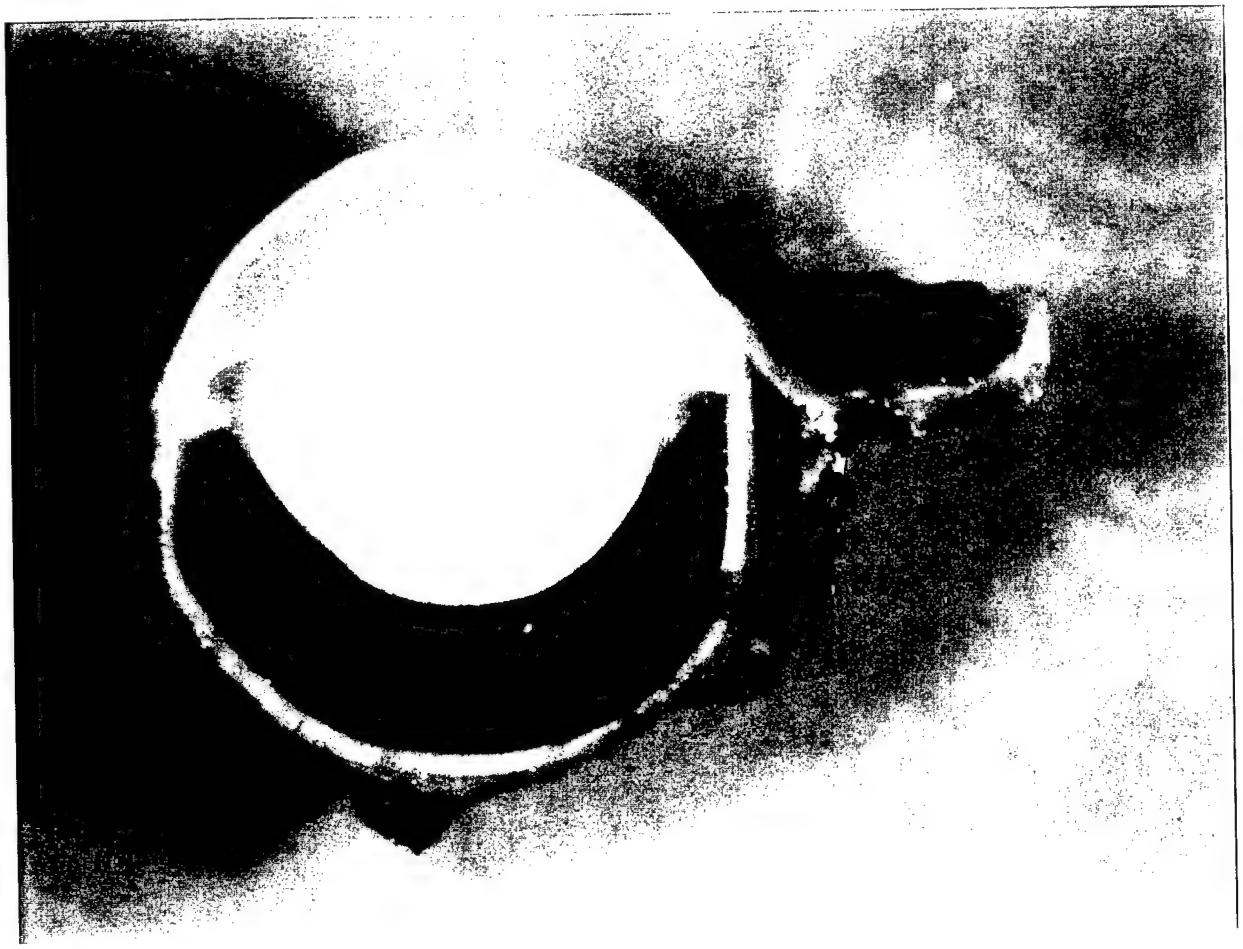

Figure 5

Area of light damage of retina after 2 hours light from above (7000 lux) plus 16 hours darkness.

Images were obtained by sectioning retinas diagonally through this region.

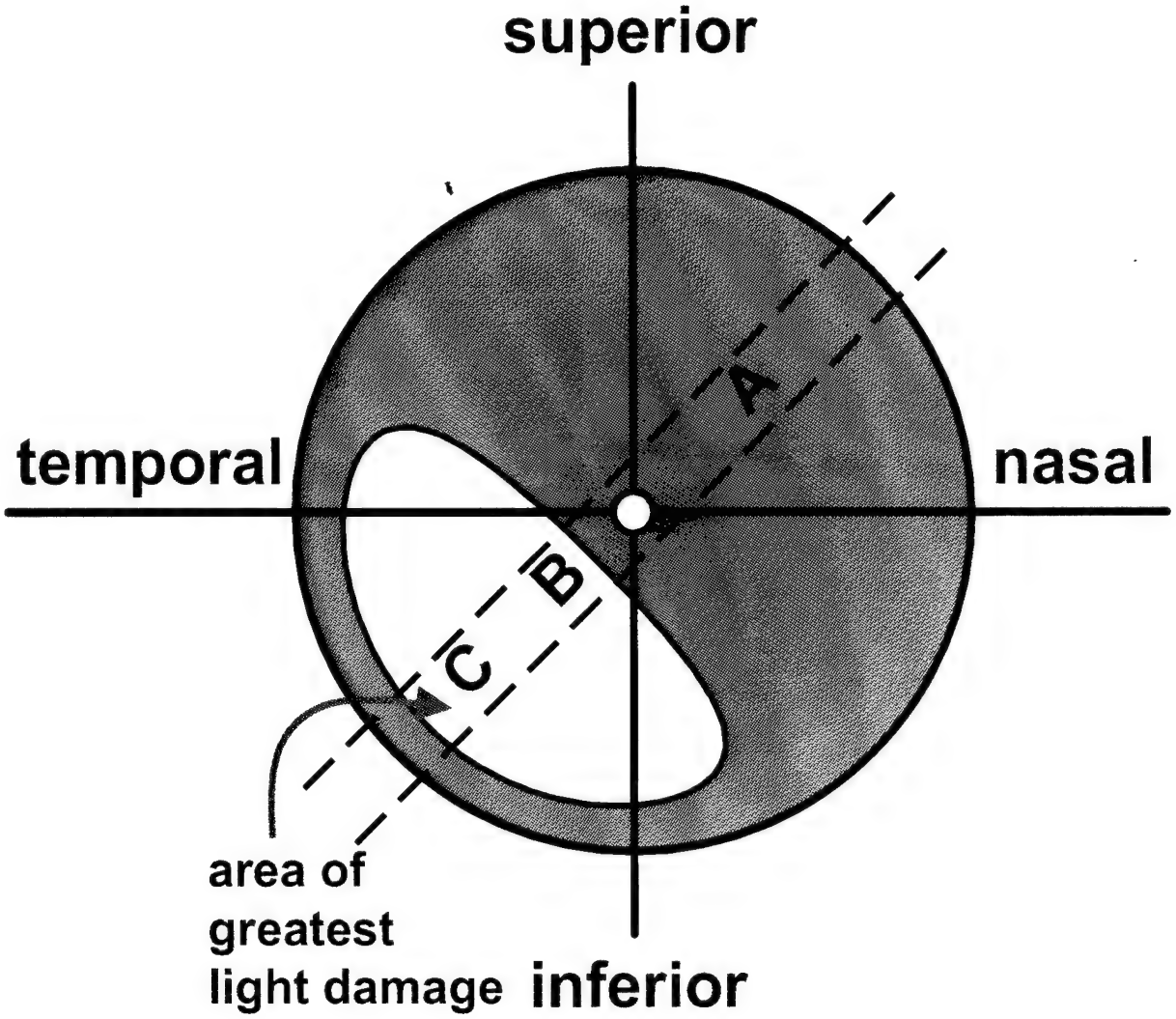
superior
temporal
nasal
A
B
C
area of
greatest
light damage
inferior

Figure 6

Illustration to show the regions of interest within a diagonal retinal section. A represents the nonstimulated "dark" half in the upper quadrant, while B and C represent two regions within the damaged area of the lower quadrant. In all following images (Figures 7-29), the sections were obtained from retinas that had been stimulated for 2 hours (7000 lux) followed by a variable amount of darkness (4-34 hours).

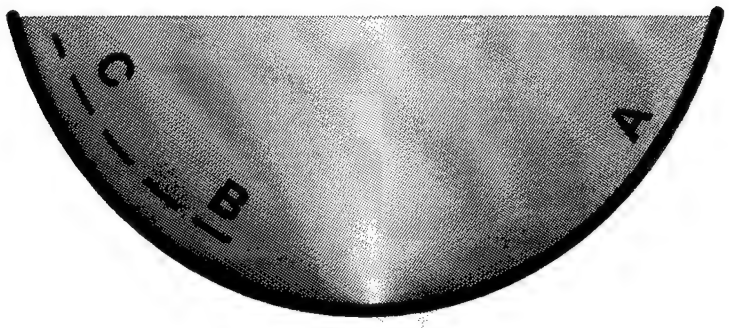
C
B
A

Figure 7

Typical pattern of TUNEL labeling showing photoreceptor cell nuclei with fragmented DNA (yellow spheres). Some DNA has already begun to bleb appearing as small fragments. Rod outer segments are green and pointing upward. Counter stained with propidium iodide (red fluorescence) to label all retinal nuclei. 200x

Figure 8

Higher power image illustrating the beginning of TUNEL labeling. As the endonucleases begin to enter the nucleus, they react first with the peripheral DNA, producing a ring or halo just inside the nucleus. As they move deeper, the entire nucleus lights up, followed by some fragmentation and blebbing. 400 x

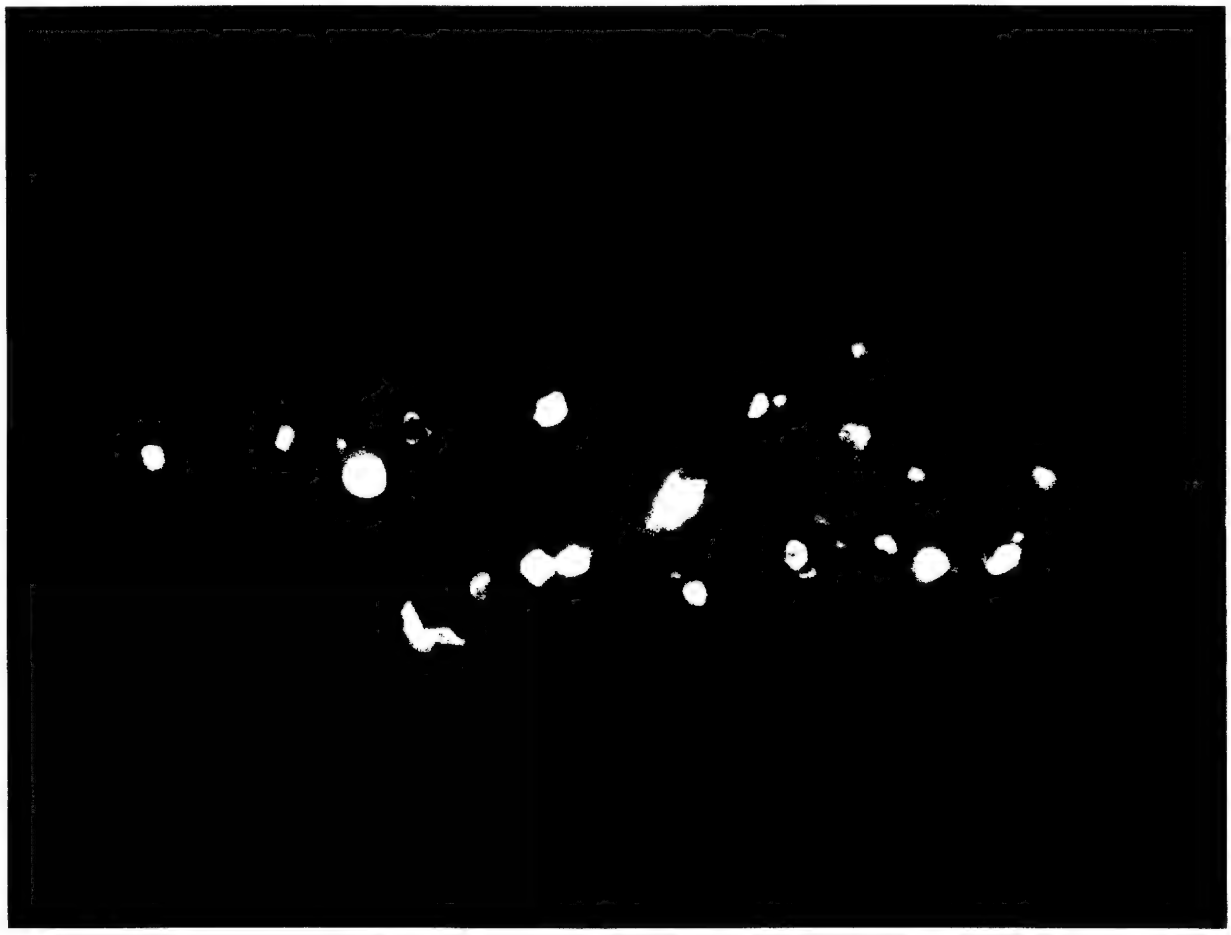

Figure 9

Time course of light induced photoreceptor apoptosis, demonstrated with FITC-12-dUTP (TUNEL). Area A; 0 hours light.

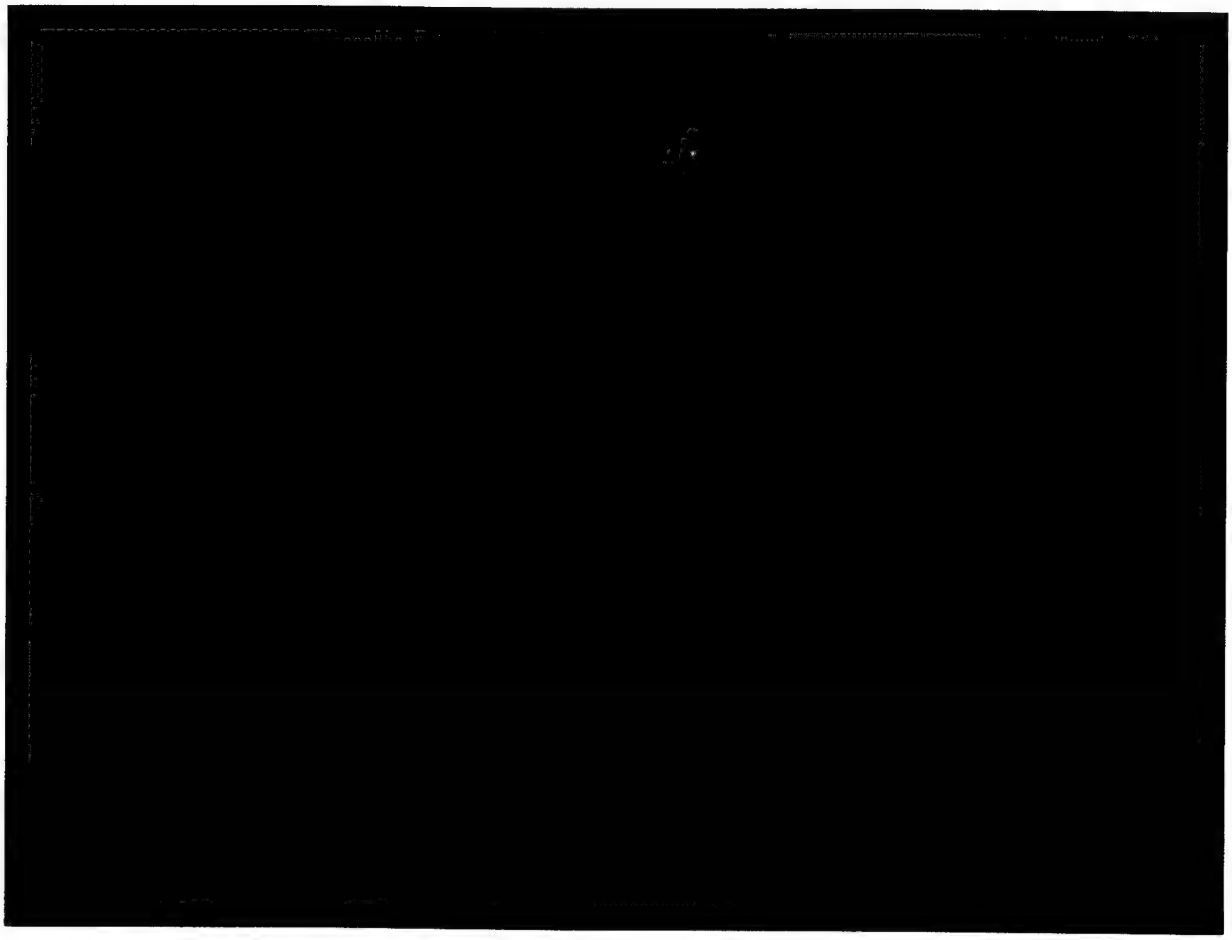

Figure 10

Time course of light induced photoreceptor apoptosis, demonstrated with FITC-12-dUTP (TUNEL). Area B; 0 hours light.

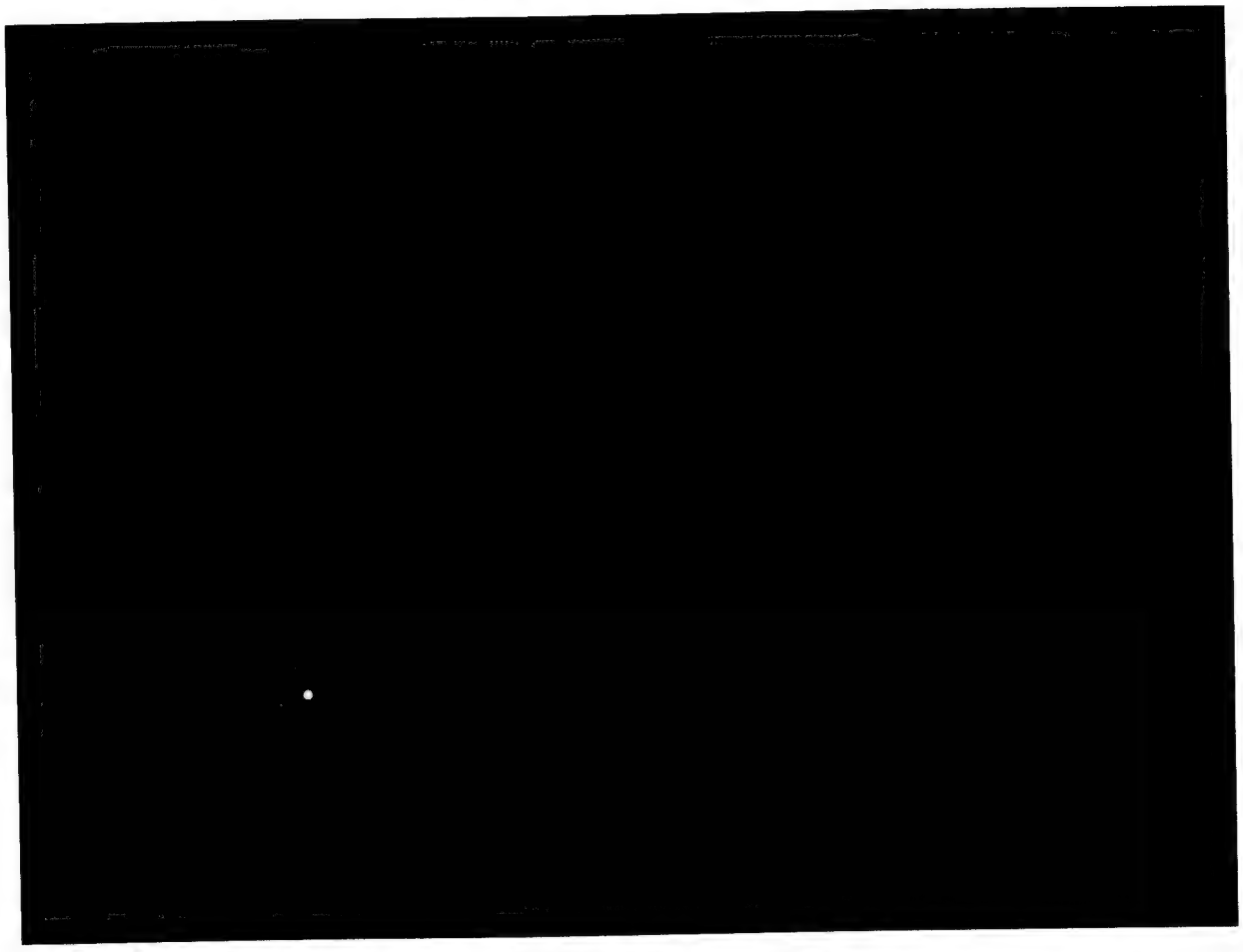

Figure 11.

Time course of light induced photoreceptor apoptosis, demonstrated with FITC-12-dUTP (TUNEL). Area C; 0 hours light.

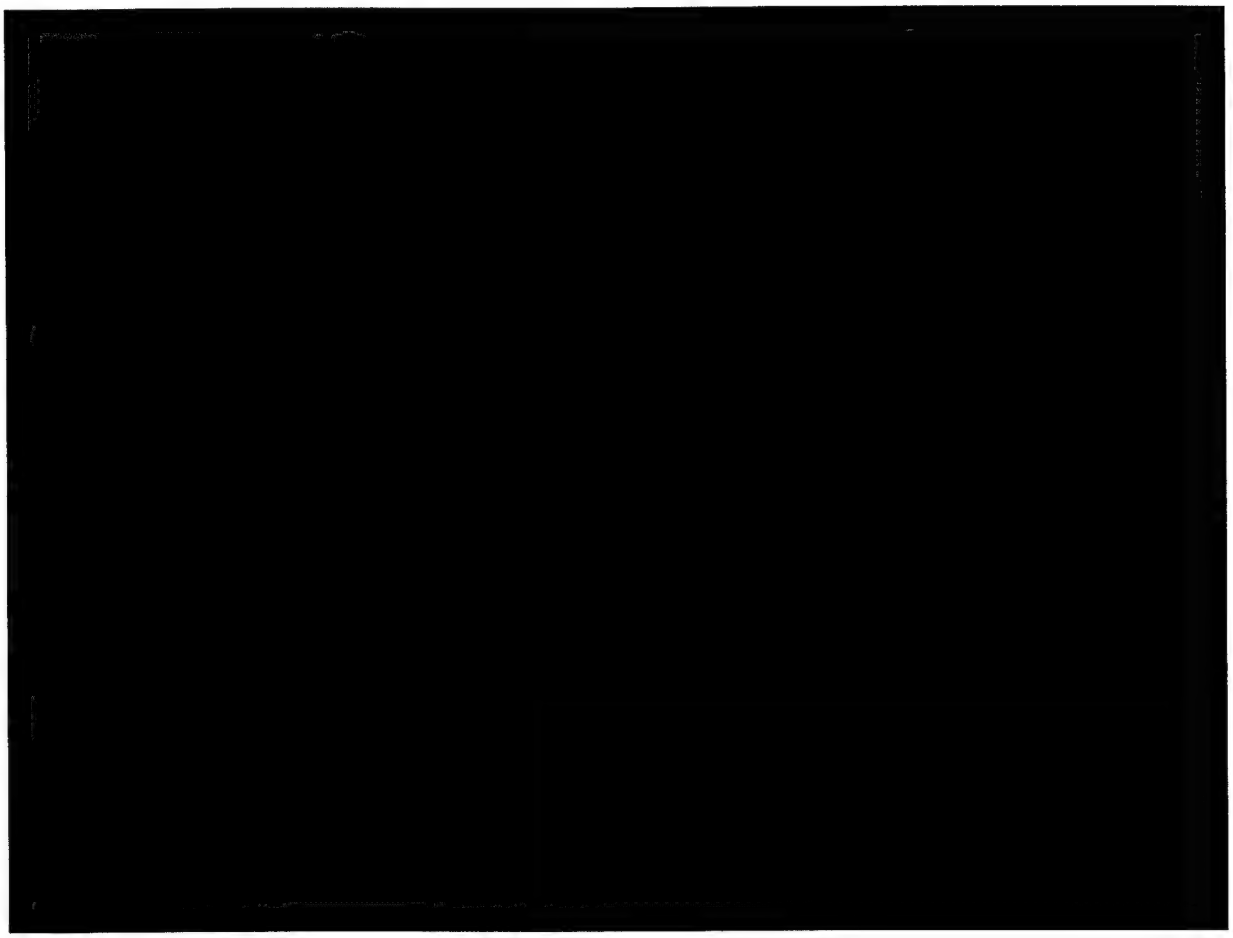

Figure 12.

Time course of light induced photoreceptor apoptosis, demonstrated with FITC-12-dUTP (TUNEL). Area A; 2 hours light plus 4 hours dark.

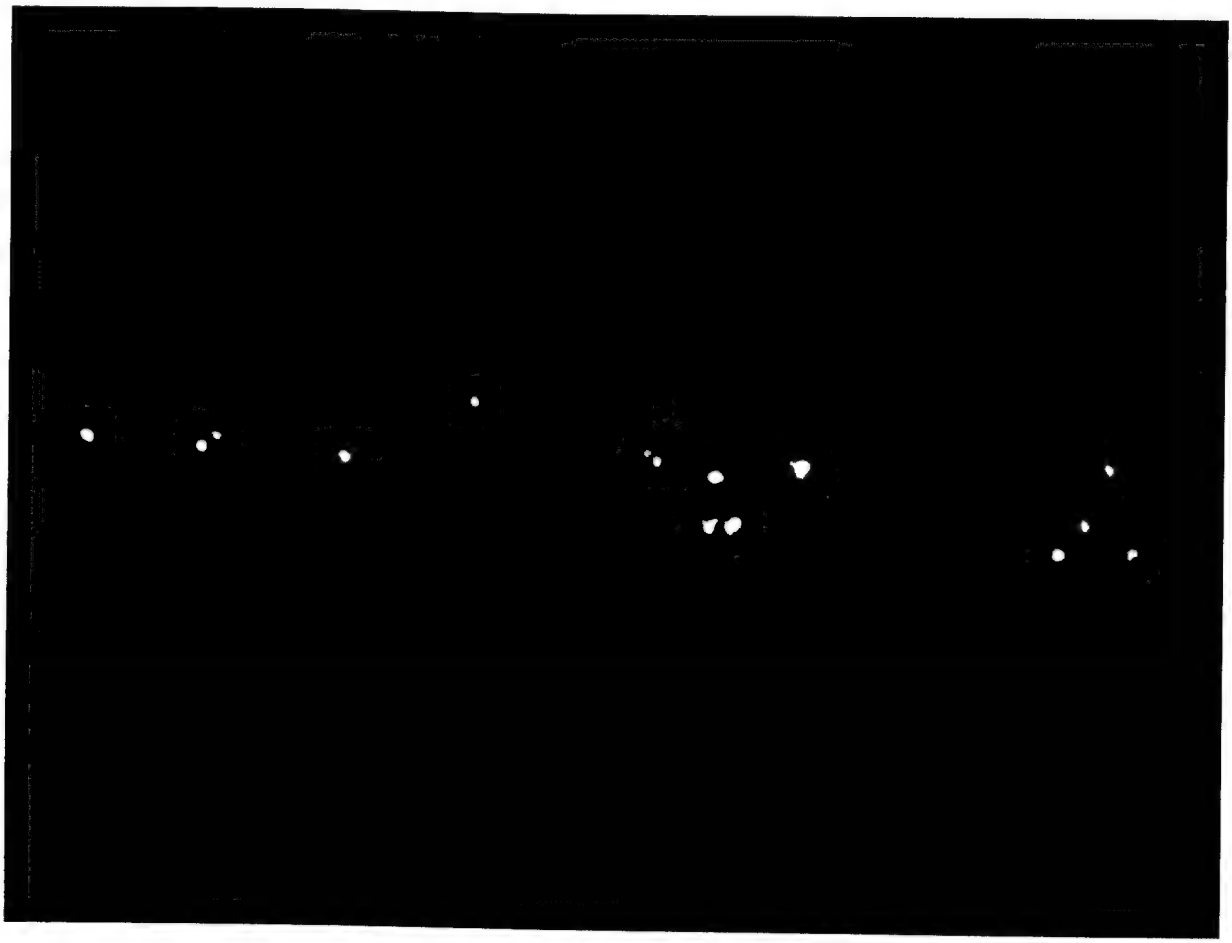

Figure 13.

Time course of light induced photoreceptor apoptosis, demonstrated with FITC-12-dUTP (TUNEL). Area B; 2 hours light plus 4 hours dark.

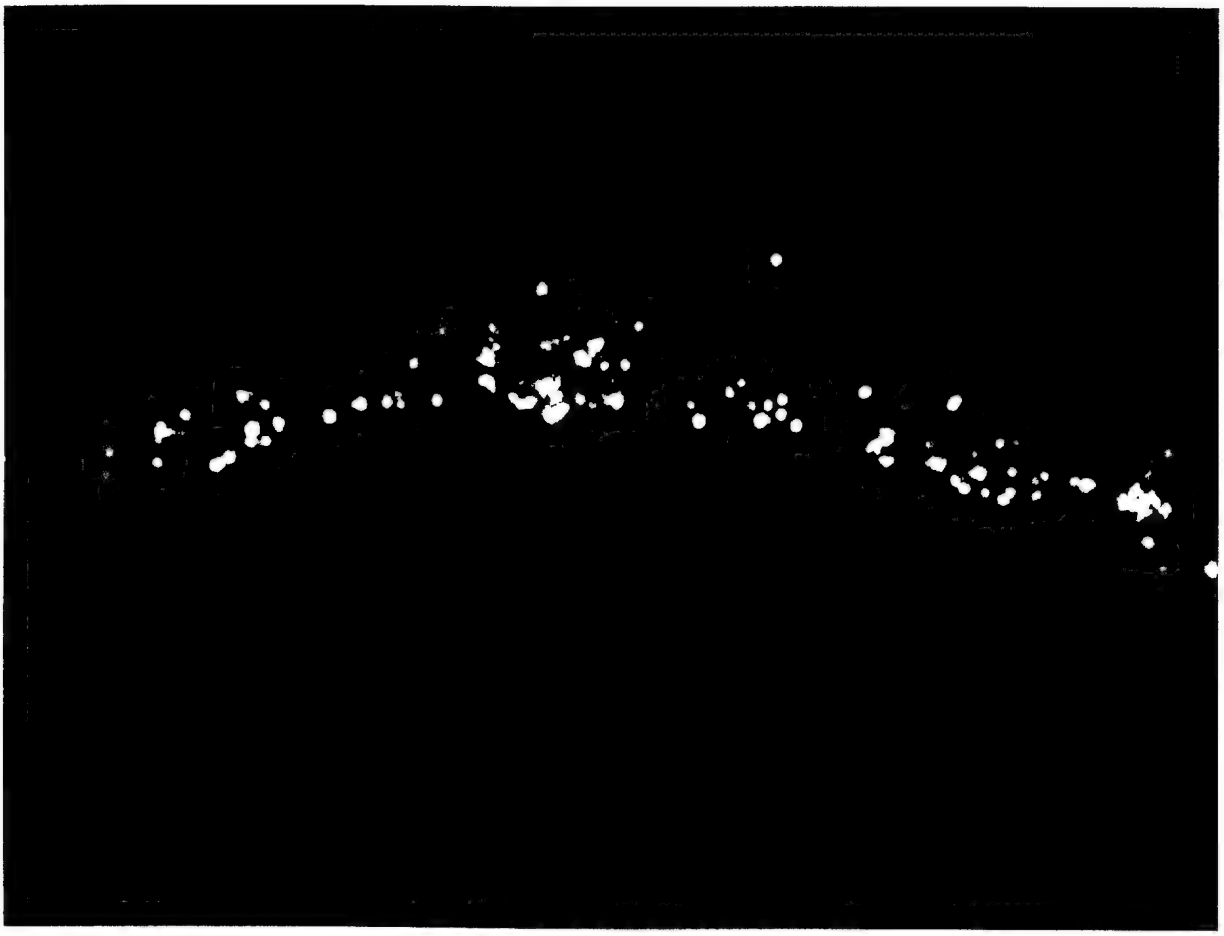

Figure 14.

Time course of light induced photoreceptor apoptosis, demonstrated with FITC-12-dUTP (TUNEL). Area C; 2 hours light plus 4 hours dark.

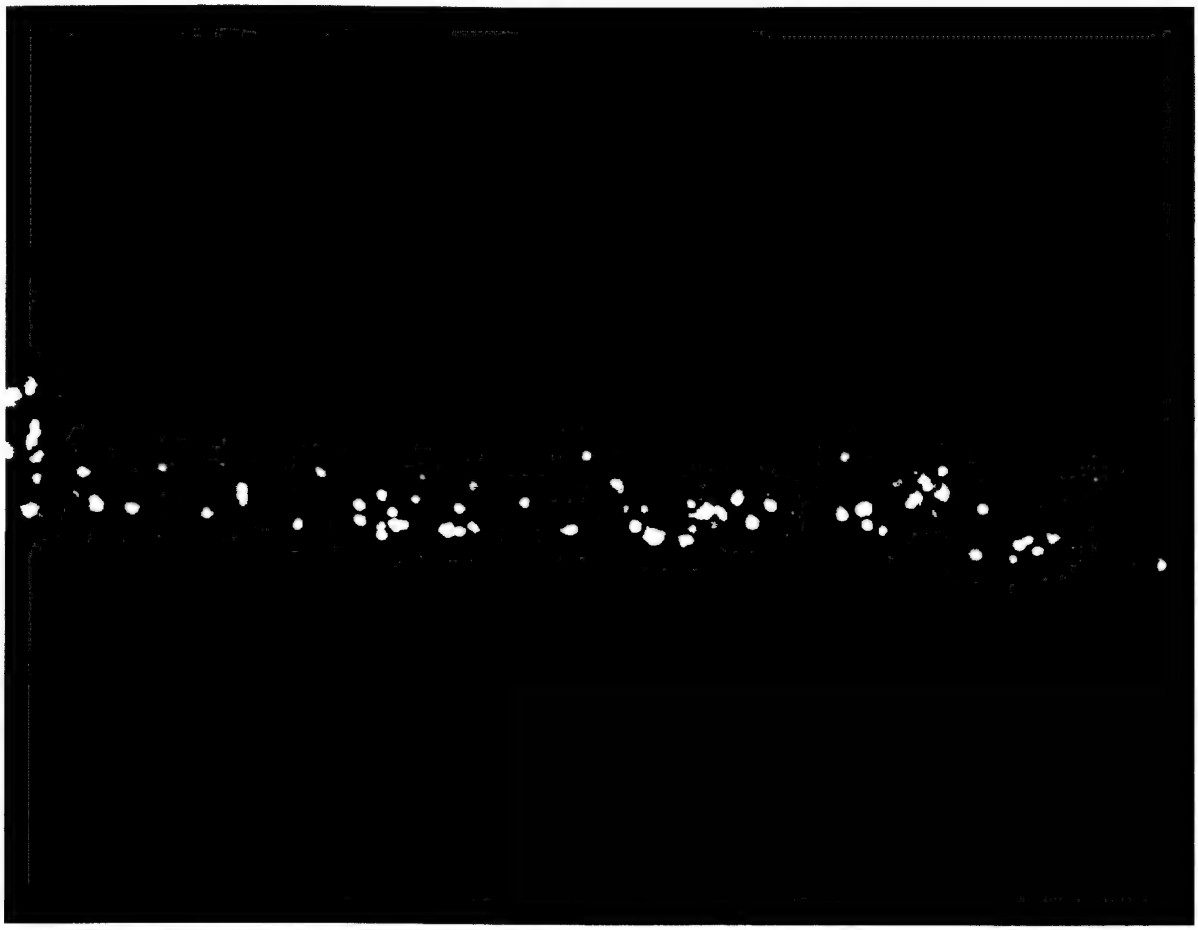

Figure 15.

Time course of light induced photoreceptor apoptosis, demonstrated with FITC-12-dUTP (TUNEL). Area A; 2 hours light plus 10 hours dark.

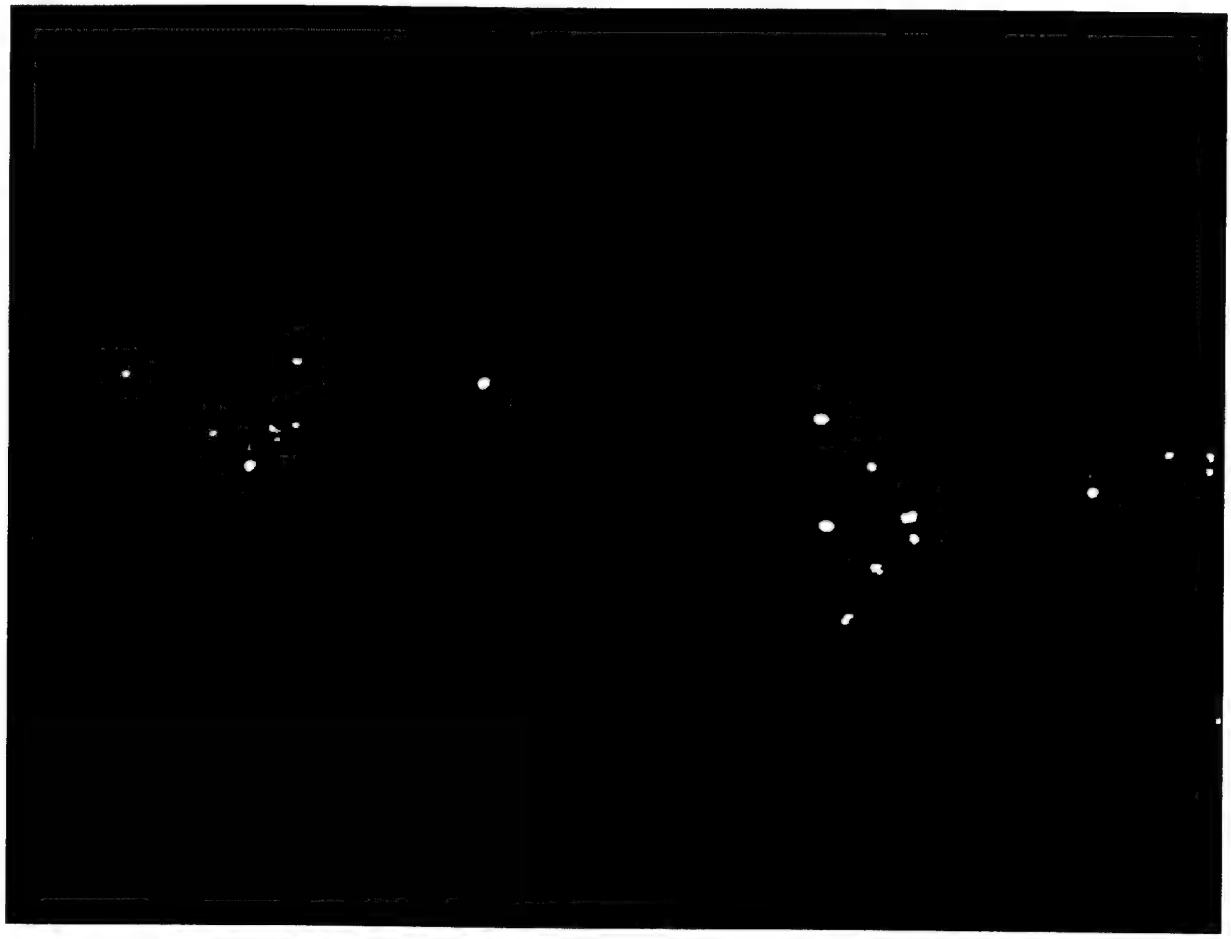

Figure 16.

Time course of light induced photoreceptor apoptosis, demonstrated with FITC-12-dUTP (TUNEL). Area B; 2 hours light plus 10 hours dark.

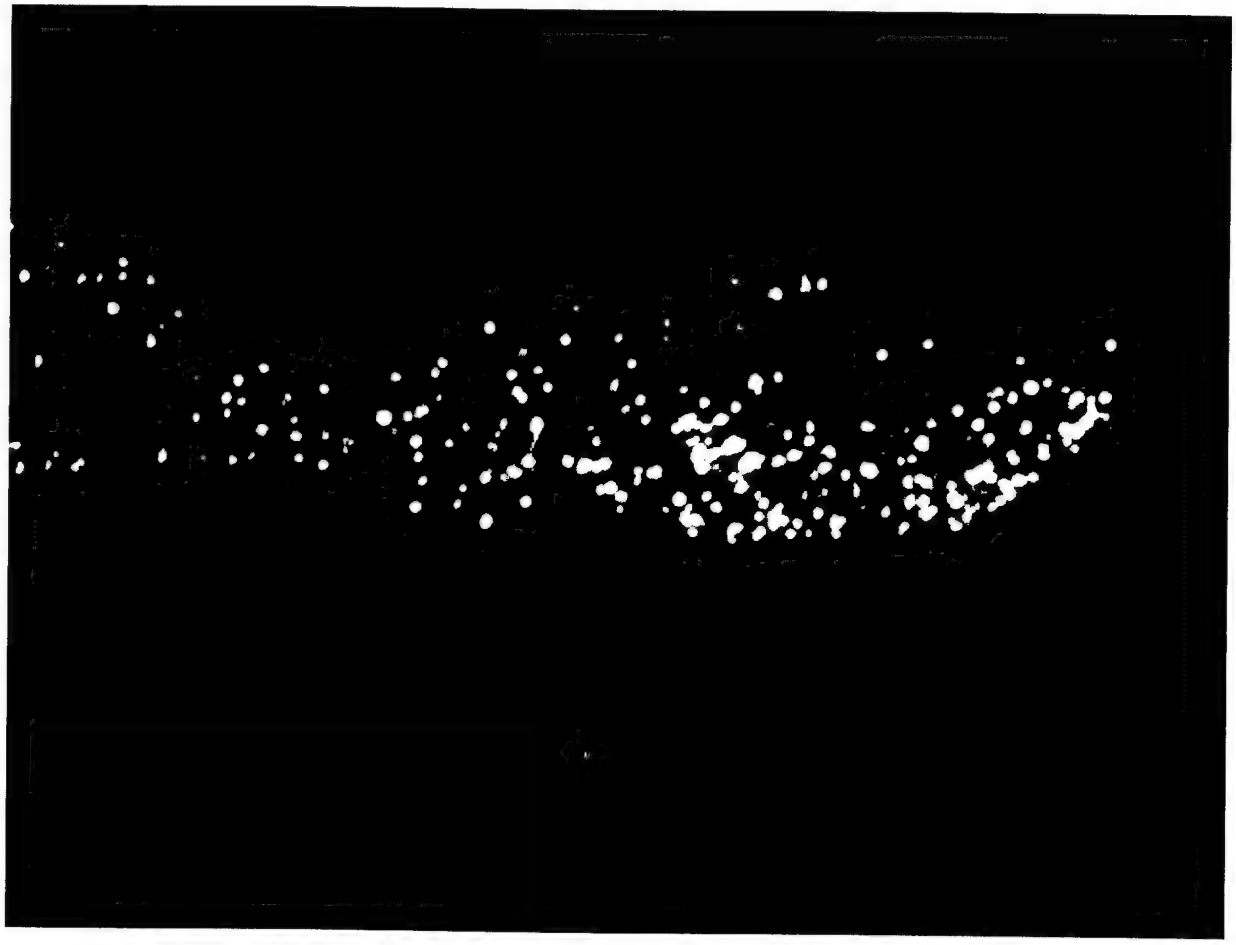

Figure 17.

Time course of light induced photoreceptor apoptosis, demonstrated with FITC-12-dUTP (TUNEL). Area C; 2 hours light plus 10 hours dark.

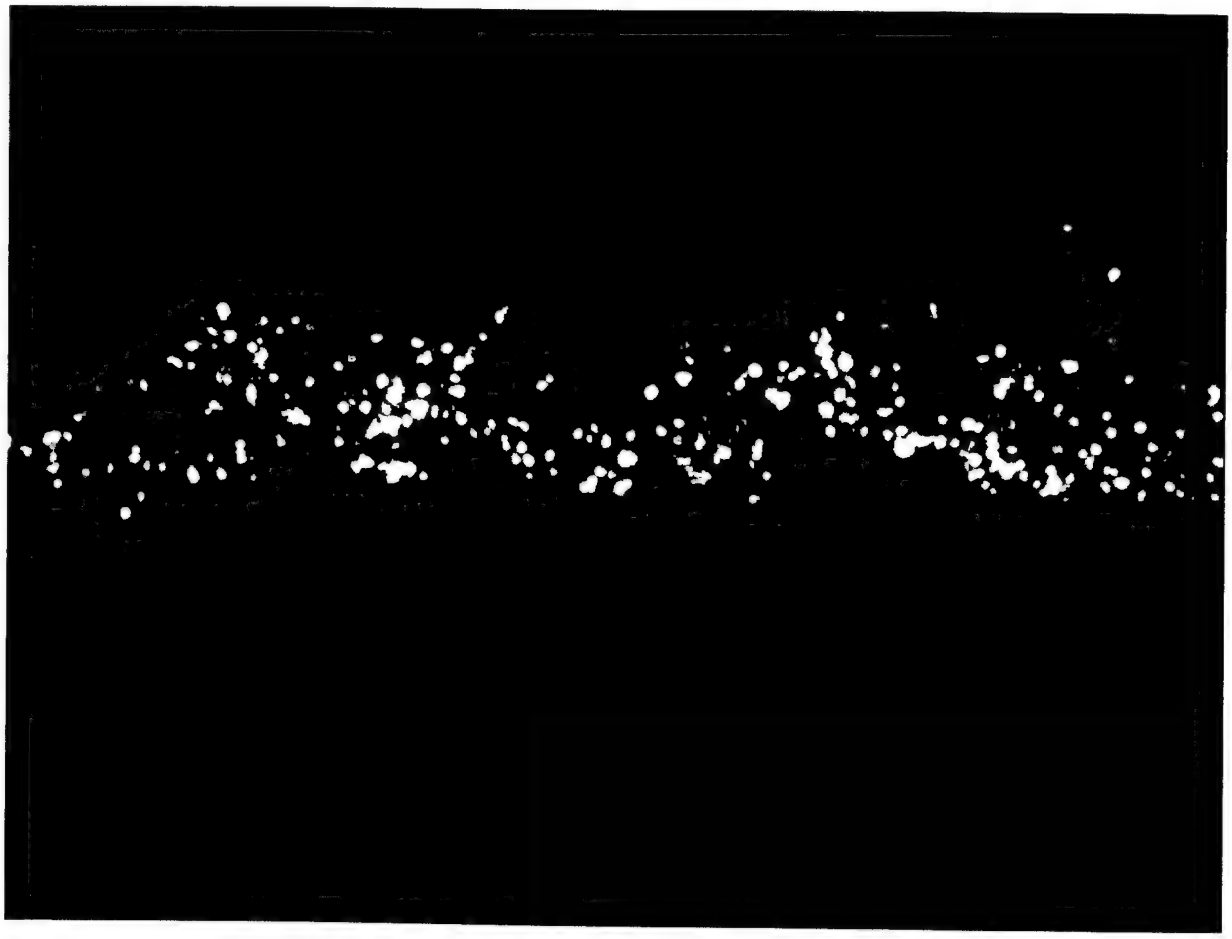

Figure 18.

Time course of light induced photoreceptor apoptosis, demonstrated with FITC-12-dUTP (TUNEL). Area A; 2 hours light plus 16 hours dark.

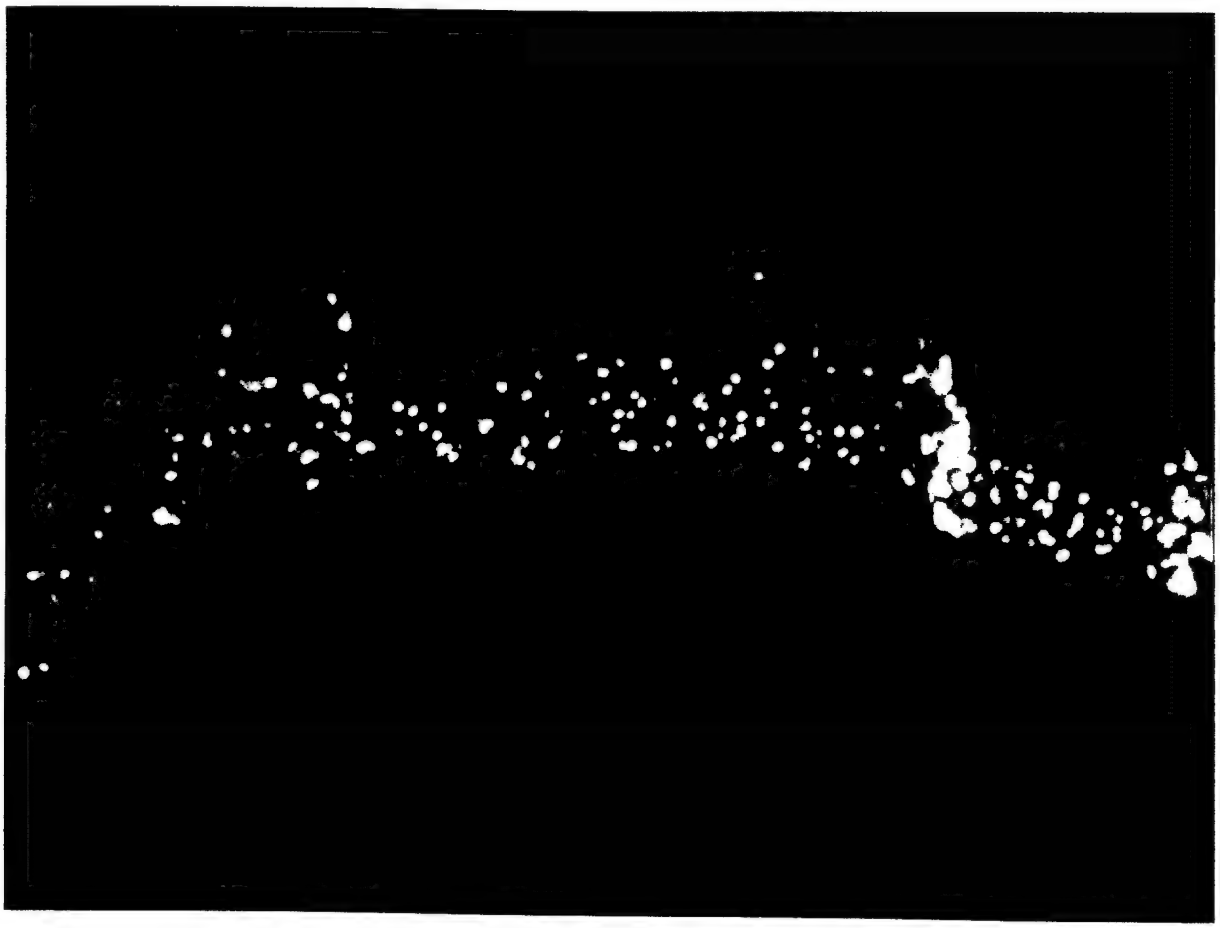

Figure 19.

Time course of light induced photoreceptor apoptosis, demonstrated with FITC-12-dUTP (TUNEL). Area B; 2 hours light plus 16 hours dark.

Figure 20.

Time course of light induced photoreceptor apoptosis, demonstrated with FITC-12-dUTP (TUNEL). Area C; 2 hours light plus 16 hours dark.

Figure 21.

Time course of light induced photoreceptor apoptosis, demonstrated with FITC-12-dUTP (TUNEL). Area A; 2 hours light plus 22 hours dark.

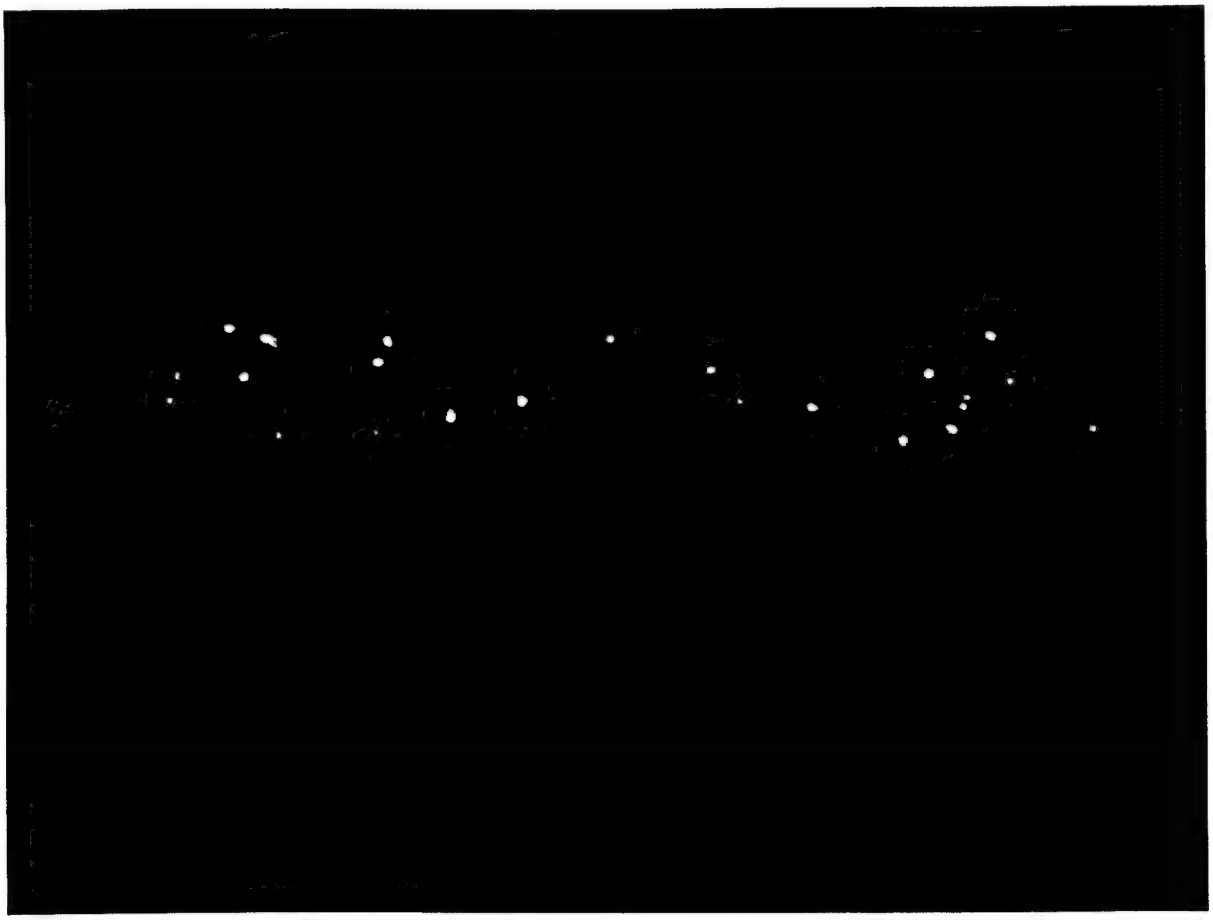

Figure 22.

Time course of light induced photoreceptor apoptosis, demonstrated with FITC-12-dUTP (TUNEL). Area B; 2 hours light plus 22 hours dark.

Figure 23.

Time course of light induced photoreceptor apoptosis, demonstrated with FITC-12-dUTP (TUNEL). Area C; 2 hours light plus 22 hours dark.

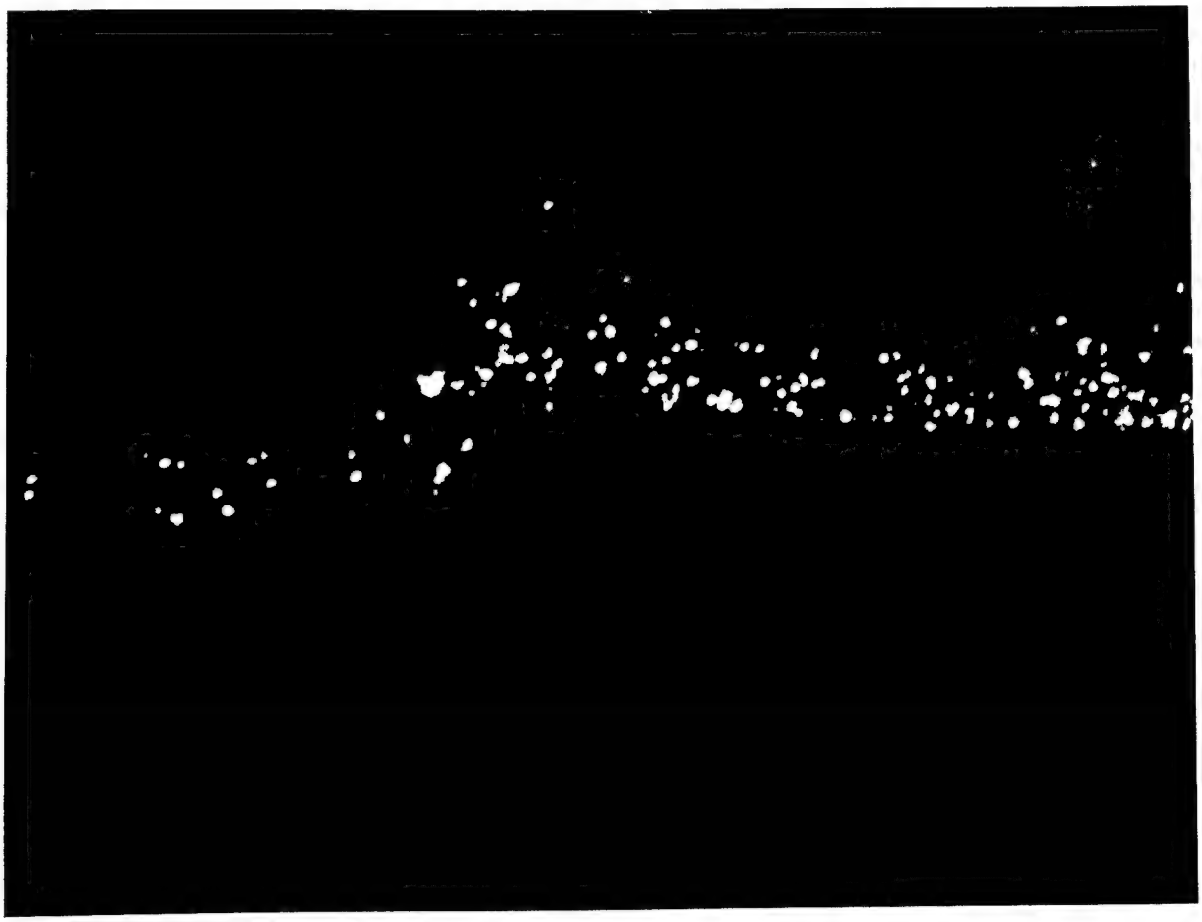

Figure 24.

Time course of light induced photoreceptor apoptosis, demonstrated with FITC-12-dUTP (TUNEL). Area A; 2 hours light plus 28 hours dark.

Figure 25.

Time course of light induced photoreceptor apoptosis, demonstrated with FITC-12-dUTP (TUNEL). Area B; 2 hours light plus 28 hours dark.

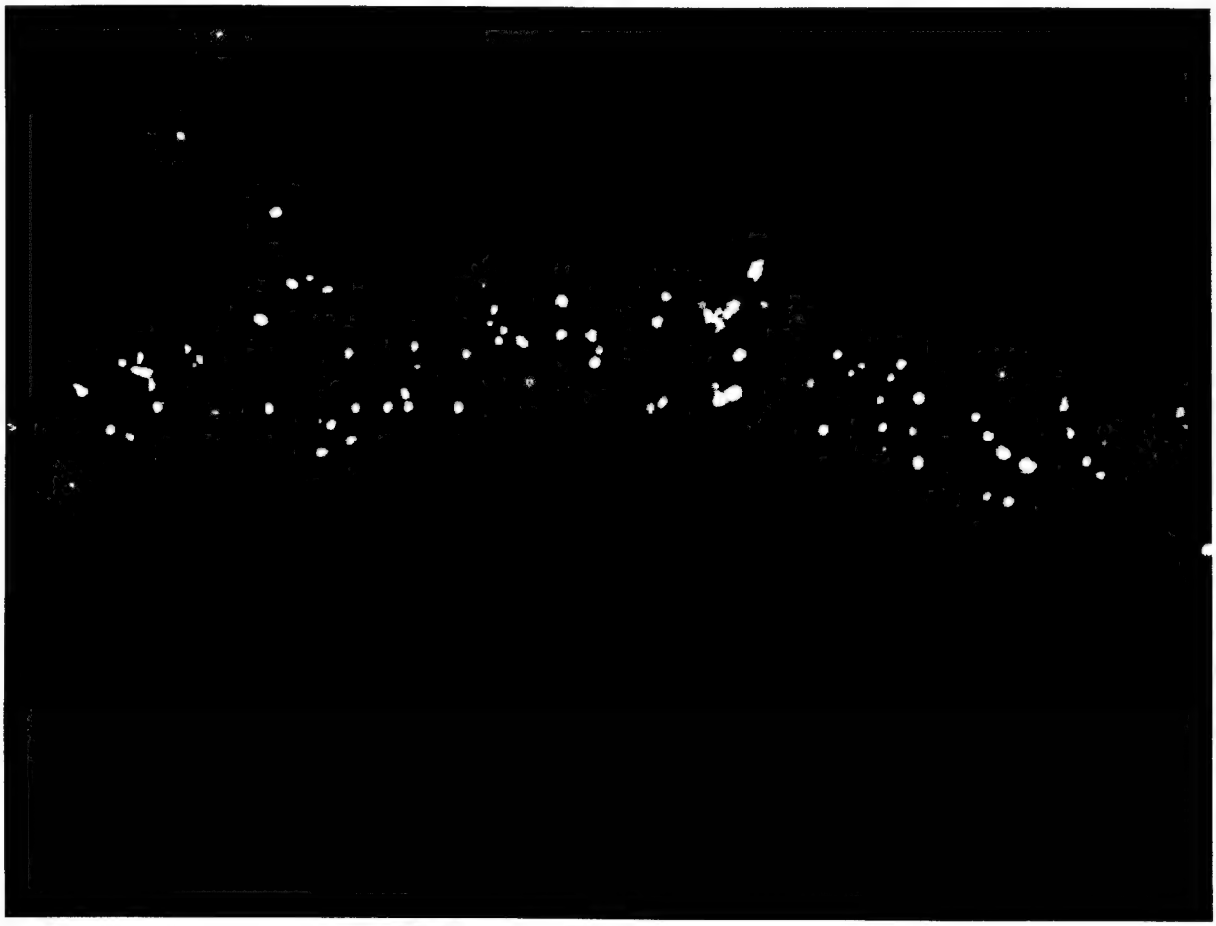

Figure 26.

Time course of light induced photoreceptor apoptosis, demonstrated with FITC-12-dUTP (TUNEL). Area C; 2 hours light plus 28 hours dark.

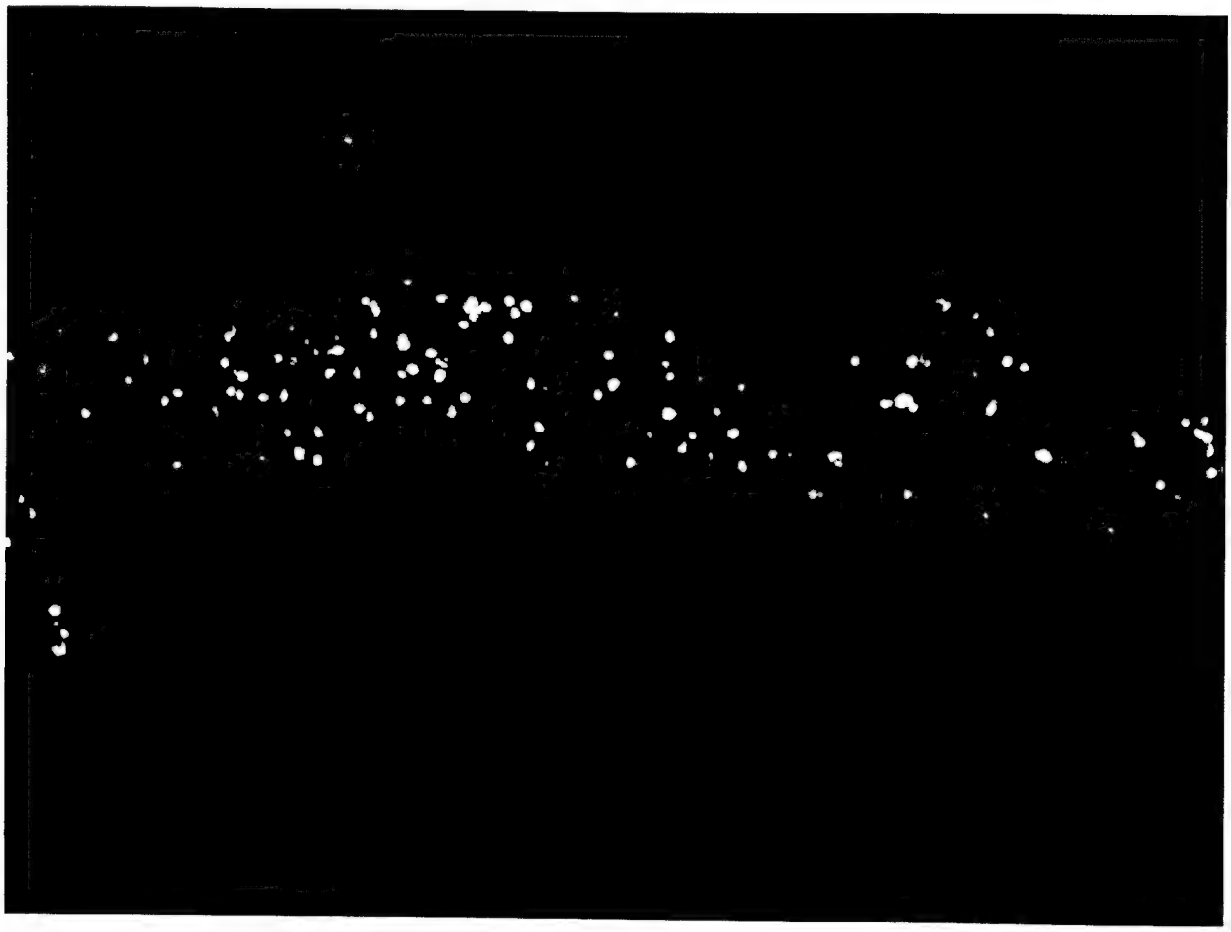

Figure 27.

Time course of light induced photoreceptor apoptosis, demonstrated with FITC-12-dUTP (TUNEL). Area A; 2 hours light plus 34 hours dark.

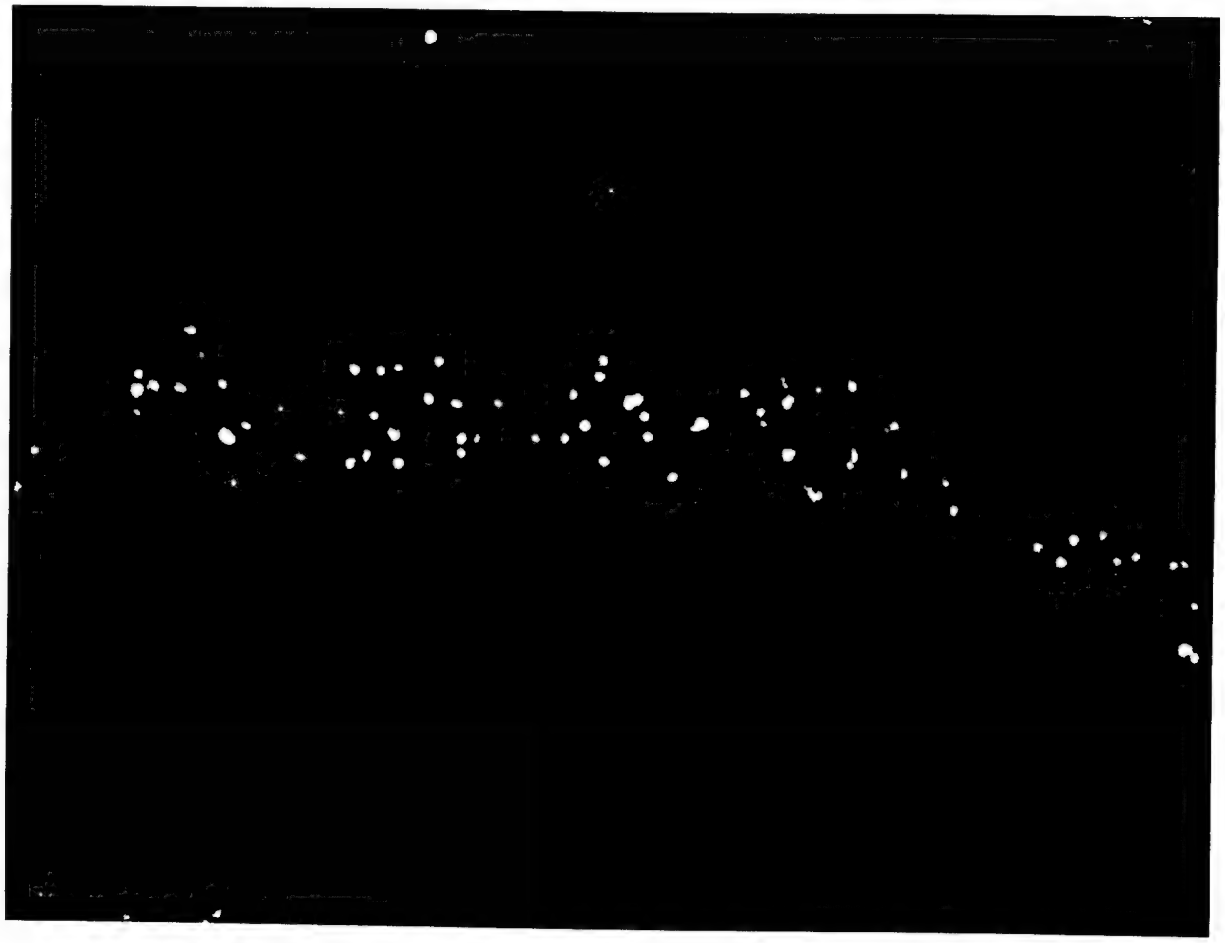

Figure 28.

Time course of light induced photoreceptor apoptosis, demonstrated with FITC-12-dUTP (TUNEL). Area B; 2 hours light plus 34 hours dark.

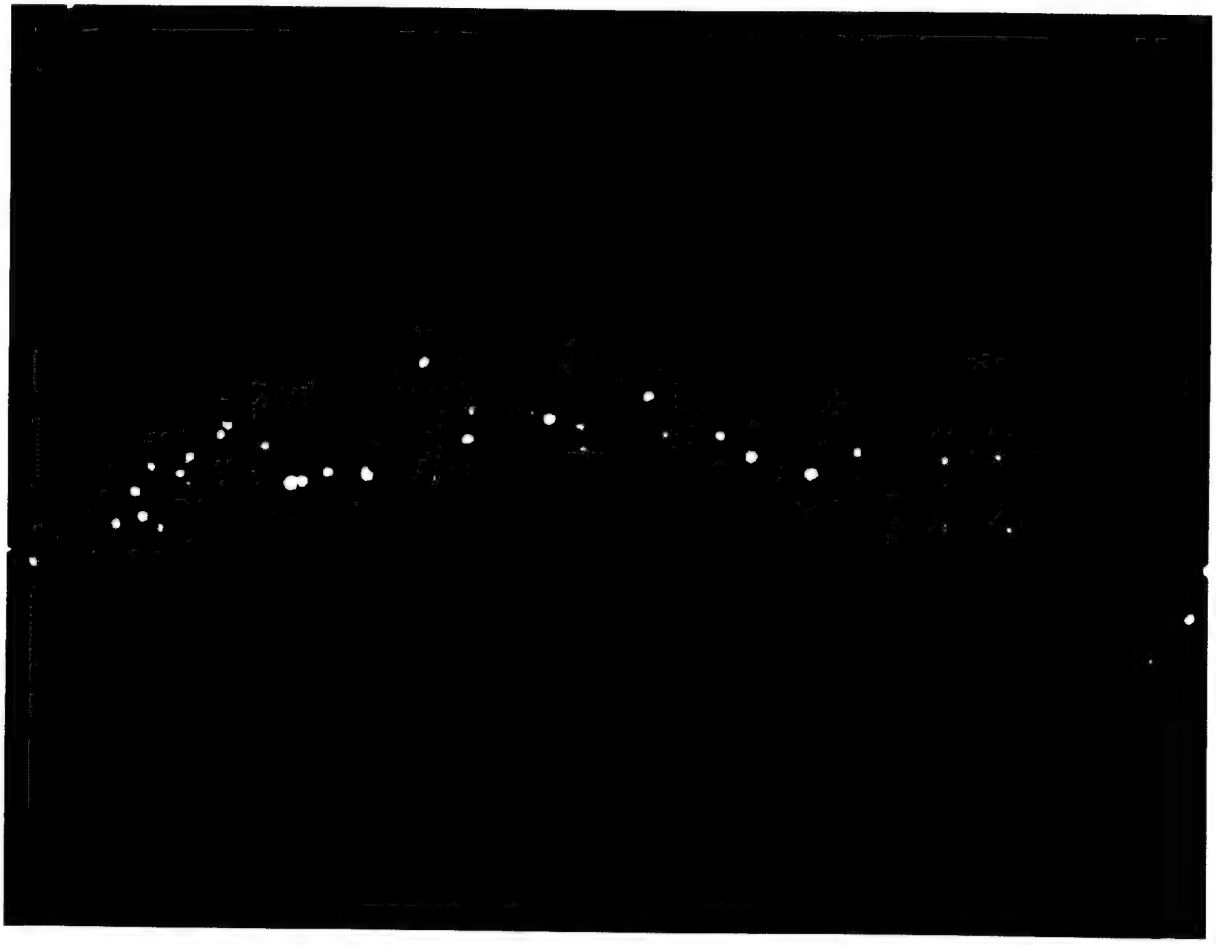

Figure 29.

Time course of light induced photoreceptor apoptosis, demonstrated with FITC-12-dUTP (TUNEL). Area C; 2 hours light plus 34 hours dark.

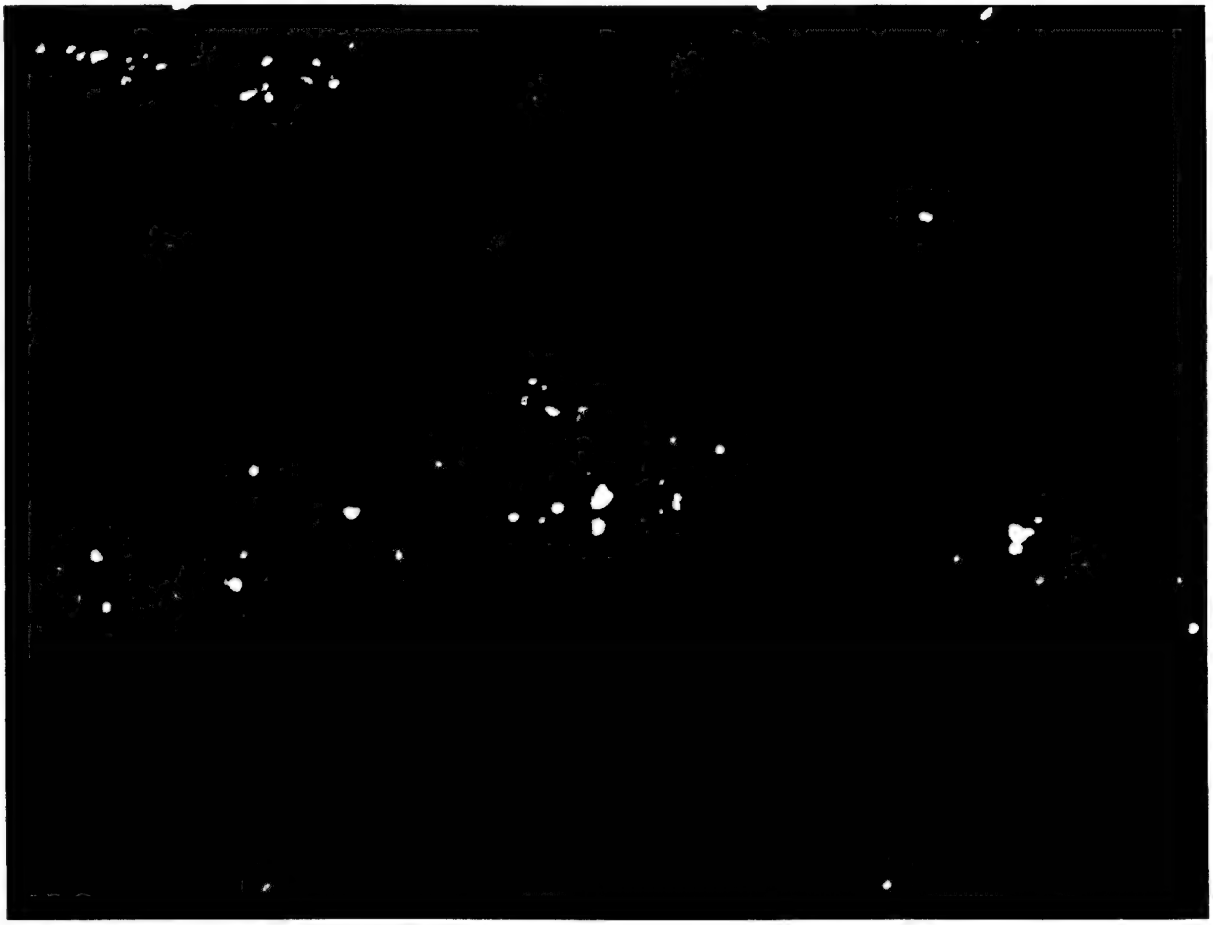

Figure 30

In this positive control retina for the BN 50730 treatment experiment, the rat was given 2 hours of light (7000 lux) originating from a fluorescent source above, and then placed in darkness for 22 hours. The TUNEL reaction demonstrates the damaged photoreceptor cell nuclei.

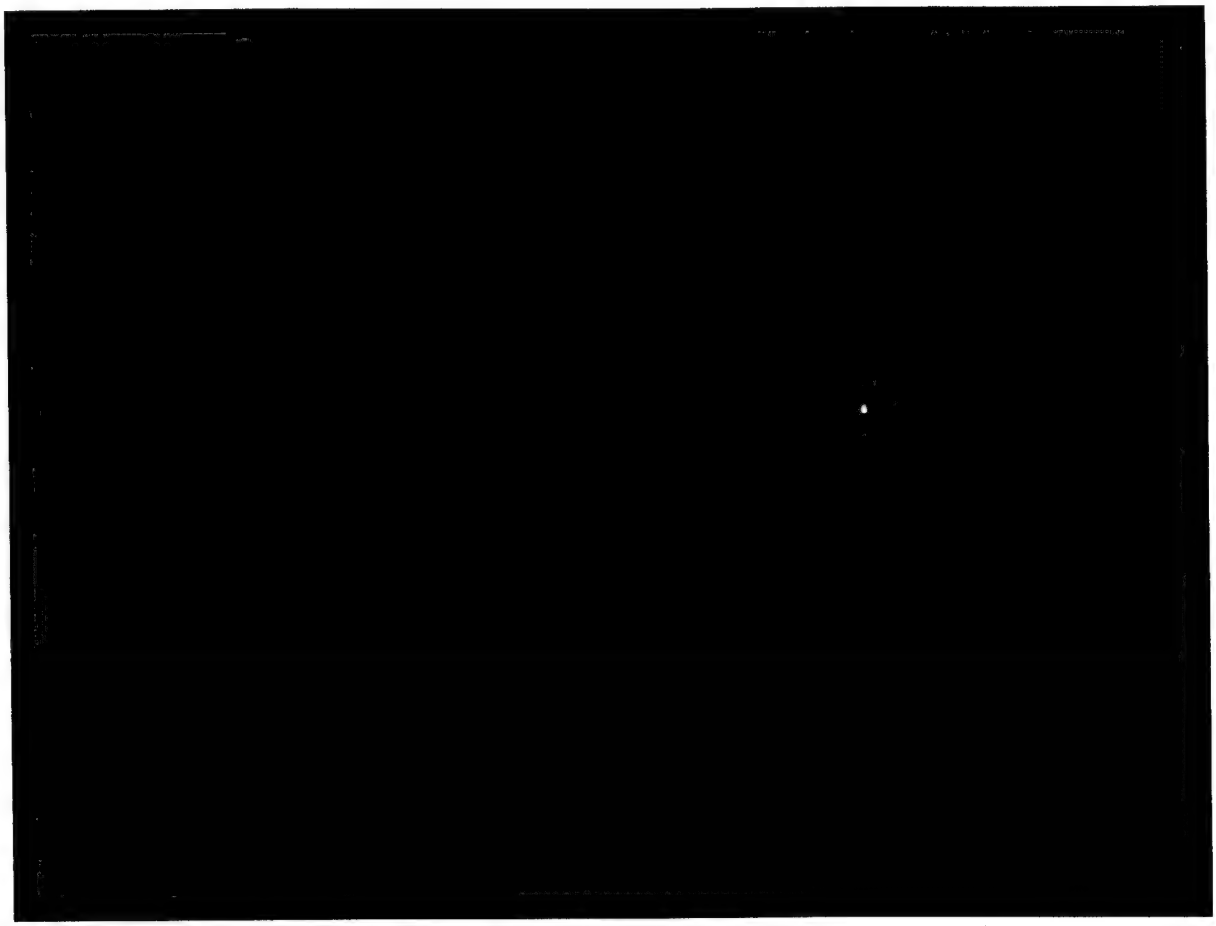

Figure 31

This retinal section was obtained from a dark adapted animal. The TUNEL reaction shows few apoptotic nuclei within photoreceptors.

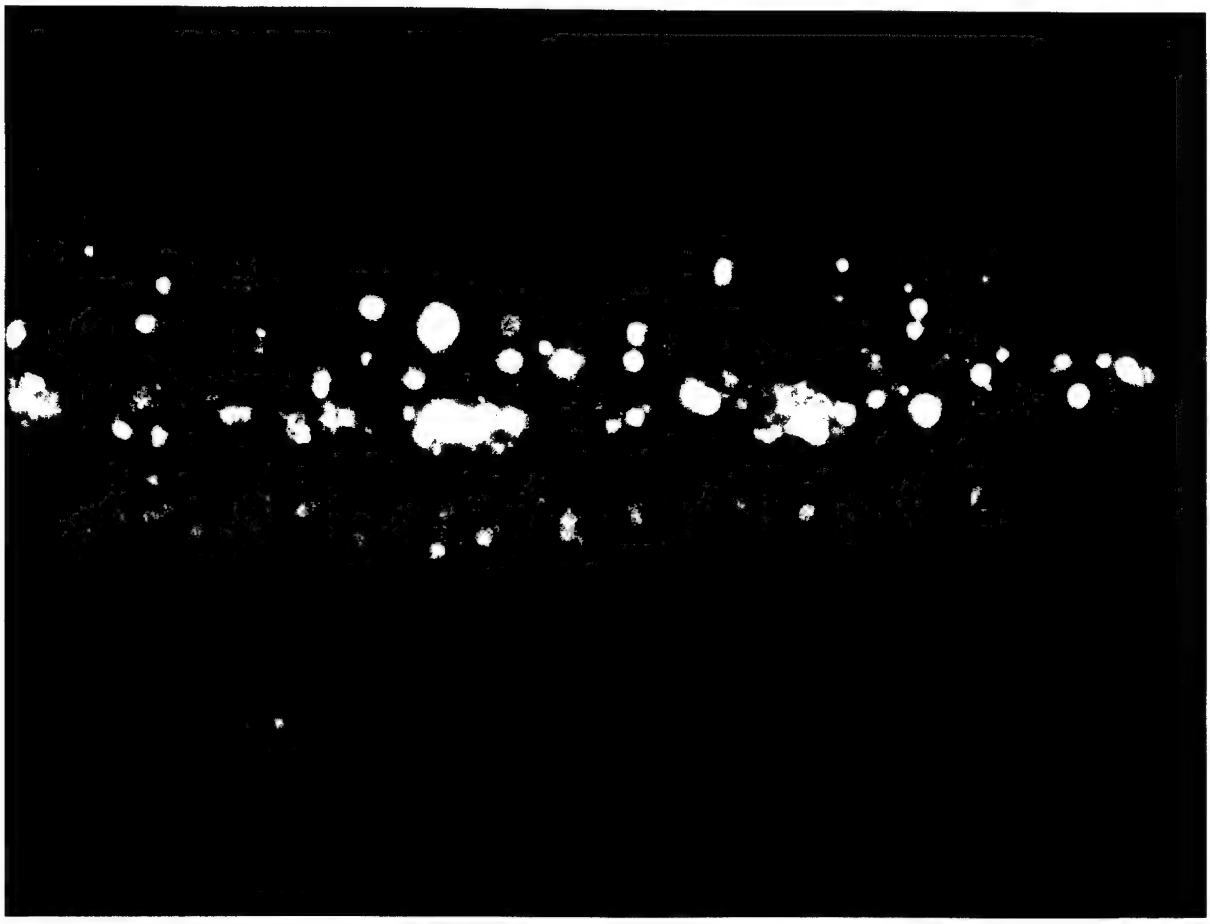

Figure 32

This animal was first treated with BN 50730 and then placed in 7000 lux for 2 hours, followed by 22 hours of darkness. Notice that there is no stimulation of nuclear labeling by light, indicating that the PAF antagonist has provided protection from light damage.

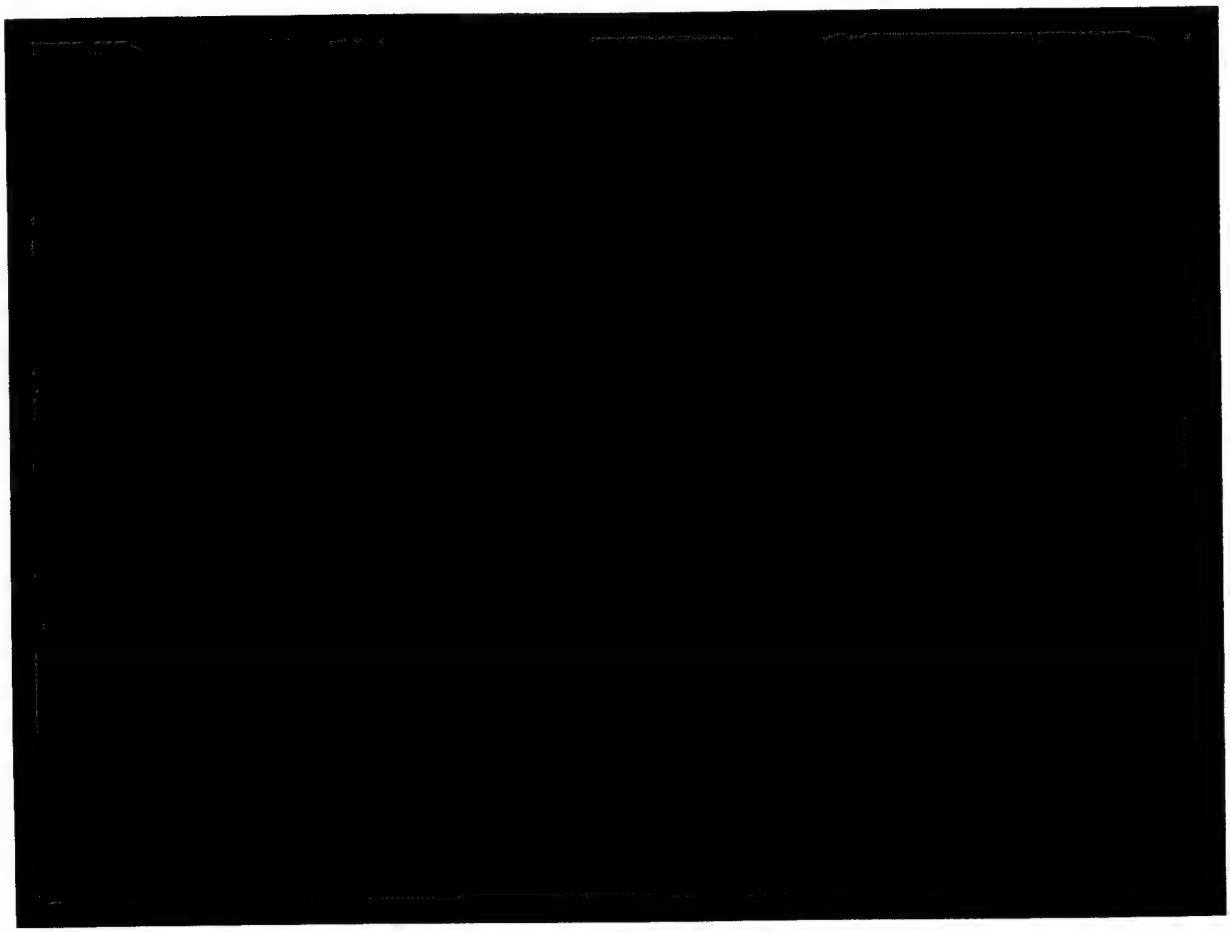

THE JOURNAL OF BIOLOGICAL CHEMISTRY
Vol. 272, No. 16, Issue of April 18, pp. 10491–10497, 1997
Printed in U.S.A.

Post-Golgi Vesicles Cotransport Docosahexaenoyl-Phospholipids and Rhodopsin during Frog Photoreceptor Membrane Biogenesis*

(Received for publication, September 19, 1996, and in revised form, December 30, 1996)

Elena B. Rodriguez de Turco‡, Dusanka Deretic§, Nicolas G. Bazan‡¶, and David S. Papermaster‖

From the ‡LSU Neuroscience Center and Department of Ophthalmology, Louisiana State University Medical Center, School of Medicine, New Orleans, Louisiana 70112, the §University of Michigan, Departments of Ophthalmology and Anatomy and Cell Biology, Ann Arbor, Michigan 48105, and ‖Univeristy of Texas, Health Science Center, Department of Pathology, San Antonio, Texas 78284-7750

Post-Golgi vesicles budding from the trans-Golgi network (TGN) are involved in the vectorial transport and delivery of rhodopsin to photoreceptor rod outer segments (ROS). We report here that newly synthesized docosahexaenoyl (DHA) phospholipids are sequestered and cotransported by rhodopsin-bearing post-Golgi vesicles to ROS. Frog retinas were pulse-labeled with [^{35}S]methionine/cysteine and [^{3}H]DHA prior to ROS isolation and subcellular fractionation. After a 1-h pulse, relatively uniform [^{3}H]DHA-lipid labeling (DPM/μg protein) was observed in all fractions enriched in post-Golgi vesicles, TGN, Golgi, and endoplasmic reticulum (ER) membranes. During the subsequent 2-h chase translocation of free [^{3}H]DHA from ROS to the photoreceptor inner segment contributed to an additional overall increase in labeling of lipids. The specific activity (dpm/nmol DHA) in ER-enriched fraction was similar or higher than in other subcellular fractions after both the pulse and the chase, indicating that the bulk of [^{3}H]DHA-lipids was synthesized in the ER. After the chase a 2-fold increase in labeling of lipids in the ER and Golgi and a 2.6-fold in lighter TGN-enriched fractions was observed. The highest labeling was in the post-Golgi vesicle fraction (4-fold increase), with [^{3}H]DHA-phosphatidylcholine and [^{3}H]DHA-phosphatidylethanolamine showing the greatest increase. At the same time, newly synthesized [^{35}S]rhodopsin shifted from the ER and Golgi toward TGN and post-Golgi fractions. Therefore, sequestration and association of [^{35}S]rhodopsin and [^{3}H]DHA-lipids in a TGN membrane domain occurs prior to their exit and subsequent vectorial cotransport on post-Golgi vesicles to ROS. Labeling of ROS lipids was very low, with phosphatidylinositol and diacylglycerols displaying the highest labeling. This indicates that other mechanisms by-passing Golgi, *i.e.* facilitated by lipid carrier proteins, may also contribute to molecular replacement of disc membrane DHA-phospholipids, particularly phosphatidylinositol.

Vertebrate photoreceptors are polarized and compartmentalized cells, with a photosensitive outer segment and a synaptic terminal domain at opposite ends of the cell. These domains are attached through a connecting cilium and a short axon, respectively, to a central region, the inner segment. The inner segment is the site where lipid and protein synthesis, polarized sorting of molecules, and initiation of membrane biogenesis for both the outer segment and synaptic terminals take place. Disc membranes in rod outer segments (ROS)[1] display a unique lipid-protein composition. The visual pigment rhodopsin, which accounts for more than 85% of disc membrane proteins (1), is embedded within a highly fluid lipid bilayer comprised of phospholipids (PLs) highly enriched in docosahexaenoic acid (DHA, 22:6*n*-3) (2–6).

Amphibian photoreceptor cells are a useful experimental model to study protein and lipid trafficking in a polarized cell. Photoreceptors actively synthesize proteins (mainly rhodopsin) and DHA-PLs to support the dynamic daily renewal of 50–80 large disc membranes in each rod cell that results in the addition of membrane at $\approx$3 μm^2/min (7, 8). ROS lack the capacity for *de novo* synthesis of PLs (4, 9). Therefore, they depend entirely on an external supply of PLs from the inner segment where they are synthesized mainly in the rough endoplasmic reticulum (ER) (10). How these highly unsaturated lipids become components of ROS membranes and at which stage of membrane biosynthesis and disc morphogenesis they become associated with rhodopsin is not yet clear.

Newly synthesized rhodopsin is vectorially transported from its site of synthesis in the rough ER to ROS by vesicles that bud from the trans-Golgi network (TGN), cluster beneath the connecting cilium, and fuse with the inner segment plasma membrane within the periciliary ridge complex (11, 12). A very low buoyant density (ρ = 1.09 g/ml) post-Golgi vesicular subcellular fraction carrying newly synthesized rhodopsin has been isolated and characterized from frog retinal photoreceptor cells (12–15). Whereas rhodopsin and the bulk of DHA-PLs are synthesized in the rough ER and both can follow a vesicle-mediated traffic through the biosynthetic pathway, other mechanisms can contribute to trafficking and selective delivery of PLs to intracellular organelles (16–18). For example, the rapid monomer transport of PLs is facilitated by transfer proteins (TP) through the cytosol (19). A transfer protein that with high affinity transfers PC to ROS membranes has also been described (20), and immunohistochemical analysis of chicken retinas at hatching revealed the presence of phosphatidylinositol (PI)-TP in retinal cells including the inner segment of photoreceptors (21).

Phospholipid renewal of ROS membranes involves both membrane replacement (as new disc membranes are assembled at the base of the ROS) and molecular replacement (*i.e.* PL

* This work was supported by funding from DAMD 17-93-V-3013 (to N. G. B.) and EY 6891 (to D. S. P. and D. D.). The costs of publication of this article were defrayed in part by the payment of page charges. This article must therefore be hereby marked "*advertisement*" in accordance with 18 U.S.C. Section 1734 solely to indicate this fact.

¶ To whom correspondence should be addressed: LSU Neuroscience Center, 2020 Gravier St., Suite B, New Orleans, LA 70112. Tel.: 504-568-6700 (ext. 321); Fax: 504-568-5801; E-mail: nbazan@lsumc.edu.

[1] The abbreviations used are: ROS, rod outer segment(s); PLs, phospholipids; DHA, 22:6n-3, docosahexaenoic acid; PA, phosphatidic acid; PC, phosphatidylcholine; PE, phosphatidylethanolamine; PS, phosphatidylserine; PI, phosphatidylinositol; DAG, diacylglycerol; ER, endoplasmic reticulum; TGN, trans-Golgi network; TP, transfer proteins.

transfer protein mediated and remodeling of disc PLs by turnover) (22, 23). Using various radiolabeled lipid precursors under experimental conditions that inhibit protein synthesis or vesicle-mediated transport, lipids can be transported to ROS by independent pathways by-passing the Golgi (24–28). However sorting of DHA-PLs, vectorial transport to ROS, and the contribution of alternative pathways to their trafficking has not been experimentally addressed. This question is especially intriguing because biochemical and autoradiographic studies of [^{3}H]DHA trafficking in frog photoreceptors after *in vitro* (29, 30) and *in vivo* (31, 32) labeling have disclosed that newly synthesized [^{3}H]DHA-PLs display a polarized delivery to ROS, where they are incorporated at the base as new discs are formed, in a pattern paralleling incorporation of radiolabeled amino acids into disk membrane proteins.

The aim of the current study was to investigate if newly synthesized DHA-lipids could be, at least in part, segregated and cotransported with rhodopsin in vesicles budding from the TGN and then enter the ROS as new membranes are formed (membrane replacement). To address this question, we pulse-labeled frog retinas for 1 h in the presence of [^{3}H]DHA and [^{35}S]methionine/cysteine, followed by a 2-h chase in a cold buffer prior to subcellular fractionation (12, 33). [^{3}H]DHA was chosen because this precursor is actively esterified into PLs in the inner segment of photoreceptor (34–38) prior to their vectorial transport to the ellipsoid region at the base of ROS and also to synaptic terminals (29, 30). Our results reveal that newly synthesized [^{3}H]DHA-PLs, especially the main components of disc membranes (*i.e.* DHA-phosphatidylcholine (PC) and DHA-phosphatidylethanolamine (PE)), are segregated and loaded together with newly synthesized [^{35}S]rhodopsin in post-Golgi vesicles. Some lipids, *i.e.* [^{3}H]DHA-PI and [^{3}H]DHA-diacylglycerols (DAG), are very rapidly synthesized and delivered to ROS probably by alternative pathways that by-pass the Golgi and may be facilitated by carrier proteins.

EXPERIMENTAL PROCEDURES

Frogs, *Rana berlandieri* (100–250 g), were purchased from Rana Co. (Brownsville, TX), maintained in a 12-h light/12-h dark cycle, and fed crickets for a week prior to the experiment. [4, 5-^{3}H]DHA (specific activity 17 Ci/mmol) and [^{35}S]Express protein labeling mixture (1,000 Ci/mmol) were from DuPont NEN. High performance thin layer chromatographic plates (10 × 10 cm, 150 μm thickness) were from Analtech (Newark, DE). Lipids and fatty acid methyl ester standards and protease inhibitors were from Sigma. High performance liquid chromatography grade solvents were from EM Science (Gibbstown, NJ). All other reagents used were of the highest purity available.

In Vitro Labeling of Retinal Lipids and Proteins with [^{3}H]DHA and [^{35}S]Methionine/Cysteine—Retinas recovered from frog eyecups 2 h before the time of light offset were dissected and subsequently incubated under dim red light. Two sets of 21 retinas were incubated in 30 ml of an oxygenated medium as described (14, 35) at 22 °C in the presence of [^{3}H]DHA (5.7 μCi/retina, final DHA concentration 0.24 μM), and [^{35}S]Express protein labeling mixture (25 μCi/retina) for 1 h. One set of retinas was further incubated for 2 h in cold buffer containing unlabeled amino acids (pulse-chase samples) prior to subcellular fractionation. Since the *in vitro* retinal metabolism of [^{3}H]DHA is altered at μM DHA concentrations (29, 30, 39), cold DHA was not added during the chase. Therefore, this chase period will hereafter be identified as "chase" to reflect this condition.

Rod Outer Segments Isolation and Retinal Subcellular Fractionation—All the procedures followed for the isolation of ROS and subcellular fractionation have been described in detail elsewhere (12, 33). Briefly, following the pulse and pulse-chase labeling, retinas were sheared through a 14-gauge needle, and ROS were separated by flotation on 34% sucrose. Retinal pellets were rehomogenized in 0.25 M sucrose in 10 mM Tris acetate, pH 7.4, containing 1 mM $MgCl_2$ and centrifuged for 4 min at 4,000 rpm (1250 g_{av}, JA20 rotor, Beckman Instruments, Inc., Palo Alto, CA). The postnuclear supernatant (3 ml) recovered after this centrifugation is enriched in photoreceptor biosynthetic membranes and organelles involved in rhodopsin transport (12, 33). To isolate post-Golgi vesicles from TGN, Golgi, and ER membranes, the postnuclear supernatant was overlaid on a 10-ml linear 20–39% (w/w) sucrose gradient in 10 mM Tris acetate buffer, pH 7.4, containing protease inhibitors and 1 mM $MgCl_2$, above a 0.5-ml cushion of 49% (w/w) sucrose in the same buffer. Gradients were centrifuged for 13 h at 4 °C in a SW40 rotor (Beckman) at 28,000 rpm (100,000 g_{av}). Fourteen fractions (0.9 ml each) were reproducibly collected from the top of the gradient. A Buchler Auto Densi-Flow fractionator was used to prepare the gradient and to collect the fractions. The subcellular fractions were diluted 4-fold with 10 mM Tris-HCl and pelleted at 50,000 rpm (240,000 g_{av}) for 40 min in a SW50 rotor. The pellets were resuspended in 210 μl of Tris acetate, pH 7.4, and divided into two aliquots, one-third for protein analysis and two-thirds for lipid analysis.

Protein Analysis—SDS-polyacrylamide gel electrophoresis was performed as described previously (12). ^{35}S-Labeled rhodopsin was determined in subcellular fractions by exposure of dried SDS gels to storage phosphor screens, and the intensity of luminescence associated with the rhodopsin band was measured and analyzed by a PhosphorImager densitometer (Molecular Dynamics). Total proteins were quantified according to Fanger (40), using bovine serum albumin as a standard.

Lipid Extraction and Analysis—Lipids were extracted from the fractions by adding 3 ml of chloroform:methanol (2:1, v/v) following the Folch procedure (41). Individual phospholipids and neutral lipids were isolated in the same TLC plate following a two-dimensional, three-step TLC procedure (6) as follows: an aliquot of the labeled lipid extract containing phospholipid and neutral lipid standards as a carriers was applied on the lower right corner (1.5 cm from each border) of 10 × 10 cm high performance thin layer chromatography plates previously sprayed with 3% magnesium acetate and activated for at least 1 h at 100 °C. The plate was developed in the first dimension twice using the Rouser I chromatographic system (chloroform/methanol/ammonia, 65:25:5, v/v) until the solvent front reached 2 cm from the top of the plate. After drying with cold air, the plate was turned to the right 90°, and neutral lipid standards (cholesterol ester, triacylglycerol, diacylglycerol, and monoacylglycerol) were spotted 1.5 cm from the bottom and 0.5 cm from the right border. Plates were then developed in hexane/ether (60:40, v/v) to isolate individual neutral lipids that had accumulated at the front of the first chromatographic system. The silica gel was cut with a vertical line to isolate neutral lipid (right) from phospholipid (left) areas of the plate (approximately 3 cm from the right border), and the silica was scraped off from the bottom right corner prior to running the plates in the Rouser II system (chloroform/acetone/ methanol/acetic acid, 30:40:10:10:5, v/v). This third chromatographic step, run in the same direction as the second step, allows the isolation of individual phospholipid classes and free fatty acids that run with the solvent front above PE. Lipid spots were visualized by iodine staining, and the radioactivity was determined in a Beckman scintillation counter.

Aliquots of lipid extracts were taken for gas-liquid chromatography analysis of endogenous fatty acid content and composition. Fatty acid methyl esters were prepared in glass tubes by transmethylation with 2 ml of toluene/methanol/sulfuric acid (100:100:4, v/v) for 4 h at 65 °C, after flushing the tubes with nitrogen and capping with a Teflon-lined cap. The tubes were cooled at room temperature, and 1 ml of water, 3 ml of hexane, and a mixture of two internal standards (17:0 and 21:0 methyl esters) were added. Fatty acid methyl esters resuspended in hexane were separated onto a SP-2330 column (30 m, 0.25 mm inner diameter, 0.2-μm film thickness, Suppelco, Bellefonte, PA) by using helium as a carrier gas, in a Varian Vista 401 gas chromatograph (Palo Alto, CA). The injector and detector temperatures were 220 and 250 °C, respectively, and the column temperature was programmed from 70 to 230 °C (42). The peaks were detected by flame ionization, identified by comparison with the retention times of authentic fatty acid methyl esters standard, and quantified using the internal standards.

Statistical Analysis—Values for [^{3}H]DHA lipid labeling and [^{35}S]rhodopsin are presented as a mean ± S.E. for n = four individual experiments. Data were compared using Student's t test for pair samples. A p value of < 0.05 was considered statistically significant.

RESULTS

Post-Golgi Vesicles Are Enriched with Newly Synthesized [^{35}S]Rhodopsin and [^{3}H]DHA-Lipids—To determine whether newly synthesized [^{3}H]DHA-PLs and [^{35}S]rhodopsin are transported together in the same population of post-Golgi vesicles recovered in fraction 5 of the sucrose gradient, retinas were pulse-labeled for 1 h in the presence of both precursors and further incubated for 2 h (chase) in cold buffer prior to subcellular fractionation. This experimental protocol gives sufficient

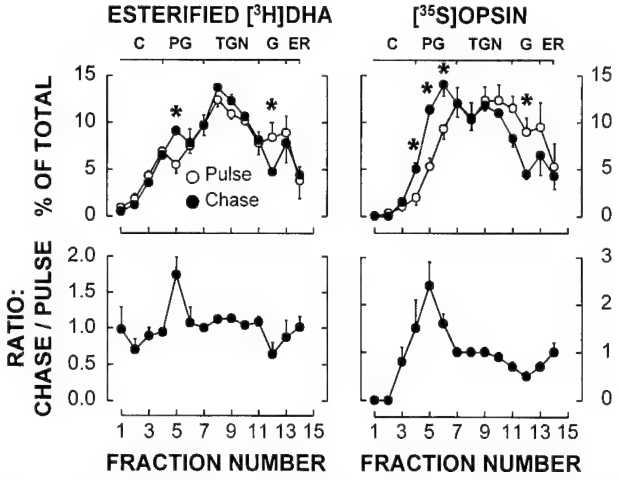

FIG. 1. **Newly synthesized [^{3}H]DHA-lipids and [^{35}S]rhodopsin exit the TGN in very low buoyant density vesicles recovered in the sucrose density gradient fraction 5.** Twenty-one frog retinas were incubated for 1 h with [^{3}H]DHA and [^{35}S]methionine/cysteine followed by a 2-h chase in cold buffer containing unlabeled amino acids. Aliquots were taken from each fraction recovered after pulse and chase labeling for lipid and protein analysis. Lipids were extracted and isolated by TLC. Esterified [^{3}H]DHA was estimated after subtraction of the free [^{3}H]DHA from total labeling. Proteins were separated by SDS-gel electrophoresis, and the radioactivity incorporated into [^{35}S]rhodopsin was determined by a PhosphorImager densitometer. Mean values ± S.E. from n = four separate experiments are shown and represent the percent distribution of total labeling recovered from the 14 fractions of the gradient. S.E. are shown when the range is larger than the symbol. *Asterisk* denotes values that are significantly different from pulse labeling ($p < 0.05$, Student's t test). *C*, cytosol; *PG*, post-Golgi vesicles; *TGN*, trans-Golgi network; *G*, Golgi; *ER*, endoplasmic reticulum.

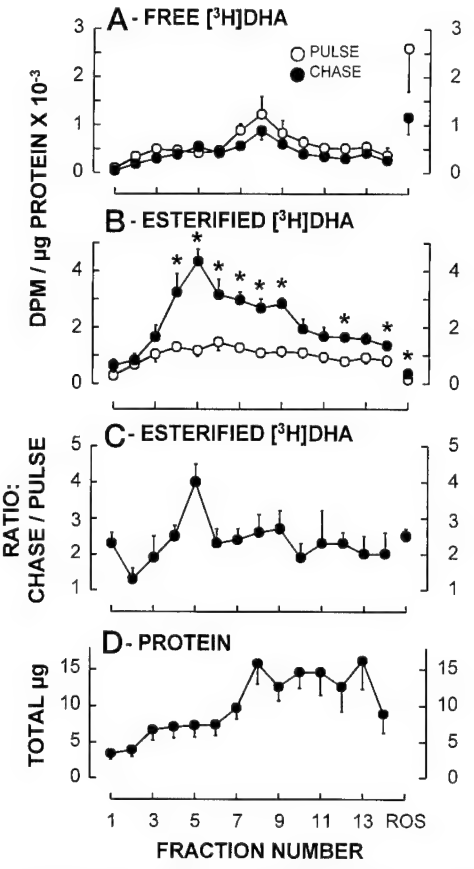

FIG. 2. **[^{3}H]DHA-lipids attain a relatively uniform labeling in all fractions after a 1-h pulse.** After a 2-h chase newly synthesized lipids accumulate in fractions containing post-Golgi vesicles recovered in fraction 5. Lipid labeling was normalized to protein content of individual subcellular fractions and shown as a mean value in dpm/μg protein ± S.E. (n = 4). *A*, free [^{3}H]DHA was isolated from phospholipids and neutral lipids by a two-dimensional, three-step TLC as detailed under "Experimental Procedures." *B*, total esterified [^{3}H]DHA is the sum of [^{3}H]DHA found esterified into phospholipids and neutral lipids. *C*, the ratio of chase/pulse labeling of total [^{3}H]DHA esterified into lipids. *D*, protein content of individual subcellular fractions. Mean values ± S.E. from n = 8 determinations including all the pulse and chase samples are shown. Other details as in Fig. 1 legend.

labeling of newly synthesized rhodopsin within 1-h pulse and a maximum labeling of the vesicles (fraction 5) during the following 2-h chase (12, 43). While the total [^{35}S]rhodopsin labeling recovered from the combined 14 fractions was similar for pulse and chase samples (data not shown), total esterified [^{3}H]DHA was increased by 2.6 ± 0.2-fold: from 1.2×10^6 dpm/21 retinas after a 1-h pulse to 3.2×10^6 dpm/21 retinas after a 2-h chase. After 1 h of pulse labeling, 58% of total [^{35}S]rhodopsin was recovered in TGN and Golgi (fractions 7–11) (Fig. 1) as expected (12). After a 2-h "chase," a shift toward post-Golgi fractions 4–6 was observed, with fraction 5 displaying the greatest increase (ratio chase/pulse: 2.4 ± 0.5). The profile of total esterified [^{3}H]DHA among subcellular fractions was similar to that of [^{35}S]rhodopsin (Fig. 1), with the highest percent values observed in those fractions that also accumulated the largest proportion of membranes (Fig. 2*D*). Remarkably after the 2-h chase only post-Golgi fraction 5 displayed significantly higher [^{3}H]DHA percent labeling (ratio chase/pulse, 1.7 ± 0.2) at the time when newly synthesized [^{35}S]rhodopsin accumulated in this fraction. Simultaneously, percent labeling in fractions 12 and 13 was lower than during the pulse.

Labeling recovered from individual subcellular fractions based upon protein content is shown in Fig. 2 and reveals four features. First, after a 1-h pulse, all fractions displayed similar labeling of esterified [^{3}H]DHA (Fig. 2*B*). Second, after the subsequent 2-h "chase," labeling of DHA-lipids increased at least 2-fold in the heavy fractions that correspond to the density of ER (13–14), Golgi (11–12), and TGN (10), by 2.6-fold in lighter TGN fractions 7–9, and peaking at 4-fold higher labeling in post-Golgi vesicles recovered in fraction 5 as compared with pulse-labeled values (Fig. 2, *B-C*). Third, no significant difference between pulse and chase labeling was observed in the free [^{3}H]DHA pool, indicating an equilibrium between the arrival of the precursor to these membrane compartments and its esterification into lipids either by *de novo* synthesis and/or turnover (Fig. 2*A*). The peak of labeling observed in fraction 8 may be the result of free [^{3}H]DHA contributed by a small proportion of heavily labeled ROS cosedimenting between fractions 7 and 9 at a buoyant density of 1.13 g/ml (12). Fourth, most of the label recovered from ROS after pulse and chase labeling was found as free DHA (92 ± 1 and 76 ± 1%, respectively) (Fig. 2*A*), whereas ROS lipids labeling was the lowest among all subcellular fractions analyzed (Fig. 2*B*). A 2.5-fold increase in ROS [^{3}H]DHA-lipids labeling after the "chase" (from 138 ± 25 to 350 ± 40 dpm/μg protein) accounted for by the concomitant loss of only 15% of free [^{3}H]DHA (from 2600 to 1160 dpm/μg protein).

The specific activity of total [^{3}H]DHA-lipids (dpm/nmol of endogenous DHA content) showed that fraction 14 (ER) displayed, after both the pulse (2790 ± 245 dpm/nmol DHA) and the "chase" (5060 ± 840 dpm/nmol DHA) labeling, similar or higher values than other fractions. After the pulse labeling, the specific activity of fraction 5 (1990 ± 115 dpm/nmol DHA) was significantly lower than that of fraction 14 ($p < 0.05$). After the chase, the specific activity of fraction 5 increased 3-fold (6580 ± 550 dpm/nmol DHA) but was not significantly different from the specific activity of fraction 14 ($p > 0.19$).

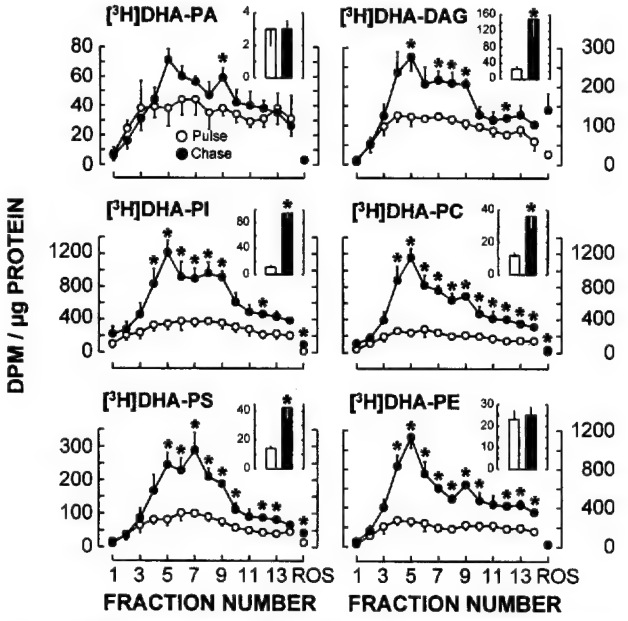

FIG. 3. **[³H]DHA-PC and [³H]DHA-PE are the phospholipids that display the highest increase of labeling in rhodopsin bearing post-Golgi vesicles after the chase.** Total dpm recovered in individual lipids per μg protein are shown. *Insets*, labeling of ROS lipids (dpm per μg of protein) after pulse (*open bars*) and chase (*closed bars*). Other details as in Fig. 1 legend.

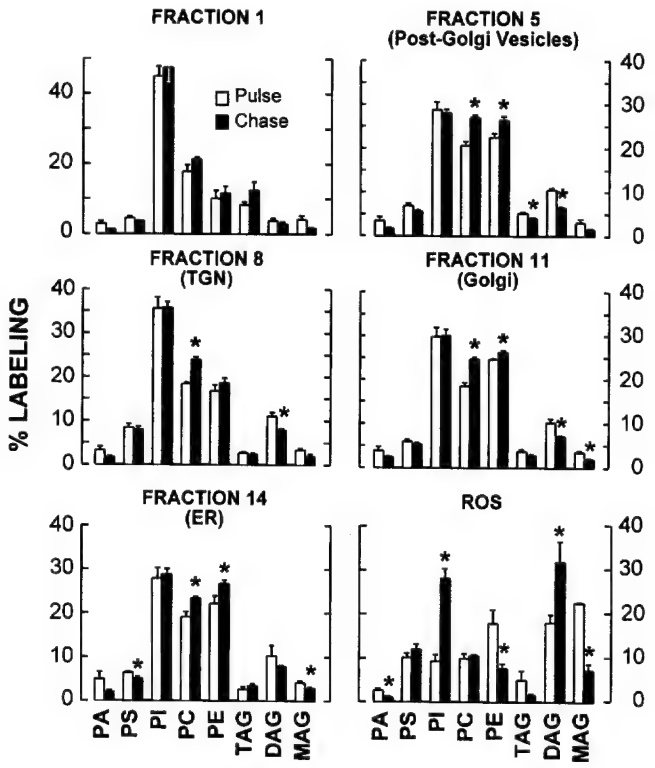

FIG. 4. **[³H]DHA-PI, [³H]DHA-PC, and [³H]DHA-PE display the highest percent labeling in all retinal subcellular fractions except for ROS which show the highest labeling in [³H]DHA-PI and [³H]DHA-DAG.** Values represent percent labeling of individual lipids with respect to total [³H]DHA recovered esterified into lipids. Other details as Fig. 1 legend.

Phosphatidylcholine, Phosphatidylethanolamine, and Phosphatidylinositol Are Highly Labeled in All Subcellular Fractions; [³H]DHA-PC and [³H]DHA-PE Preferentially Shift toward Post-Golgi Vesicles (Fraction 5) after the Chase—The two most abundant PLs in retinal membranes, PC and PE, reveal a similar labeling profile after a 2-h "chase" (Fig. 3). [³H]DHA-PC and [³H]DHA-PE gradually increased from fractions enriched in ER to heavy fractions of the TGN, with a sharp peak in post-Golgi fraction 5 reaching a 5.2- and 4.6-fold increase, respectively, above pulse labeling. The profile of [³H]DHA-PI was very similar to that of [³H]diacylglycerol (DAG), and their labeling was significantly increased only in TGN fractions 7–9, with the highest increase in post-Golgi fraction 5 (3.9- and 2.5-fold, respectively). PS was the only phospholipid that did not show a peak of labeling in fraction 5 but displayed 3-fold increase between fractions 5 and 7. Phosphatidic acid (PA) labeling gradually increased from ER fractions to post-Golgi fraction 5 with no significant differences from the 1-h pulse labeling.

[³H]DHA-PL labeling in ROS was very low (Fig. 3, *insets*) with a different pattern of distribution than all other subcellular fractions (Fig. 4). Although the small amount of ROS that is recovered in the gradient between fraction 7 and 9 may contribute to their highly free [³H]DHA labeling (Fig. 2), it cannot contribute to but rather results in an underestimation of lipid labeling in these fractions that arise from inner segment membranes. [³H]DHA-PI displayed, by far, the highest labeling in ROS, with a 7.9-fold increase after a 2-h "chase," followed by DAG (4.8-fold), PC, and PS (3-fold each). No differences were observed between a 1-h pulse and 2-h "chase" labeling in [³H]DHA-PE and [³H]DHA-PA (Fig. 3, *insets*). This short-term incubation may reflect the labeling of disc membrane lipids by molecular replacement including (*a*) [³H]DHA incorporation by turnover, (*b*) the fast transport from the inner segment of a portion of newly synthesized [³H]DHA-lipids (*i.e.* [³H]DHA-PI), and/or (*c*) further metabolism of newly incorporated [³H]DHA-PLs into ROS such as *N*-methylation of [³H]DHA-PE to [³H]DHA-PC (4, 44).

The percent distribution of esterified [³H]DHA displayed high values for PI, PC, and PE in all fractions except for ROS (Fig. 4). In fraction 5 they reached a similar value (28%), although in other fractions, PI labeling alone prevailed. The highest percent labeling of PI was observed in fraction 1 (48%) and to a lesser extent in fraction 2 (34%), probably associated with cytosolic proteins recovered at the top of the gradient that may sediment after the 40,000 centrifugation (12). The ratio PI to PC labeling was higher in TGN fractions as compared with post-Golgi fractions 4–6, showing the highest value in fraction 8 of the TGN after both pulse and chase labeling (Fig. 5).

The Content of Endogenous Fatty Acyl Chains of Lipids from Post-Golgi Vesicular Fractions—Total fatty acyl group content, reflecting mainly membrane phospholipids, increased gradually from the heaviest, ER-enriched fractions (2 nmol/μg protein) to the post-Golgi light vesicular fractions 4–5 (4 nmol/μg protein) (Fig. 6). The endogenous DHA content was very similar for all fractions (approximately 20% of total acyl groups) except for TGN fractions 7–9 where ROS, not completely removed prior to subcellular fractionation, cosedimented. In ROS, DHA accounted for 50% of total acyl groups. The lower % DHA content in fraction 5 as compared with ROS suggests that either the lipids from the vesicles bearing rhodopsin are less enriched in DHA-lipid and/or that lipids contributed by other vesicles with a lower degree of unsaturation are recovered in this fraction. The latter possibility is unlikely since immunoisolation of rhodopsin-bearing post-Golgi vesicles with anti-rhodopsin antibody indicated that they constitute >85% of the vesicles sedimenting in fraction 5 of the gradient (12). The net amount of DHA per protein in ROS (1.93 nmol/μg) was twice that of lipids from fraction 5 vesicles (0.85 nmol/μg protein). Although rhodopsin is the most abundant protein recovered in fraction 5, its contribution to the total proteins in the fraction

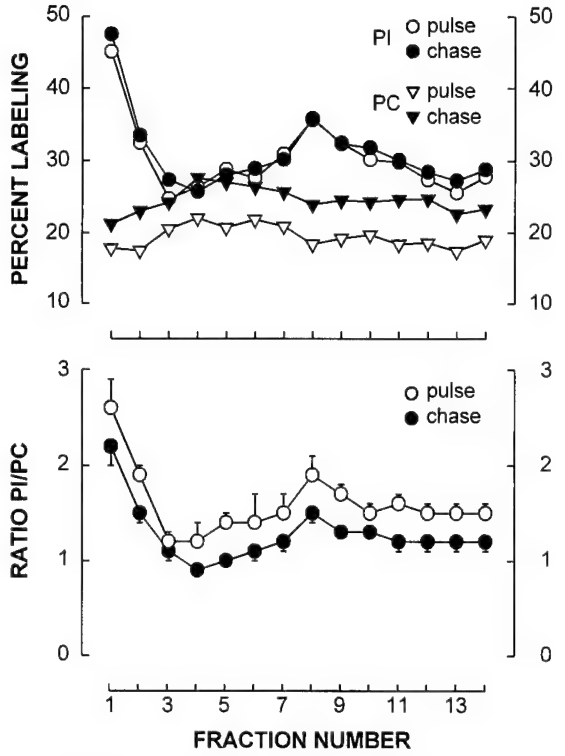

FIG. 5. **Lipids from TGN fraction 8 display the highest [^{3}H]DHA-PI/[^{3}H]DHA-PC ratio.** *Upper panel*, values represent percent labeling of PI and PC with respect to total esterified [^{3}H]DHA recovered in lipids from individual subcellular fractions. *Lower panel*, ratios of percent [^{3}H]DHA-PI/[^{3}H]DHA-PC after pulse and chase labeling. Other details as Fig. 1 legend.

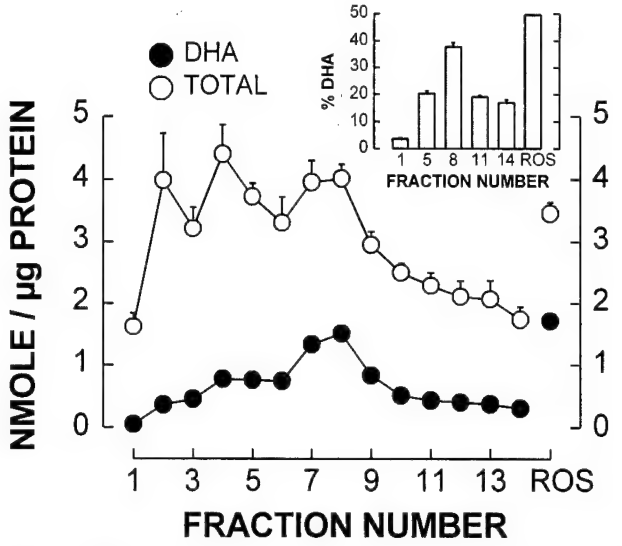

FIG. 6. **Lipids from post-Golgi vesicle fraction 5 display a similar content of lipid-acyl groups but a lower content of DHA as compared with ROS membranes.** An aliquot of lipid extracts was derivatized to fatty acid methyl esters, and their content and acyl group composition was analyzed by GLC as detailed under "Experimental Procedures." The observed higher content of DHA in fractions 7–8 is probably due to their contamination with ROS membranes. Mean values ± S.E. from n = 8–10 individual determinations are shown and expressed as nmol of fatty acids/µg of protein. *Inset*, mol % content of DHA in subcellular fractions.

is less than 50%, whereas rhodopsin accounts for 85–90% of total ROS proteins (12). Therefore, the net amount of DHA-PLs with respect to rhodopsin protein in these post-Golgi vesicles may reach values similar to that of ROS.

DISCUSSION

This study provides the first available information about the closely coordinated trafficking, sorting, and association of newly synthesized [^{3}H]DHA-PLs with [^{35}S]rhodopsin in frog photoreceptors as the two major membrane components initiate their journey from the rough ER, where they are synthesized, move through the Golgi, and leave the TGN on post-Golgi vesicles vectorially driven to ROS for the assembly of new disc membranes. Our results also yield several other important findings: (*a*) free [^{3}H]DHA may be incorporated by turnover in disc PLs although much less efficiently than when utilized in the inner segment for [^{3}H]DHA-PLs synthesis; (*b*) some [^{3}H]DHA-PLs, mainly [^{3}H]DHA-PI, are actively synthesized in the inner segment, rapidly transported to ROS, and incorporated into disc membranes; (*c*) during the short period of *in vitro* labeling (1–3 h), the fast labeling of all disc membranes by molecular replacement (*i.e.* protein-mediated transport of [^{3}H]DHA-PLs and/or [^{3}H]DHA incorporation by turnover) as compared with the labeling of a few discs at the base by membrane replacement, makes it difficult to assess the contribution of the latter mechanism to the overall labeling of ROS lipids.

The time course of [^{35}S]rhodopsin labeling through the different compartments of the secretory pathway reflects its vesicle-mediated vectorial traffic from the site of synthesis at the rough ER to only one destination, ROS. The well defined early accumulation of [^{35}S]rhodopsin in Golgi fractions by 1 h of labeling followed by its displacement during the subsequent 2-h chase toward TGN and post-Golgi vesicles recovered in fraction 5 (14 and Fig. 1) was used as a marker of membrane flow to follow the fate of newly synthesized [^{3}H]DHA-lipids. Labeled lipids recovered in Golgi and TGN-enriched fractions at any time represent newly synthesized lipids that become constitutive components of the membranes as well as the different [^{3}H]DHA-lipid pools that are in transit through these compartments to different destinations. [^{3}H]DHA-lipids labeling of post-Golgi vesicles (fraction 5), however, is a clear indication of those newly synthesized [^{3}H]DHA-lipids cotransported with [^{35}S]rhodopsin to ROS.

Within the first hour of pulse labeling, [^{3}H]DHA incorporation into lipids reached similar values in all subcellular fractions. This rapid equilibrium [^{3}H]DHA-lipids among all fractions was also reflected in a similar mol % content of endogenous DHA (20%). Only fractions 7–9, contaminated with ROS membranes, displayed higher mol % values. Thus, newly synthesized [^{3}H]DHA-lipids were rapidly transported throughout the multiple compartments of the biosynthetic pathway either by vesicle budding and fusion, by carrier proteins, and/or by lateral diffusion through intermembrane bridges (17, 18). Incorporation of [^{3}H]DHA by turnover in lipids trafficking along the transport pathway could also contribute to the uniform labeling distribution observed among subcellular fractions.

After the 2-h "chase" labeling in cold buffer, it became apparent that the high labeling of free [^{3}H]DHA in ROS was not paralleled by an efficient esterification into disc membrane phospholipids but rather by a translocation to the inner segment where it was actively esterified. This could be accomplished by the presence of (*a*) DHA-fatty acid binding proteins in ROS (45) and in the cytosolic fraction of retinas (46, 47) and (*b*) DHA-CoA synthetase in microsomes. This enzyme that activates DHA prior to its esterification into lipids displays the highest activity in microsomes from frog retinas and very low activity in ROS (48). Although free DHA can be incorporated in disc membrane PLs by turnover of their acyl groups (49–51), our present results indicate that the bulk of DHA is incorporated into lipids in the inner segment prior to their delivery to ROS (52). Indeed, the similar or higher specific activity of total

[^{3}H]DHA-lipids observed in the ER-enriched fractions as compared with other fractions enriched in membranes of the Golgi and post-Golgi supports this notion.

An interesting observation after the 2-h cold chase incubation was that the increase in [^{3}H]DHA-lipids labeling was not of the same magnitude for all subcellular fractions (Figs. 2 and 3). It showed a clear trend from a 2-fold increase in ER and Golgi, to 2.5-fold in TGN, and the highest 4-fold increase in post-Golgi vesicles (gradient fraction 5). Because these fractions also became heavily labeled with newly synthesized [^{35}S]rhodopsin after the chase, it appears that some newly synthesized [^{3}H]DHA-PLs are sorted, along with newly synthesized [^{35}S]rhodopsin in transit toward the TGN exit. The highest [^{3}H]DHA-PLs labeling observed in [^{35}S]rhodopsin-bearing post-Golgi vesicles suggests that they budded from microdomains in the TGN enriched in both [^{3}H]DHA-PLs and [^{35}S]rhodopsin. In fact, rhodopsin shows a preference for association with more fluid lipids (53), and in ROS PLs with high DHA content are in closer association with rhodopsin than less unsaturated ones (54). That the highest [^{3}H]DHA-PLs labeling in post-Golgi vesicles observed after the 2-h "chase" could be the result of differences in lipid turnover in this fraction is unlikely since (*a*) labeling gradually increased from Golgi to post-Golgi vesicles, (*b*) no differences in the specific activity (total [^{3}H]DHA-PLs/endogenous DHA content) between post-Golgi vesicles and ER fraction was observed, and (*c*) after 1-h pulse labeling post-Golgi vesicles did not show higher labeling than other fractions. Taken together these data strongly argue in favor of a progression of label through a series of compartments. Moreover, the similar [^{3}H]DHA-lipid labeling observed after 1 h among all subcellular fractions also suggests an early association between newly synthesized DHA-lipids and newly synthesized rhodopsin rather than with older rhodopsin molecules already moving ahead in transit through the Golgi.

The profile of individual [^{3}H]DHA-lipids labeling in subcellular fractions after the 2-h "chase" was very similar for the two main membrane components PE and PC, which also displayed the highest increase of labeling in post-Golgi vesicles (Fig. 3). This observation and the very low labeling of [^{3}H]DHA-PC and [^{3}H]DHA-PE recovered in ROS (Figs. 3 and 4) suggests that their incorporation into disc membranes mainly occurs by membrane replacement. Our preliminary studies using brefeldin A, which perturbs rhodopsin trafficking, show that [^{3}H]DHA-PL and [^{35}S]rhodopsin transfer into fraction 5, PE and PC, in particular, were successfully blocked, and also that ROS lipid labeling was reduced.[2] At difference with PE and PC, [^{3}H]DHA-PI displayed a more sustained increase throughout TGN peaking in post-Golgi fracton 5. Although the labeling of [^{3}H]DHA-DAG was much lower than that of [^{3}H]DHA-PI (Fig. 4), both followed a very similar profile (Fig. 3), probably reflecting an active phosphodiesteratic catabolism of PI with the consequent generation of labeled DAG along the TGN compartment. In ROS, [^{3}H]DHA-DAG and [^{3}H]DHA-PI displayed the highest labeling (Fig. 4), suggestive of their active translocation and incorporation in disc membranes by molecular replacement. Several lines of experimental evidence appear to indicate that PI, synthesized *de novo* in the inner segment of photoreceptors, can actively be transferred to ROS by-passing the Golgi (24, 28). In ROS, PI can be further phosphorylated to phosphatidylinositol 4,5-bisphosphate (9, 55). Because ROS contains a light-stimulated phosphoinositide-specific phospholipase C (56, 57), the presence of a photoreceptor cytosolic PI-TP, possibly similar to the one found in rat brain cytosol (58), could contribute to sustain and modulate the inositol lipid-derived signals triggered by light.

Frog and primate retinas labeled *in vitro* and/or *in vivo* with [^{3}H]DHA display an early high level of labeling of PI, reaching values similar to that of PC and PE (29, 30, 59). In the present study, we confirm and further extend our previous observation to show that [^{3}H]DHA-PI preferentially accumulates in the lightest fractions 1–3 of the gradient where cytosolic proteins are recovered (12), and also in ROS and in TGN fractions. The high ratio [^{3}H]DHA-PI to [^{3}H]DHA-PC found in TGN fractions 7–9 of frog retinas is the first evidence indicating a relative enrichment with newly synthesized [^{3}H]DHA-PI of membranes located at the exit from the TGN compartment. As previously shown in yeast (19) and on PC12 cells (60), the high PI/PC ratio may also be essential for budding of rhodopsin-bearing vesicles from TGN and further suggests the involvement of PI/PC-TP in the dynamics of Golgi function in photoreceptors. Moreover, PI-TP has been identified as a cytosolic factor that stimulates the formation of secretory vesicles in PC12 cells (60). Since membranes recovered in TGN-enriched fractions 6–11 also contain synaptophysin, a synaptic membrane protein (12), further studies are necessary to evaluate the possible contribution of [^{3}H]DHA-PI, in transit together with synaptophysin toward synaptic terminals, to the high [^{3}H]DHA-PI in TGN fractions 7–9. The overall contribution of synaptic protein biosynthesis in this fraction must be relatively minor, however, since rhodopsin synthesis greatly exceeds the rate of synthesis of all other retinal membrane proteins (61).

Post-Golgi vesicles recovered from the gradient fraction 5 (ρ = 1.09 g/ml) display lower density than ROS which sediments in fractions 7–8 (ρ = 1.12–1.13) and therefore must have a higher lipid to protein ratio (12). This is also supported by freeze-fracture EM studies (62) showing that vesicles clustered around the connecting cilium display half the density of the intramembranous particle of ROS disks. Since in post-Golgi vesicles the total acyl group content, derived mainly from PLs (4.2 nmol/μg protein), was similar to that of the ROS (3.9 nmol/μg protein), other lipids such as sterols presumably contribute to their lower density. Cholesterol delivery to ROS may be accomplished either by a pathway(s) independent from that followed by integral plasma membrane proteins (18, 63) and/or together with rhodopsin and DHA-lipid-containing post-Golgi vesicles. As vesicles fuse with the plasma membrane adjacent to the base of the connecting cilium, they could generate the cholesterol-enriched domains observed in frog photoreceptors surrounding the periciliary ridge complex (64, 65) and in nascent discs at the base of the ROS (66).

In summary, this study shows that newly synthesized [^{3}H]DHA-PLs, mainly [^{3}H]DHA-PC and [^{3}H]DHA-PE, are vectorially cotransported to ROS by rhodopsin-bearing post-Golgi vesicles, and other PLs such as [^{3}H]DHA-PI may also reach ROS and the TGN by-passing the Golgi carried by transfer proteins. Moreover, in the complex process of membrane biogenesis, addition of rhodopsin and DHA-PLs at the base of ROS could be "the driving force" for the incorporation of other PLs that do not contain DHA (approximately 40–50% of total PLs in disc membranes) possibly reaching the periciliary region by independent pathways. Current studies aim to delineate the mechanism(s) that contribute to the complex polarized trafficking of DHA-PLs either by vesicular and/or by transfer protein-mediated transport to ROS.

Acknowledgments—We thank R. E. Anderson for thoughtful discussions of the results and Nilda Parkins, Belen Puleo-Scheppke, and Claudia Trippe for their excellent technical assistance.

[2] D. Deretic *et al.*, manuscript in preparation.

REFERENCES

1. Papermaster, D. S., and Dreyer, W. J. (1974) *Biochemistry* **13,** 2438–2444
2. Aveldaño de Caldironi, M. I., and Bazan, N. G. (1980) *Neurochem. Int.* **1,**

381–392
3. Aveldaño, M. I., and Bazan, N. G. (1983) *J. Lipid Res.* **24,** 620–627
4. Fliesler, S. J., and Anderson, R. E. (1983) *Prog. Lipid Res.* **22,** 79–131
5. Wiegand, R. D., and Anderson, R. E. (1983) *Exp. Eye Res.* **37,** 150–173
6. Choe, H.-G., and Anderson, R. E. (1990) *Exp. Eye Res.* **51,** 159–165
7. Besharse, J. C. (1986) in *The Retina: A Model for Cell Biological Studies* (Adler, R., and Farber, D., eds) pp. 297–352, Academic Press, Inc., New York
8. Deretic, D., and Papermaster, D. S. (1995) in *Progress in Retinal and Eye Research* (Osborne, N. N., and Chadek, G. J., eds) Vol. 14, pp. 249–265, Pergamon Press Inc., Tarrytown, NY
9. Choe, H.-G., Ghalayini, A. J., and Anderson, R. E. (1990) *Exp. Eye Res.* **51,** 167–176
10. Mercurio, A. M., and Holtzman, E. (1982) *J. Neurocytol.* **11,** 295–322
11. Papermaster, D. S., Schneider, B. G., Defoe, D., and Besharse, J. C. (1986) *J. Histochem. Cytochem.* **34,** 5–16
12. Deretic, D., and Papermaster, D. S. (1991) *J. Cell Biol.* **113,** 1281–1293
13. Deretic, D., and Papermaster, D. S. (1993) *J. Cell Sci.* **106,** 803–813
14. Deretic, D., Aebersold, R. H., Morrison, H. D., and Papermaster, D. S. (1994) *J. Biol. Chem.* **269,** 16853–16861
15. Deretic, D., Huber, L. A., Ransom, N., Mancini, M., Simons, K., and Papermaster, D. S. (1995) *J. Cell Sci.* **108,** 215–224
16. Bishop, W. R., and Bell, R. M. (1988) *Annu. Rev. Cell Biol.* **4,** 579–610
17. Pagano, R. E. (1990) *Curr. Opin. Cell Biol.* **2,** 652–663
18. Voelker, D. R. (1991) *Microbiol. Rev.* **55,** 543–560
19. Cleves, A., McGee, T., and Bankaitis, V. (1991) *Trends Cell Biol.* **1,** 30–34
20. Dudley, P. A., and Anderson, R. E. (1978) *FEBS Lett.* **95,** 57–60
21. Sellner, P. A., Dalton, T. P., and Helmkamp, G. M. (1991) *Invest. Ophthalmol. & Visual Sci.* **32,** Suppl. ARVO, 1149
22. Bibb, C., and Young, R. W. (1974) *J. Cell Biol.* **61,** 327–343
23. Young, R. W. (1976) *Invest. Ophthalmol.* **15,** 700–725
24. Fliesler, S. J., and Basinger, S. F. (1987) *J. Biol. Chem.* **262,** 17516–17523
25. Fliesler, S. J., Florman, R., and Keller, R. K. (1995) *Exp. Eye Res.* **60,** 57–69
26. Matheke, M. L., Fliesler, S. J., Basinger, S. F., and Holtzman, E. (1984) *J. Neurosci.* **4,** 1086–1093
27. Matheke, M. L., and Holtzman, E. (1984) *J. Neurosci.* **4,** 1093–1103
28. Wetzel, M. G., Bendala-Tufanisco, E., and Besharse, J. C. (1993) *J. Neurocytol.* **22,** 397–412
29. Rodriguez de Turco, E. B., Gordon, W. C., and Bazan, N. G. (1991) *J. Neurosci.* **11,** 3667–3678
30. Rodriguez de Turco, E. B., Gordon, W. C., and Bazan, N. G. (1993) *Curr. Eye Res.* **13,** 21–28
31. Gordon, W. C., and Bazan, N. G. (1990) *J. Neurosci.* **10,** 2190–2202
32. Gordon, W. C., and Bazan, N. G. (1993) *Invest. Ophthalmol. & Visual Sci.* **34,** 2402–2411
33. Deretic, D., and Papermaster, D. S. (1993) in *Methods for the Study of Photoreceptor Cells* (Hargrave, P., ed) Vol. 15, pp 108–120, Rockefeller University Press, New York
34. Louie, K., Wiegand, R. D., and Anderson, R. E. (1988) *Biochemistry* **27,** 9014–9020
35. Bazan, N. G. (1982) *Phospholipids in the Nervous System* (Horrocks, L. A., Ansell, G. B., and Porcellati, G., eds) pp. 49–62 Raven Press, NY
36. Bazan, N. G., Reddy, T. S., Bazan, H. E. P., and Birkle D. L. (1986) *Prog. Lipid Res.* **25,** 595–606
37. Rotstein, N. P., and Aveldaño, M. I. (1987) *Biochim. Biophys. Acta* **921,** 221–234
38. Rotstein, N. P., and Aveldaño, M. I. (1987) *Biochim. Biophys. Acta* **921,** 235–244
39. Rodriguez de Turco, E. B., Gordon, W. C., and Bazan, N. G. (1992) *Invest. Ophthalmol. & Visual Sci.* **32,** Suppl. ARVO, 702
40. Fanger, B. O. (1987) *Anal. Biochem.* **162,** 11–17
41. Folch, J., Lees, M., and Stanley, G. H. S. (1957) *J. Biol. Chem.* **226,** 497–509
42. Marcheselli, V. L., and Bazan, N. G. (1990) *J. Nutr. Biochem.* **1,** 231–237
43. Deretic, D., Puleo-Scheppke, B., and Trippe, C. (1996) *J. Biol. Chem.* **271,** 2279–2286
44. Roque, M. E., and Giusto, N. M. (1995) *Exp. Eye Res.* **60,** 631–643
45. Jiao, X., Gentleman, S., Wetzel, M. G., O'Brien, P., and Chader, G. F. (1993) *Invest. Ophthalmol. & Visual Sci.* **34,** (suppl.) 1328
46. Sellner, P. (1994) *Invest. Ophthalmol. & Visual Sci.* **35,** 443–452
47. Lee, J., Jiao, X., Gentleman, S., Wetzel, M. G., O'Brien, P., and Chader, G. F. (1995) *Invest. Ophthalmol. & Visual Sci.* **36,** 2032–2039
48. Reddy, T. S., and Bazan, N. G. (1984) *Curr. Eye Res.* **3,** 1225–1232
49. Giusto, N. M., Boschero, M. I., Sprecher, H., and Aveldaño, M. I. (1986) *Biochim. Biophys. Acta* **860,** 137–148
50. Zimmerman, W. F., and Keys, S. (1988) *Exp. Eye Res.* **47,** 247–260
51. Louie, K., Zimmerman, W. F., Keys, S., and Anderson, R. E. (1991) *Exp. Eye Res.* **53,** 309–316
52. Bazan, N. G. (1990) *Nutrition and the Brain*, pp. 1–24, Raven Press, Ltd, New York
53. Chen, Y. S., and Hubbel, W. L. (1973) *Exp. Eye Res.* **17,** 517–532
54. Aveldaño, M. I. (1988) *Biochemistry* **27,** 1229–1239
55. Giusto, N. M., and Ilincheta de Boschero, M. G. (1986) *Biochim. Biophys. Acta* **877,** 440–446
56. Ghalayini, A. J., and Anderson, R. E. (1984) *Biochem. Biophys. Res. Commun.* **124,** 503–506
57. Ghalayini, A. J., and Anderson, R. E. (1992) *J. Biol. Chem.* **267,** 17977–17982
58. Thomas, G. M. H., Cunningham, E., Fensome, A., Ball, A., Totty, N. F., Troung, O., *et al.* (1993) *Cell* **74,** 919–928
59. Rodriguez de Turco, E. B., Gordon, W. C., Peyman, G. A., and Bazan, N. G. (1990) *J. Neurosci. Res.* **27,** 522–532
60. Ohashi, M., de Vries, K. J., Frank, R., Snoek, G., Bankaitis, V., Wirtz, K., and Hutter, W. B. (1995) *Nature* **377,** 544–547
61. Papermaster, D. S., Converse, C. A., and Siu, J. (1975) *Biochemistry* **14,** 1343–1352
62. Besharse, J. C., and Pfenninger, K. H. (1980) *J. Cell Biol.* **87,** 451–463
63. Urbani, L., and Simoni, R. D. (1990) *J. Biol. Chem.* **265,** 1919–1923
64. Andrews, L. D., and Cohen, A. I. (1981) *Exp. Eye Res.* **33,** 1–10
65. Andrews, L. D., and Cohen, A. I. (1983) *J. Cell Biol.* **97,** 749–755

448.7

EFFECTS OF CHOLINERGIC, NORADRENERGIC, SEROTONERGIC AND HISTAMINERGIC MODULATION ON SPIKE TIMING IN NEOCORTICAL NEURONS Akaysha C. Tang*, Andreas Bartels and Terrence J. Sejnowski. The Salk Institute, Computational Neurobiology Laboratory, La Jolla, CA 92037.

Acetylcholine, norepinephrine, serotonin and histamine are neuromodulators that affect several potassium currents, including the calcium-dependent potassium current, I_{sAHP}. When applied to neocortical neurons in slice preparations they increase the firing rates of pyramidal neurons as well as alter the interspike intervals in response to square pulse current injection by decreasing spike rate adaptation. We examined the effects of these neuromodulators on the responses of neocortical neurons in the rat visual cortex to fluctuating inputs that resembled synaptic inputs in vivo. Bath application of carbachol (5-7.5μM), norepinephrine(500μM), serotonin (500μM) and histamine (500μM) produced additional spikes to an identical fluctuating stimulus but the displacement of existing spikes was only a few milliseconds. Thus, the effects of neuromodulation are compatible with the preservation of information in spike timing which could augment information contained in the firing rate. Using a compartmental model of neocortical neurons and a two-pulse stimulation paradigm, we isolated two factors underlying changes in spike timing due to neuromodulation, a direct effect of changing I_{sAHP} and an indirect effect of spike insertion due to an increased firing rate. This model provides a framework for studying the relationship between the effects of neuromodulation on spike timing and the firing rate.

Sponsored by Howard Hughes Medical Institute.

448.8

SYNAPTIC PLASTICITY AT MINIATURIZED SPINES ON PURKINJE CELLS EXPRESSING CONSTITUTIVELY ACTIVE Rac GTPase. T.K. Hensch[*1,3], L. Luo[2,3] L.Y. Jan[3], and Y.N. Jan[3]. [1]Frontier Research Program, RIKEN, Saitama, JAPAN; [2]Stanford University, Stanford, CA; [3]HHMI, Univ. of California, San Francisco, CA.

The Rac/Rho/Cdc42 subfamily of small GTPases mediates two distinct functions: regulation of the actin cytoskeleton and transduction of signals from the membrane to the nucleus. We previously demonstrated a role for Rac in the elaboration of neurites during mouse development by selective expression of a constitutively active form of human Rac1 in Purkinje cells (PCs) using the L7 promoter (Luo et al, Nature, 1996). Axons of transgenic PCs largely failed to reach their target in deep cerebellar nuclei, while their dendritic arbors bore numerous 'mini' spines that were greatly reduced in size with no obvious spine necks. Here we report the intrinsic membrane properties and plasticity at parallel fiber (PF) synapses onto these morphologically-altered PCs.

As expected from their complex dendrites which grew to normal height within the molecular layer, PCs in mutant cerebellar slices exhibited normal resting membrane potential and input resistance. Strong hyperpolarization activated inwardly-rectifying potassium currents (I_h) with a typical current-voltage relationship. However, unlike the trains of sodium spikes usually evoked in wild type PCs, depolarizing pulses often elicited none or only one in transgenic neurons, consistent with a perturbed axonal compartment where action potential initiation occurs.

PF inputs onto mutant 'mini' spines produced graded EPSPs that could be blocked completely by AMPA receptor antagonists. Presynaptic facilitation of paired PF pulses was pronounced and decayed similarly to wild type. PF inputs paired with postsynaptic depolarization persistently depressed EPSPs by about 25%, reflecting the appropriate activation of calcium channels on mutant PCs. Thus, long-term depression (LTD) of PF synapses was not impeded by constitutive activation of Rac signaling. Moreover, our results provide direct *in vivo* evidence that morphological compartmentalization of synaptic machinery at spines is not essential for LTD induction. *Supported by HHMI.*

448.9

A SECRETORY PHOSPHOLIPASE A_2 ($sPLA_2$) RECEPTOR AGONIST INDUCES EXPRESSION OF PROSTAGLANDIN ENDOPEROXIDE SYNTHASE-2 (COX-2) IN PRIMARY CORTICAL NEURONS BUT NOT GLIAL CULTURES. M. Serou, V.L. Marcheselli, M.A. DeCoster, P. Homavoun* and N.G. Bazan. LSUMC Neuroscience Center, New Orleans, USA.

The sPLA2 receptor agonist sPLA2 from bee venom, as well as the excitatory amino acid agonists, glutamate and kainate, cause significant cell death to primary cortical neuronal cultures. Coadministration of glutamate and sPLA2 synergistically activates cell death and arachidonic acid turnover (J Biol Chem 271:32722-8, 1996). Kainate causes a platelet activating factor (PAF)-dependent induction of prostaglandin endoperoxide synthase 2 (COX-2) in hippocampus (J Biol Chem 271:24794-9, 1996). Here we studied the effects of sPLA2 (10 or 25 ng/ml) added to primary cortical neurons, either alone or in combination with 100 µM glutamate. We followed the induction of COX-2 and inducible nitric oxide synthase (iNOS) mRNA and protein levels. Chemiluminescence showed that iNOS, neuronal specific NOS (nNOS), and COX-1 were expressed at comparable levels in neurons and astrocytes, while COX-2 was detectable in neurons only. iNOS and COX-2 protein and COX-2 mRNA were induced in neurons after treatment with either glutamate or sPLA2, while no changes were seen in nNOS and COX-1. Combination of glutamate and sPLA2 produced additive induction of iNOS and COX-2 protein and COX-2 mRNA levels. Preincubation of cultures with 1µM BN50730, an intracellular PAF antagonist, attenuated COX-2 mRNA induction by glutamate and by sPLA2, but this inhibition is overcome by combining 100µM glutamate and 25ng/ml sPLA2. We suggest that glutamate and sPLA2 induce COX-2 gene expression by PAF-dependent mechanisms. (NS 23002).

448.10

DEVELOPMENTAL CHANGES OF POSTSYNAPTIC CALCINEURIN AND IP_3 RECEPTORS IN REGULATING SYNAPTIC TRANSMISSION. *JIN-HUI WANG* & PAUL T. KELLY. Dept. of Neurobiology & Anatomy, Univ. of Texas Houston, TX 77030.*

We have shown that postsynaptic calcineurin (CaN) activity limits synaptic transmission by decreasing Ca^{2+} release via inositol-1,4,5-triphosphate (IP_3) and ryanodine receptor-channels in hippocampal slices of adult rats [Wang & Kelly(1997) *J Neurosci* in press]. Although CaN activity increases dramatically during brain maturation [Tallant and Cheung (1983) Biochem 22, 3630-3635], its role in regulating synaptic activity during development is unknown. Whole-cell patch pipettes were used to record excitatory postsynaptic currents (EPSCs; holding potential, -80 mV), and to perfuse agents that inhibit CaN activity or activate IP_3 receptors into CA1 pyramidal neurons in hippocampal slices from rats between postnatal days (PND) 8-28. Postsynaptic perfusions of a CaN autoinhibitory peptide (50 µM) produced a progressive, age-related potentiation of synaptic transmission (>250% at PND 25-28 vs. 25% at PND 10-11; n=16). Postsynaptic perfusions of adenophostin-A (an IP_3 receptor agonist; 1 µM) induced synaptic potentiation starting from PND 8 (20%) and reaching near maximum (>250%) about PND 21 (n=13). EPSCs recorded with control pipette solution appeared stable during PND 8-24 (n=8). These results show that postsynaptic basal CaN activity that limits synaptic responses and IP_3 receptor-mediated Ca^{2+} release that increases synaptic strength undergo a progressive change during postnatal brain maturation. Western blot results indicate that CaN and a CaN binding protein (FKBP-12) in hippocampal extracts display parallel developmental increase, with maximal levels at PND 22 (n=3). Together with previous results that postsynaptic injections of FK-506, which disrupts FKBP-12 function in anchoring CaN and inhibits CaN activity, did not affect basal synaptic transmission between PND 14-21 [Wang and Kelly (1997) *J Neurosci* in press], we propose that functional convergence of postsynaptic CaN and FKBP-12 does not occur in immature brain.

448.11

RECEPTOR SUBUNIT COMPOSITION AND SINGLE- CHANNEL KINETICS GOVERN THE TIME COURSE OF GLYCINERGIC SYNAPTIC TRANSMISSION IN THE DEVELOPING BRAINSTEM. JH Singer[1]*, JS Isaacson[1], EM Talley[2], DA Bayliss[2], and AJ Berger[1]. [1]Dept. of Physiology and Biophysics, Univ. of WA, Seattle, WA 98195 and [2]Dept. of Pharmacology, Univ. of VA, Charlottesville, VA 22908.

We examined the contribution of channel kinetics to the time course of glycinergic inhibitory postsynaptic currents (IPSCs) in developing rat hypoglossal motoneurons (HMs). Whole-cell and outside-out patch recordings (V_m= -70mV, room temp.) were made from HMs in brainstem slices. Spontaneous miniature IPSCs (mIPSCs) were recorded in the presence of TTX, DNQX, APV, bicuculline, and cadmium. Glycine (1 mM) was rapidly applied (<1 ms) to outside-out, somatic patches, and single-channel currents were studied during steady-state application of 5-10 µM glycine.

In situ hybridization of brainstem slices revealed that glycine receptor (GlyR) α2 mRNA was replaced by GlyR α1 mRNA during early postnatal development (P0-18). In contrast, GlyR β mRNA expression was high and remained unchanged during this time. Single-channel currents recorded in patches from neonate (P0-3) HMs showed a developmental decrease in burst duration relative to those from juveniles (P10-18) (18.3 ms vs. 11.1 ms, n= 9 patches total). Consistent with this change in single-channel properties, the time course of unitary-evoked and spontaneous miniature IPSCs became faster with postnatal development. Synaptic currents were fit with a biexponential function: mIPSC τ_{mean}= 14.2±2.4 ms in neonates and 6.3±0.8 ms in juveniles, a change of 56% (n=21). The time course of currents activated by brief pulses of glycine to outside-out patches was similar to that of mIPSCs, and showed an equivalent developmental decrease (68%, n=38 patches). Patch currents did not desensitize in response to applications of 70-150 ms. These changes in GlyR subunit composition and the resultant channel kinetics indicate that channel deactivation is an important determinant of IPSC decay at all stages of postnatal development.

Supported by NS-33583 to DAB and a NS-14857 and HL-33583 to AJB.

448.12

SIGNAL ENCODING IN SPIKING AND GRADED POTENTIAL NEURONS.

J. Haag* and A. Borst, Friedrich-Miescher-Laboratory of the Max-Planck-Society, Spemannstrasse 37-39, D-72076 Tuebingen, Germany

The large motion-sensitive interneurons located in the posterior part of the third visual neuropile (lobula plate) of the blowfly spatially integrate with their extended dendrites the signals of numerous local motion-sensitive elements. While some of these neurons (e.g. HS-cells) respond to visual motion mainly with a graded shift of their membrane potential, others respond with an increase in spike-frequency (e.g. H1-cells). Since both cell types receive the same synaptic input it is possible to compare the accuracy and reliability by which these different neurons encode visual motion information. We measured the responses of HS- and H1-cells to a pseudo-random velocity waveform where a visual grating is moving along the horizontal axis of the eye. To determine the encoding accuracy of both cell types, we used the reverse reconstruction method (Bialek et al., *Science* 252:1854-1857, 1991; Theunissen et al., J Neurophysiol 75:1345-1364) and calculated the coherence between the stimulus and the neural signals as a function of stimulus frequency. We found that information about visual motion is well preserved in the neural signal of HS- and H1-cells at frequencies up to about 10 Hz. With a coherence value of about 70% HS-cells performed slightly better than H1-cells (coherence value: 60%). The lower coherence value of the spiking neuron is due to its low spontaneous firing frequency which allows to encode inhibitory, null-direction motion stimuli in only a small dynamic range. To disentangle how much coherence is deteriorated by noise and by nonlinear encoding, we measured the signal-to-noise spectra of both cell types. We found that the deviation of the coherence value from 100% for both cell types is partly due to noise and partly due to nonlinear encoding. The amount of nonlinear encoding increases with increasing maximal stimulus velocity in both neurons in about the same way.

This work was supported by the Max-Planck-Society.

1.9

UROENDOCRINE BIOMARKERS OF ESTROGEN ACTIVITY IN OMEN WITH ALZHEIMER'S DISEASE. S. Asthana,* S. Craft, L.D. ker, E. Avery, M.A. Raskind, S.R. Plymate. Geriatric Res., Edu. and nical Center (GRECC), VA Puget Sound Health Care System, attle/Tacoma, WA, and Univ. of Washington School of Med., Seattle, WA.

We have recently reported that treatment with transdermal 17 ß-estradiol straderm™) significantly enhances attention and verbal memory in stmenopausal women with Alzheimer's disease (AD). In an attempt to ntify neuroendocrine biomarkers of estrogen activity in patients with AD, measured plasma concentrations of insulin-like growth factor-I (IGF-I) d its major binding protein IGFBP-3.

Twelve postmenopausal women with probable AD completed the study. x women were randomized to receive a 2-month treatment with 0.05 g/day of transdermal 17 ß-estradiol and the remaining six received a acebo skin patch. Treatment was discontinued after 2-months, and bjects were followed for additional five weeks. Following baseline sessment, subjects were evaluated at weeks 1, 3, 5, and 8 on treatment, and weeks 9, 10, 11, and 13 off treatment. For each testing visit, cognition as evaluated by neuropsychological tests and blood samples were collected measure plasma concentrations of estradiol, IGF-I, and IGFBP-3. In the strogen-treated group, a significant negative correlation (r= -0.93, p=0.02) as observed between mean plasma concentrations of estradiol and IGF-I. Moreover, for subjects treated with estrogen, a significant negative orrelation was found between a measure of verbal memory (i.e., mean cued elayed recall test score of Buschke Test) and mean plasma concentrations ach of IGF-I (r= -0.903, p<0.04) and IGFBP-3 (r= -0.99, p<0.01). No uch significant relationships were identified for the placebo-treated group.

The results of this prospective, controlled clinical study demonstrate that lasma concentrations of IGF-I and IGFBP-3 are potential biologic markers f cognition enhancing efficacy of estrogen in women with AD. Supported y a grant from the Alzheimer's Assoc. and by Ciba-Geigy Corporation.

843.10

THE PUTATIVE ANTI-DEMENTIA DRUG N-(4-ACETYL-1-PIPERAZINYL)-*P*-FLUOROBENZAMIDE MONOHYDRATE (FK960) HAS CONCENTRATION-DEPENDENT ACTIONS ON GLUTAMATERGIC TRANSMISSION IN THE HIPPOCAMPUS. J.P.Hodgkiss, H.M.Marston* and J.S.Kelly, F.I.N.E., Department of Pharmacology, University of Edinburgh, EDINBURGH EH8 9JZ, U.K.

The amelioration by FK960 of memory impairment in rats induced by scopolamine may involve serotonergic, somatostatinergic and cholinergic transmitter systems in the CNS (Yamazaki et al (1996) JPET 279, 1157). We show here that FK960 enhances glutamatergic transmission in rat hippocampal CA1 neurones *in vitro*. Whole cell recordings of excitatory post-synaptic potentials (EPSPs) evoked by stimulation (0.25-0.33 Hz) of the stratum radiatum were made from CA1 neurones at 20°C using a K gluconate-based pipette solution. The slices were exposed to an artificial CSF containing picrotoxin (100µM), bicuculline (10µM) and D-AP5 (25-50µM). FK960 (94-100nM) significantly increased EPSP amplitude by on average 62% (2.68±0.45 mV (SEM, n=6) in control; 4.19±0.71 mV after 22-32 mins in FK960; p<0.008 paired t-test). At 50 nM FK960 the mean percent increase in EPSP amplitude was 24% (1.96±0.62 mV in control; 2.44±0.77 mV in FK960, n=3) and at 200 nM it was 7% (2.52±0.27 mV in control; 2.71±0.38 mV in FK960, n=4) neither change in amplitude was significant, suggesting a bell-shaped dose-response relationship (Yamazaki et al. *ibid*). In 3 experiments in which the recording lasted for more than 55 mins EPSP amplitude gradually fell below control in 200 nM FK960; this was not seen with the other 2 concentrations of FK960. We conclude that over a narrow concentration range FK960 enhances glutamatergic transmission. It has yet to be determined whether the locus of action of FK960 at each of these concentrations is pre- or postsynaptic or a combination of both. The nature of the relationship between glutamatergic transmission and transmitter systems already implicated in the action of FK960 also requires clarification. Supported by Fujisawa Pharmaceutical Co., Ltd.

843.11

STAGE DEPENDENT FORMATION OF AMYLOID PLAQUES, NEURITIC PLAQUES AND PHF-τ-PROTEIN IN CORRELATION TO THE ASSOCIATED INFLAMMATORY REACTION AND TO THE DEGREE OF DEMENTIA IN ALZHEIMER'S DISEASE. D.R. Thal[1,2], T. Arendt[3], M. Holzer[3], G. Waldmann[1], D. Zedlick[3], R. Schober[1]. [1]Department of Neuropathology, Institute of Pathology, [2]Department of Neuroanatomy, Paul Flechsig Institute of Brain Research and [3]Department of Psychiatrics, University of Leipzig, Leipzig, Germany

Alzheimer's disease (AD) is characterized by the progressive accumulation of neurofibrillary tangles and senile plaques. The occupation with neurofibrillary tangles starting in the transentorhinal region and spreading to the limbic system and then to the neocortex is the basis of the staging system of Braak and Braak (Acta Neuropath. 82: 239; 1991). To correlate progressive accumulation of neurofibrillary tangles with the degree of dementia, with the state of the inflammatory reaction and with the formation of amyloid and neuritic plaques and hyperphosphorylated τ-protein (τ-P), we have investigated 160 autopsy cases including all stages of AD and control cases. The frequency of β-amyloid positive plaques, of neuritic plaques and HLA-DR positive microglial cells in the cortex and in the white matter was examined semiquantitativly in immunostained sections of the hippocampal, entorhinal, temporal and occipital cortex and adjacent white matter. The content of τ-P was determined with quantitative ELISA. The degree of dementia (CDR-score) was estimated according to CERAD. All investigated parameters showed an increase up to stage V. The CDR-score increased with increasing stage displaying a linear progression throughout all stages. Although stage VI patients displayed dementia and large numbers of plaques the frequency of plaques and of reactive microglial cells was lower than in stage V. The results show that the occupation of the AD-brain with neurofibrillary tangles is correlated to an increasing degree of dementia throughout all stages. The maximum frequency of amyloid and neuritic plaques and of reactive microglial cells in stage V may indicate resorptive phenomena involving the amyloid burden or the frequency of neurofibrillary tangles with a subsequent shift in staging. Supported by BMBF grant No. 01 KS 9504, TP C1.

843.12

INTERACTION OF PRESENILIN 2 WITH APP. D.E. Merriam, R.M. Moir, A.C. Crowley, D.M. Romano and R.E. Tanzi, W. Wasco*, Genetics and Aging Unit, Department of Neurology, Massachusetts General Hospital, Harvard Medical School, Boston, MA 02129-9142

To date, autosomal dominant mutations in the genes encoding the amyloid ß protein precursor (APP) and presenilins 1 and 2 (PS1, PS2) have been identified and are believed to account for up to 50% of the early onset forms of familial AD (FAD). APP is the precursor of Aß, the 39-43 amino acid peptide that is the main component of senile plaques. PS1 and PS2 are members of an evolutionarily conserved gene family which also includes two *C. elegans* proteins, *spe-4* and *sel-12*. Although it is now clear that the FAD-associated mutations in the presenilins are linked to modifications in the amounts and types of Aß produced, it is not known if the observed changes in Aß production are a result of mutation-induced alterations of a direct interaction between the presenilins and APP, or between the presenilins and other unidentified proteins in the Aß-producing pathway. We have utilized co-immunoprecipitation, *in vivo* crosslinking and modified ELISA assays (see abstract by Moir et al.) to demonstrate that there is a direct interaction between PS2 and APP, and that the PS2 FAD-associated Volga German mutation adversely affects this interaction. In addition, immunofluorescence and subcellular fractionation have been used to demonstrate that APP and PS2 co-localize in the intracellular membranes of the ER and Golgi and that while normal, regulated cleavage of PS2 appears to takes place within the Golgi, an alternative cleavage of PS2, which is more prominently associated with FAD-associated N141I mutant forms of the molecule, takes place in the ER.

This work was supported by a grant from the NINDS. WW is a Pew Scholar.

843.13

CYCLOOXYGENASE-2 (COX2) RNA MESSAGE STABILITY IN ALZHEIMER'S DISEASE (AD) NEOCORTEX. W.J. Lukiw* and N.G. Bazan, LSUMC Neuroscience Center, New Orleans LA 70112, USA

Recent studies indicate that long term treatment by nonsteroidal antiinflammatory drugs (NSAIDs) are beneficial for the prevention of Alzheimer's disease (AD). Our laboratory has shown that inflammatory mediators promote transcriptional activation of cyclooxygenase-2 (COX2) in brain [PNAS 91:5252,1994; JBC 271:24794,1996]. Using RT-PCR analysis and human-specific COX2 and b-actin primers, we have determined in 25 human post-mortem neocortical samples (age range 60-82 yrs, post-mortem interval range 0.7-12.0 hrs) the levels of COX2 RNA message signal in relation to b-actin RNA message levels. Our results indicate a large variation in the signal intensity for the COX2 transcript in control and AD neocortex, ranging from 3.2-10.4% of the b-actin signal in controls to 3.4-13.5% of the b-actin signal in AD affected brain. Although there was a trend for higher COX2 RNA message abundance in AD neocortex to +11.5% of that of controls, it did not reach statistical significance (ANOVA=0.45). We noted a strong positive correlation between the post-mortem interval and the intensity of the COX2 RNA signal (ANOVA=0.006). Linear regression analysis indicated that the COX2 transcript is a relatively short-lived RNA species (half-life~3.5 hr) typical of primary response elements. The individual variability in COX2 RNA message abundance may reflect various degrees of expression of AD-related inflammatory processes.

843.14

SYNAPTIC AND CYTOSKELETAL RNA MESSAGE LEVELS IN ALZHEIMER NEOCORTEX. E.I. Rogaev[1], W.J. Lukiw[2], V.L. Marcheselli[2]* and N.G. Bazan[2], [1]Academy of Medical Sciences, Moscow, Russia, [2]LSUMC Neuroscience Center, New Orleans, LA, USA;

Neuropathology of Alzheimer's disease (AD) neocortex reveals only marginal correlations between the degree of cognitive decline and plaque and tangle density. Deficits in the organization of the synapse have suggested that the integrity of the synaptic contact may be a more meaningful marker for AD. To evaluate the contribution of brain-specific transcription products to the signaling capacity of AD-affected cells, we have quantitated RNA message levels for 12 synapse- and cytoskeletal-related genes in 23 normal and sporadic AD neocortical samples (mean age 68.4 yr; age range 60-82 yr). RNA message levels were evaluated for synaptophysin, synapsin, synaptobrevin, GAP43, NFL, NFM, β-actin, α-tubulin, APP, tau and GFAP. APP and tau RNAs were not found to be significantly altered in abundance. Synaptophysin, synapsin, synaptobrevin, NFL and α-tubulin messages were reduced in AD to 51, 46, 55, 33 and 58 per cent of controls, respectively (p=0.04-0.001). RT-PCR analysis for synaptophysin RNA message, using β-actin as an internal control, confirmed a significant reduction for this synaptic vesicle glycoprotein in AD affected neocortex. In normally aging brain, transcription products for synapse- and cytoskeletal-related genes constitute an abundant RNA message class. We propose that their selective reductions in neocortices afflicted with sporadic AD contribute to the altered synaptic cytoarchitecture characteristic of the AD brain.

441.5

BLOCKADE OF NMDA RECEPTORS POTENTIATES APOPTOSIS INDUCED BY SERUM DEPRIVATION IN CORTICAL CELL CULTURES. F. Terro*, M. Lesort, C. Yardin, J. Hugon. Neurobiol and Cell Path Unit, ERS CNRS 6101, Lab Histol and Cell Biol, Fac. Medicine Limoges - FRANCE

Glutamate (Glu) can induce both apoptosis and necrosis while trophic factor removal leads exclusively to apoptosis. In mature cerebellar granule cell cultures, serum deprivation-induced apoptosis can be prevented by Glu receptor antagonists. In this study, using rat primary neuronal cortical cultures at 9 days *in vitro*, apoptosis was induced by serum deprivation and quantified by DNA staining with DAPI and by detection of DNA fragmentation with the TUNEL procedure. The percentages of apoptosis were 14.6± 0.7% (mean ± SD) and 14.4± 1.4%, respectively in cultures incubated for 24h and 48h in serum containing medium. In 24h serum-deprived cultures the percentages of apoptosis were respectively 26±4.7%, 41.9± 5.2% with MK801 [10 µM] and 40.9± 2.8% with AP-7 [25 µM]. In 48h serum-deprived cultures, apoptosis was 36.8± 2.9%, 53.8±3.6% when MK801 [10 µM] was added and 41.1± 3.7% in presence of CNQX [10 µM]. Some 48h serum-deprived cultures were exposed to Glu or NMDA both used at low concentrations. The percentages of apoptotic neurons were respectively 19.2±3.7% and 24.1±2.6% in serum-deprived cultures treated with Glu 5 µM and NMDA 5 µM. These findings suggest that the blockade of NMDA receptors potentiates apoptosis induced by serum deprivation, while their activation by low concentration of agonists is protective. In this model of apoptosis, the effects of trophic support removal is effeciently reversed by NMDA receptor activation.

441.6

SYNERGISTIC BREAKDOWN OF SYNAPTIC PHOSPHATIDYLCHOLINE AND PHOSPHATIDYLETHANOLAMINE BY SPLA$_2$ AND GLUTAMATE DURING CORTICAL NEURONAL CELL DEATH. E.B. Rodriguez de Turco[1], E. Richardson[1], M. Kolko[1], H.E.P. Bazan[1]*, G. Lambeau[2], M. Lazdunski[2] and N.G. Bazan[1], LSUMC Neuroscience Center, [1]New Orleans, USA and [2]Inst. Pharm. Molec. Et. Cell. CNRS, Valbonne, France.

Cytosolic phospholipase A_2 (cPLA$_2$) is activated by glutamate (Glu). Secretory PLA$_2$ (sPLA$_2$), present in synaptic vesicles (Biochem. J.318:701, 1996), may contribute to Glu neurotoxicity, and we have shown that the sPLA$_2$ type II, OS$_2$ and type III from bee venom (BV), elicit synergy in inducing neuronal cell death (J. Biol. Chem. 271:32722, 1996). We addressed the question of which synaptic membrane phospholipids are hydrolyzed under these conditions. [^{3}H] arachidonic acid labeled cortical neurons in primary culture were treated for 45 min with Glu (80 µM), OS$_2$ (25 ng/ml) and BV (25 ng/ml). Twenty four hours after treatment, [^{3}H] arachidonate lipids labeling was analyzed 24 hours later. Glu preferentially hydrolyzed [^{3}H] PE. After OS2 treatment, degradation of [^{3}H] PC was greater than that of [^{3}H] PE, while both lipids were similarly hydrolyzed by BV. Simultaneous treatment of the cells with OS2 and Glu resulted in a synergistic degradation of PE and to a lesser extent PC, concomitantly with a two-fold higher accumulation of free [^{3}H] arachidonic acid than when the agonists were individually added. Pretreatment of the cells with the NMDA antagonist MK801 blocked the changes induced by Glu, as well as the synergistic or additive responses of sPLA$_2$s and Glu. These results indicate that neurotoxicity induced by Glu-NMDA and sPLA$_2$ involves a sustained activation of degradative pathways that affect different neuronal membrane phospholipids and, when both antagonists are present together, result in a synergistic response leading to neuronal cell death. (NS23002).

441.7

BAX FACILITATES "ISCHEMIC" APOPTOSIS BUT NOT EXCITOTOXIC NECROSIS IN CORTICAL NEURONAL CULTURE. F. J. Gottron[†*], M. M. Behrens[†], C. M. Knudson[‡], S. J. Korsmeyer[‡], and D.W. Choi[†]. † Center for the Study of Nervous System Injury and Dept. of Neurology, ‡ Dept. of Medicine and Pathology and Howard Hughes Medical Institute Washington Univ. School of Medicine, St. Louis, MO 63110.

As a death promoting member of the BCL2-related family of proteins, BAX may play an important role in neuronal apoptosis associated with neurodegenerative disease or acute insults such as ischemia. Cultured mouse cortical neurons undergo apoptosis when exposed for 24 hr to 100 nM staurosporine. This death was greatly attenuated in cultures prepared from *Bax* deficient mice. Similarly, neuronal apoptosis induced in near-pure neuronal cultures by removal of serum for 24 hr was much lower in cultures from *Bax* deficient mice as compared to those prepared from their wildtype littermates.

However, neurons in mixed neuronal-glial cultures prepared from *Bax* null mice were equivalently vulnerable to excitotoxic necrosis as cultures prepared from wildtype littermates. Excitotoxicity was induced by a 5 min exposure to 100 µM NMDA, 24 hr exposure to 100 µM kainate, or 90 min exposure to combined oxygen-glucose deprivation. If however, the prominent excitotoxic component of oxygen-glucose deprivation-induced death was blocked by the addition of MK-801 and 6-cyano-7-nitroquinoxaline-2,3-dione (CNQX), and the duration of insult was extended to compensate for the protective effect of adding glutamate antagonists, then wildtype but not *Bax* gene-deficient neurons underwent apoptosis. These data suggest that BAX facilitates apoptosis of cortical neurons, in response to several insults including oxygen-glucose deprivation. Supported by NIH NINDS grants NS 30337 and NS 32636 (DWC).

441.8

SUPPRESSION OF BUTYRYLCHOLINESTERASE GENE EXPRESSION BY ANTISENSE 5'BChE mRNA INCREASES APOPTOSIS IN EMBRYONIC CHICK RETINOSPHEROIDS. A. Robitzki, A. Mack and P. G. Layer*. Institute for Zoology, Division of Developmental and Neurobiology, Darmstadt University of Technology, D-64287 Darmstadt, FRG.

The enzymes butyryl- and acetylcholinesterase (BChE, AChE) have been suggested to represent key proteins in retinal proliferation and differentiation. We here have transfected reaggregated embryonic chick retinal cells, so-called *retinospheroids* with an antisense 5'BChE-expression vector including 577 bp of the 5' upstream region and the first 106 bp of exon 1 of rabbit BChE. Thus, these cells will produce their own antisense mRNA to suppress the expression of BChE. As verified both on the transcriptional and the translational level, BChE expression and proliferation were suppressed, while AChE expression and morphological differentiation were advanced. As determined by vital propidium iodide uptake, TdT-mediated dUTP nick end labeling (TUNEL) and DNA fragmentation assays, BChE inhibition doubles the rate of programmed cell death. Furthermore, AChE-positive cells increased, whereas rod- and cone-specific opsin immunoreactivity decreased. Interestingly, the red and green cone precursors seem to be almost completely degenerated. These observations suggest that the proliferation marker BChE plays a role in the intracellular balance between proliferation, differentiation and apoptosis. The suppression of BChE is followed by a higher differentiation of AChE-positive cells, and by a higher rate of apoptosis of photoreceptor precursors.

441.9

JNK3 IS REQUIRED FOR STRESS-INDUCED APOPTOSIS OF HIPPOCAMPAL NEURONS *IN VIVO*. *C. Kuan, D. Yang, A.J. Whitmarsh, R.J. Davis, P. Rakic and R.A. Flavell. Section of Neurobiol. and Immunobiol., Yale Univ. Sch. of Med., New Haven, CT 06510. Program in Mol. Med., Univ. of Mass. Medical Sch. Worcester, MA 01605.

JNK3 is the neural isoform of the c-Jun NH_2-terminal kinases (JNK) that are activated by exposure of cells to environmental stress. Its restricted expression to the nervous system as well as its activation by noxious stimuli suggests that JNK3 may mediate stress-induced neuronal apoptosis. To test this hypothesis, we have generated JNK3-deficient mice which develop normally and exhibit remarkable resistance to kainic acid (KA)-induced seizures and apoptosis of hippocampal neurons compared to wild-type littermates (30 mg/kg). The observed neurotoxicity is likely caused by a JNK3-mediated signal transduction pathway since the administration of KA induces phosphorylation of the NH_2-terminal domain of c-Jun within the hippocampus and an increased AP-1 transcriptional activity in the wild-type but not in JNK3-deficient mice. This explanation is further supported by a comparable induction of c-Fos by KA and the equivalent sensitivity to other epileptogenic agents such as pentetrazole between wild-type and mutant mice. Our results suggest that the JNK signaling pathway may be involved in the mechanism of excitotoxicity underlying a variety of neurological diseases.

441.10

MATERNAL DEPRIVATION INDUCES NEURONAL DEATH. L.X. Zhang*[1], G. O. Xing[1], S. Levine[2], R. M. Post[1] & M. A. Smith[3]. [1]Biological Psychiatry Branch, NIMH, Bethesda, MD 20892, [2]Dept. of Psychology, U. of Delaware, Newark, DE, and [3]CNS Diseases Research, DuPont Merck Research Labs, Wilmington, DE 19880

Prolonged separation from the mother interferes with normal growth and development and is a significant risk factor for adult psychopathology. Altered hippocampal function is thought to underlie some of the long-term changes in behavioral sensitivity to stress that occur after early maternal deprivation (DEP). We hypothesized that DEP might increase apoptosis of neurons in the hippocampal formation which continues to develop during the first two postnatal weeks. To identify cells undergoing apoptosis, we labeled the 3' end of DNA fragments with digoxigenin nucleotides using terminal transferase (ApopTag, Oncor). We found that the number of ApopTag-positive cells in the area extending from the hippocampus to the surrounding alveus was doubled following 24 hr of DEP at postnatal day 12. We also observed a dramatic induction of c-fos mRNA in cells located in this same area and extending into the dentate gyrus. ApopTag-positive cells were also increased in the cerebral cortex and some white matter regions. The mechanisms underlying the increase in neuronal death following DEP are not known. However, the distribution of the ApopTag-labeled cells paralleled an observed increase in the expression of Bax (a cell suicide gene) and a decrease in brain-derived neurotrophic factor mRNA levels. Thus maternal separation during critical stages of brain development may affect the structure and function of areas such as the hippocampus which could lead to abnormal behavior as an adult.

(Supported by NIH intramural and extramural funds)

650.7

THE NEURONAL MITOCHONDRIAL PERMEABILITY TRANSITION. Janet M. Dubinsky*, Dept. of Physiology, University of Minnesota, Minneapolis MN 55455.

Elevations in cytosolic calcium and production of reactive oxygen species are hypothesized to contribute to glutamate excitotoxicity by inducing the mitochondrial permeability transition (mPT). The mPT is a nonspecific putative pore in the mitochondrial inner membrane with a nS conductance. MPT induction by calcium, inorganic phosphate, oxidant, or combinations of these is characterized by mitochondrial swelling, mitochondrial depolarization, and inhibition by cyclosporin A (CsA). To provide independent evidence for the existence of the mPT, cultured hippocampal neurons were stained with JC-1 and pretreated with the calcium ionophore, 4Br-A23187. When a high calcium-containing solution replaced the pretreatment high magnesium-containing solution, neuronal mitochondria changed from rod-like structures to very rounded forms, observed with a Leica confocal microscope. Comparable swelling was observed following toxic glutamate treatments (500μM for 5 min). Glutamate-induced swelling was prevented when Ba^{2+} was substituted for Ca^{2+} or when 1μM CsA was added to all solutions. Glutamate-induced neuronal death was ameliorated by 1μM CsA. Dose response curves were shifted to higher doses but the shift in log ED_{50} did not achieve significance (p=0.052). Higher doses of CsA were themselves toxic. Thus the mPT exists in neurons and may contribute to excitotoxic neuronal death. Supported by NIA AG10034 and the Minnesota affiliate, American Heart Association.

650.8

ROLE OF CASPASES IN NMDA-INDUCED APOPTOSIS OF CEREBROCORTICAL NEURONS. Lalitha Tenneti,*[1] Danielle D'Emilia[1], Carol M. Troy[2] and Stuart A. Lipton[1]. [1]Dept. of Neurology, Children's Hospital; Program in Neuroscience, Harvard Med. Schl, Boston, MA 02115, and [2]Dept. of Pathology, Columbia University, NY 10032.

Excessive activation of glutamate receptors is an important mediator of cell death in a number of acute and chronic neurodegenerative diseases. The intracellular processes that mediate this neuronal death are poorly understood. Following mild insults to neurons, *N*-methyl-D-aspartate (NMDA) receptor activation induces apoptosis but with fulminant insults such as high concentrations of NMDA necrosis will intervene (Bonfoco *et al.*, PNAS,1995). Members of the caspase family of cysteine proteases are necessary for neuronal apoptosis both *in vivo* and *in vitro*. To determine the possible role of caspases in NMDA-induced apoptosis, we have utilized two functionally distinct approaches. One is to use a novel peptide ($V\text{-}ICE_{inh}$) that contains the catalytic site of caspases and appears to act as a pseudoenzyme that binds caspase substrates and prevents their cleavage. The other is a peptide (Z-VAD) that inhibits caspase activity. Pretreatment with either $V\text{-}ICE_{inh}$ or Z-VAD protects cultured rat cortical neurons from NMDA-induced apoptosis, but not from necrosis, indicating a selective role for caspases in NMDA-induced apoptosis. Pretreatment with either $V\text{-}ICE_{inh}$ or Z-VAD did not affect NMDA-induced Ca^{2+} influx or mitochondrial membrane potential. In contrast, formation of reactive oxygen species (ROS) and lipid peroxidation during NMDA-induced apoptosis were blocked by both $V\text{-}ICE_{inh}$ and Z-VAD. Our results suggest that while Ca^{2+} influx through NMDA receptors occurs upstream of caspase activation, ROS formation and lipid peroxidation may be downstream events in the pathway leading to neuronal apoptosis. [Funded by NIH grant PO1 HD29587 (S.A.L.) and MDA ; APDF grants (C.M.T)].

650.9

ERYTHROPOIETIN PROTECTS RAT CENTRAL NEURONS FROM NMDA- AND NO-INDUCED APOPTOSIS. Haydar M. Digicaylioglu, Stuart A. Lipton*. Department of Neurology, Children's Hospital and Program in Neuroscience, Harvard Medical School, Boston, MA 02215.

Erythropoietin (EPO), which was recently detected in the mammalian brain, is produced predominantly by astrocytes. EPO receptors (EPO-R) have been demonstrated on cortical and hippocampal neurons. Additionally, human astrocytes induced by cytokines, as well as neurons stimulated by NMDA produce nitric oxide (NO), which can contribute to neuronal damage mediated by formation of peroxynitrite ($ONOO^-$). Erythropoietin production in HepG2 cells has been shown to decrease in the presence of NO donors, implying the existence of an autocrine feedback loop. Conversely, we hypothesized that EPO might feedback in a paracrine manner to protect neurons from NO-related toxicity. To test this, we studied NO-induced apoptosis in cultured rat cerebrocortical neurons in the presence or absence of EPO, and verified apoptosis by a variety of techniques including morphology and propidium iodide staining of permeabilized cells (Bonfoco et al., *PNAS* 1995). Incubation with 300 μM NMDA for 20 min resulted in apoptosis of 47 ± 4.5% of the neurons, but incubation with 5U (0.55 pM) human recombinant EPO decreased this to 20 ± 5%. EPO also decreased neuronal apoptosis due to the NO donors spermine/NO (200 μM) or S-nitrosocysteine (SNOC, 200 μM). An 18 hr incubation in spermine/NO resulted in apoptosis of 42 ± 6.6% of the neurons, and SNOC induced apoptosis in 45 ± 2.2%. Coincident exposure to EPO decreased apoptosis ~2-fold, to 21 ± 1.7% (spermine/NO) and 20 ± 0.6% (SNOC). These findings suggest that EPO may represent an endogenous protective mechanism from NMDA receptor-mediated and NO-related neuronal injury in the mammalian CNS. *Supported by NIH grant P01 HD29587 (to S.A.L.).*

650.10

NEUROPROTECTION BY RECOMBINANT PLATELET-ACTIVATING FACTOR ACETYLHYDROLASE (rPAF-AH) ON NMDA-INDUCED EXCITOTOXICITY IN HIPPOCAMPAL NEURONS. F. Ogden, M.A. DeCoster, and N.G. Bazan*. LSUMC Neuroscience Center, New Orleans, LA 70112

The bioactive lipid, platelet-activating factor (PAF) is generated in brain during seizures and ischemia. Plasma-type recombinant PAF-AH (ICOS, Corp., Inc. Bothell, WA) was used to test the hypothesis that PAF is involved in early events leading to apoptosis in neurons during injury to the brain. Treatment of primary hippocampal neuronal cultures with NMDA (50 μM) for two hours caused a 2-fold increase in apoptosis and a 3-fold increases in excitotoxicity (lactate dehyrdrogenase release). Apoptosis was quantified with TUNEL-Fluorescein and Propidium Iodide staining, fluorescence microscopy, a 3CCD color camera, and 2D graphics analysis software. rPAF-AH (20 μg/ml) was added exogenously to the cultures up to two hours at 37°C prior to treatment with NMDA. NMDA (50 μM) was then added for two hours at 37°C. Following NMDA treatment, the media was changed to remove any exogenous NMDA and rPAF-AH, and the cells were incubated in replacement media containing rPAF-AH (10 μg/ml) for 22 hours. rPAF-AH treatment decreased excitotoxicity by 50% at 30 minutes, 52% at 1 hour, and 45% at two hours of pretreatment time. Apoptosis was decreased by 21%, 42%, and 45%, respectively. Interestingly, rPAF-AH was protective against injury mediated by both NMDA and glutamate treatments, but not against that mediated by kainic acid induced toxicity. Neuroprotection provided by rPAF-AH suggests the involvement of PAF as an injury mediator in excitotoxicity via the NMDA receptor (NIH/NS23002).

650.11

BRAIN DERIVED NEUROTROPHIC FACTOR MEDIATES THE NEUROPROTECTIVE EFFECT OF NMDA IN RAT CEREBELLAR GRANULE CELLS. A. M. Marini*, S. J. Rabin, R. H. Lipsky and I. Mocchetti. Dept. of Neurology and Clinical Investigation, Walter Reed Army Med. Center, Washington, DC, 20307, Depts. of Neurology and Pathology, U. S. U. H. S., Bethesda, MD 20814, and Dept. of Cell Biology, Div. of Neurobiology, Georgetown Univ., Sch. of Med., Washington, DC 20007.

Cerebellar granule cells in culture are vulnerable to glutamate or N-methyl-D-aspartate (NMDA). Paradoxically, pretreatment of these cells with subtoxic concentrations of NMDA (100μM) markedly blocked the neurotoxicity resulting from subsequent exposure to glutamate or NMDA. The NMDA-mediated neuroprotection is antagonized by pretreatment of these cells with protein synthesis inhibitors, suggesting an involvement of protein(s) with neuroprotective properties, most likely neurotrophic factors. This study was undertaken to characterize which trophic factor(s) plays a role in the NMDA-mediated neuroprotective activity. Among the neurotrophins, only brain derived neurotrophic factor (BDNF) prevented glutamate-mediated cell death in cultured cerebellar granule cells (DIV8). Exposure of neurons to subtoxic concentrations of NMDA resulted in an increase in BDNF mRNA beginning at 1 hr, peaking at 3-8 hr and declining by 24 hr. The accumulation of BDNF mRNA, NMDA-mediated, was followed by an increase in trkB tyrosine phosphorylation by 3 hr. Because the effect of BDNF occurs via activation of its high affinity receptor trkB, we examined whether the NMDA-mediated neuroprotection could be blocked by K252a, an inhibitor of trk receptor signal transduction. K252a (5nM) inhibited completely the neuroprotective properties of NMDA. Thus, NMDA, by enhancing synaptic activity, activates an autocrine BDNF loop promoting neuronal survival. Supported by Research Career Development Award NS 01675 and H.H.S. grant NS 29664 to I.M., and DCI 7163 and USU RO9276 to A.M.M.

843.9

NEUROENDOCRINE BIOMARKERS OF ESTROGEN ACTIVITY IN WOMEN WITH ALZHEIMER'S DISEASE. S. Asthana,* S. Craft, L.D. Baker, E. Avery, M.A. Raskind, S.R. Plymate. Geriatric Res., Edu. and Clinical Center (GRECC), VA Puget Sound Health Care System, Seattle/Tacoma, WA, and Univ. of Washington School of Med., Seattle, WA.

We have recently reported that treatment with transdermal 17 ß-estradiol (Estraderm™) significantly enhances attention and verbal memory in postmenopausal women with Alzheimer's disease (AD). In an attempt to identify neuroendocrine biomarkers of estrogen activity in patients with AD, we measured plasma concentrations of insulin-like growth factor-I (IGF-I) and its major binding protein IGFBP-3.

Twelve postmenopausal women with probable AD completed the study. Six women were randomized to receive a 2-month treatment with 0.05 mg/day of transdermal 17 ß-estradiol and the remaining six received a placebo skin patch. Treatment was discontinued after 2-months, and subjects were followed for additional five weeks. Following baseline assessment, subjects were evaluated at weeks 1, 3, 5, and 8 on treatment, and at weeks 9, 10, 11, and 13 off treatment. For each testing visit, cognition was evaluated by neuropsychological tests and blood samples were collected to measure plasma concentrations of estradiol, IGF-I, and IGFBP-3. In the estrogen-treated group, a significant negative correlation ($r= -0.93$, $p=0.02$) was observed between mean plasma concentrations of estradiol and IGF-I. Moreover, for subjects treated with estrogen, a significant negative correlation was found between a measure of verbal memory (i.e., mean cued delayed recall test score of Buschke Test) and mean plasma concentrations each of IGF-I ($r= -0.903$, $p<0.04$) and IGFBP-3 ($r= -0.99$, $p<0.01$). No such significant relationships were identified for the placebo-treated group.

The results of this prospective, controlled clinical study demonstrate that plasma concentrations of IGF-I and IGFBP-3 are potential biologic markers of cognition enhancing efficacy of estrogen in women with AD. Supported by a grant from the Alzheimer's Assoc. and by Ciba-Geigy Corporation.

843.10

THE PUTATIVE ANTI-DEMENTIA DRUG N-(4-ACETYL-1-PIPERAZINYL)-*P*-FLUOROBENZAMIDE MONOHYDRATE (FK960) HAS CONCENTRATION-DEPENDENT ACTIONS ON GLUTAMATERGIC TRANSMISSION IN THE HIPPOCAMPUS. I.P.Hodgkiss, H.M.Marston* and J.S.Kelly, F.I.N.E., Department of Pharmacology, University of Edinburgh, EDINBURGH EH8 9JZ, U.K.

The amelioration by FK960 of memory impairment in rats induced by scopolamine may involve serotonergic, somatostatinergic and cholinergic transmitter systems in the CNS (Yamazaki et al (1996) JPET 279, 1157). We show here that FK960 enhances glutamatergic transmission in rat hippocampal CA1 neurones *in vitro*. Whole cell recordings of excitatory post-synaptic potentials (EPSPs) evoked by stimulation (0.25-0.33 Hz) of the stratum radiatum were made from CA1 neurones at 20°C using a K gluconate-based pipette solution. The slices were exposed to an artificial CSF containing picrotoxin (100µM), bicuculline (10µM) and D-AP5 (25-50µM). FK960 (94-100nM) significantly increased EPSP amplitude by on average 62% (2.68±0.45 mV (SEM, n=6) in control; 4.19±0.71 mV after 22-32 mins in FK960; $p<0.008$ paired t-test). At 50 nM FK960 the mean percent increase in EPSP amplitude was 24% (1.96±0.62 mV in control; 2.44±0.77 mV in FK960, n=3) and at 200 nM it was 7% (2.52±0.27 mV in control; 2.71±0.38 mV in FK960, n=4) neither change in amplitude was significant, suggesting a bell-shaped dose-response relationship (Yamazaki et al. *ibid*). In 3 experiments in which the recording lasted for more than 55 mins EPSP amplitude gradually fell below control in 200 nM FK960; this was not seen with the other 2 concentrations of FK960. We conclude that over a narrow concentration range FK960 enhances glutamatergic transmission. It has yet to be determined whether the locus of action of FK960 at each of these concentrations is pre- or postsynaptic or a combination of both. The nature of the relationship between glutamatergic transmission and transmitter systems already implicated in the action of FK960 also requires clarification. Supported by Fujisawa Pharmaceutical Co., Ltd.

843.11

STAGE DEPENDENT FORMATION OF AMYLOID PLAQUES, NEURITIC PLAQUES AND PHF-τ-PROTEIN IN CORRELATION TO THE ASSOCIATED INFLAMMATORY REACTION AND TO THE DEGREE OF DEMENTIA IN ALZHEIMER'S DISEASE. D.R. Thal[1*], T. Arendt[2], M. Holzer[2], G. Waldmann[2], D. Zedlick[2], R. Schober[1]. [1]Department of Neuropathology, Institute of Pathology, [*]Department of Neuroanatomy, Paul Flechsig Institute of Brain Research and [2]Department of Psychiatrics, University of Leipzig, Leipzig, Germany

Alzheimer's disease (AD) is characterized by the progressive accumulation of neurofibrillary tangles and senile plaques. The occupation with neurofibrillary tangles starting in the transentorhinal region and spreading to the limbic system and then to the neocortex is the basis of the staging system of Braak and Braak (Acta Neuropath. 82: 239; 1991). To correlate progressive accumulation of neurofibrillary tangles with the degree of dementia, with the state of the inflammatory reaction and with the formation of amyloid and neuritic plaques and hyperphosphorylated τ-protein (τ-P), we have investigated 160 autopsy cases including all stages of AD and control cases. The frequency of β-amyloid positive plaques, of neuritic plaques and HLA-DR positive microglial cells in the cortex and in the white matter was examined semiquantitativly in immunostained sections of the hippocampal, entorhinal, temporal and occipital cortex and adjacent white matter. The content of τ-P was determined with quantitative ELISA. The degree of dementia (CDR-score) was estimated according to CERAD. All investigated parameters showed an increase up to stage V. The CDR-score increased with increasing stage displaying a linear progression throughout all stages. Although stage VI patients displayed dementia and large numbers of plaques the frequency of plaques and of reactive microglial cells was lower than in stage V. The results show that the occupation of the AD-brain with neurofibrillary tangles is correlated to an increasing degree of dementia throughout all stages. The maximum frequency of amyloid and neuritic plaques and of reactive microglial cells in stage V may indicate resorptive phenomena involving the amyloid burden or the frequency of neurofibrillary tangles with a subsequent shift in staging. Supported by BMBF grant No. 01 KS 9504, TP C1.

843.12

INTERACTION OF PRESENILIN 2 WITH APP. D.E. Merriam, R.M. Moir, A.C. Crowley, D.M. Romano and R.E. Tanzi, W. Wasco*, Genetics and Aging Unit, Department of Neurology, Massachusetts General Hospital, Harvard Medical School, Boston, MA 02129-9142

To date, autosomal dominant mutations in the genes encoding the amyloid ß protein precursor (APP) and presenilins 1 and 2 (PS1, PS2) have been identified and are believed to account for up to 50% of the early onset forms of familial AD (FAD). APP is the precursor of Aß, the 39-43 amino acid peptide that is the main component of senile plaques. PS1 and PS2 are members of an evolutionarily conserved gene family which also includes two *C. elegans* proteins, *spe-4* and *sel-12*. Although it is now clear that the FAD-associated mutations in the presenilins are linked to modifications in the amounts and types of Aß produced, it is not known if the observed changes in Aß production are a result of mutation-induced alterations of a direct interaction between the presenilins and APP, or between the presenilins and other unidentified proteins in the Aß-producing pathway. We have utilized co-immunoprecipitation, *in vivo* crosslinking and modified ELISA assays (see abstract by Moir et al.) to demonstrate that there is a direct interaction between PS2 and APP, and that the PS2 FAD-associated Volga German mutation adversely affects this interaction. In addition, immunofluorescence and subcellular fractionation have been used to demonstrate that APP and PS2 co-localize in the intracellular membranes of the ER and Golgi and that while normal, regulated cleavage of PS2 appears to takes place within the Golgi, an alternative cleavage of PS2, which is more prominently associated with FAD-associated N141I mutant forms of the molecule, takes place in the ER.

This work was supported by a grant from the NINDS. WW is a Pew Scholar.

843.13

CYCLOOXYGENASE-2 (COX2) RNA MESSAGE STABILITY IN ALZHEIMER'S DISEASE (AD) NEOCORTEX. W.J. Lukiw* and N.G. Bazan, LSUMC Neuroscience Center, New Orleans LA 70112, USA

Recent studies indicate that long term treatment by nonsteroidal antiinflammatory drugs (NSAIDs) are beneficial for the prevention of Alzheimer's disease (AD). Our laboratory has shown that inflammatory mediators promote transcriptional activation of cyclooxygenase-2 (COX2) in brain [PNAS 91:5252,1994; JBC 271:24794,1996]. Using RT-PCR analysis and human-specific COX2 and b-actin primers, we have determined in 25 human post-mortem neocortical samples (age range 60-82 yrs, post-mortem interval range 0.7-12.0 hrs) the levels of COX2 RNA message signal in relation to b-actin RNA message levels. Our results indicate a large variation in the signal intensity for the COX2 transcript in control and AD neocortex, ranging from 3.2-10.4% of the b-actin signal in controls to 3.4-13.5% of the b-actin signal in AD affected brain. Although there was a trend for higher COX2 RNA message abundance in AD neocortex to +11.5% of that of controls, it did not reach statistical significance (ANOVA=0.45). We noted a strong positive correlation between the post-mortem interval and the intensity of the COX2 RNA signal (ANOVA=0.006). Linear regression analysis indicated that the COX2 transcript is a relatively short-lived RNA species (half-life~3.5 hr) typical of primary response elements. The individual variability in COX2 RNA message abundance may reflect various degrees of expression of AD-related inflammatory processes.

843.14

SYNAPTIC AND CYTOSKELETAL RNA MESSAGE LEVELS IN ALZHEIMER NEOCORTEX. E.I. Rogaev[1], W.J. Lukiw[2], V. L. Marcheselli[2*] and N.G. Bazan[2], [1]Academy of Medical Sciences, Moscow, Russia, [2]LSUMC Neuroscience Center, New Orleans, LA, USA;

Neuropathology of Alzheimer's disease (AD) neocortex reveals only marginal correlations between the degree of cognitive decline and plaque and tangle density. Deficits in the organization of the synapse have suggested that the integrity of the synaptic contact may be a more meaningful marker for AD. To evaluate the contribution of brain-specific transcription products to the signaling capacity of AD-affected cells, we have quantitated RNA message levels for 12 synapse- and cytoskeletal-related genes in 23 normal and sporadic AD neocortical samples (mean age 68.4 yr; age range 60-82 yr). RNA message levels were evaluated for synaptophysin, synapsin, synaptobrevin, GAP43, NFL, NFM, β-actin, α-tubulin, APP, tau and GFAP. APP and tau RNAs were not found to be significantly altered in abundance. Synaptophysin, synapsin, synaptobrevin, NFL and α-tubulin messages were reduced in AD to 51, 46, 55, 33 and 58 per cent of controls, respectively ($p=0.04$-0.001). RT-PCR analysis for synaptophysin RNA message, using β-actin as an internal control, confirmed a significant reduction for this synaptic vesicle glycoprotein in AD affected neocortex. In normally aging brain, transcription products for synapse- and cytoskeletal-related genes constitute an abundant RNA message class. We propose that their selective reductions in neocortices afflicted with sporadic AD contribute to the altered synaptic cytoarchitecture characteristic of the AD brain.

343.5

RAT BRAIN ADENOSINE A1 RECEPTOR ANTISENSE DECREASES SPECIFIC ADENOSINE LIGAND BINDING - T.H. Swanson*, S.E. Krahl, S.A. Rivkees, and O.A. Timofeeva - Department of Medicine, Medical College of Ohio, Toledo, OH 43699.

Many inhibitory effects of adenosine in the brain are mediated through adenosine A1 receptors. Blockade of A1 receptors has led to important observations regarding the mechanism of adenosine inhibition. However, many adenosine antagonists have actions which may be independent of A1 receptor inhibition. To study the effects of A1 receptor antagonism further, we developed antisense oligonucleotides to the A1 receptor. Targeting the methionine initiator, 1st intracellular loop, 3rd intracellular loop, and 2nd extracellular loop domains of the A1 receptor messenger RNA, we constructed 20 mer oligonucleotides in an antisense configuration. These oligos were infused into the right lateral ventricle of the rat via osmotic minipumps at 0.45µL/hr for 7 days, along with sense oligos, and saline as controls. Receptor binding assays using standard autoradiography techniques with $^{H}3$ dipropyl, cyclopentylxanthine, demonstrated that the 2nd extracellular loop antisense decreased antagonist binding. The other antisense were either toxic (caused tissue destruction) or ineffective. Saline infusion was not toxic. Longer (14 day) infusions were uniformly toxic. These data are the first to demonstrate an effective antisense oligo to the adenosine A1 receptor in rat brain.

Supported by NIH RO1 #NS33539

343.6

SELECTIVE INDUCTION BY SEIZURES OF THE EXPRESSION OF GAMMA ISOFORM OF THE PEROXISOME PROLIFERATION-ACTIVATED RECEPTOR (PPARγ) IN CEREBRAL CORTEX AND HIPPOCAMPUS. M. Hardy, G. Allan, S. Nguyen, A. Ershov, H.J. Gould* and N.G. Bazan, LSU Medical Center, Neuroscience Center, New Orleans, LA, USA.

Seizure activity is marked by a rapid increase in free fatty acids, eicosanoids, platelet-activating factor and other bioactive lipids. Some of these short-lived messengers may exert long-term effects on neuronal gene expression. The PPARγ is a member of the steroid/retinoid superfamily of ligand-dependent transcription factors. There are three different PPAR subtypes α, β/δ, and γ, each with a specific tissue distribution. PPAR transcriptional activity is stimulated by peroxisome proliferators, including fibrates and fatty acids, and some potential ligands have been identified, including prostaglandin J2 derivatives and leukotriene B4. PPARs are thus thought to allow short-term messengers to stimulate long-term effects. The ability of seizures to activate PPAR expression was assessed in two models, a single electroconvulsive shock (ECS), and kainic acid (KA)-induced status epilepticus. Messenger RNA levels for PPARγ were elevated by 7 hrs post-seizure in the hippocampus, but not the cerebral cortex in the KA model, whereas levels were elevated in the cortex, but not the hippocampus in the ECS model. Levels of PPAR α and β/δ mRNAs were unchanged in both models. PPARγ induction in the KA model was greater in animals showing more severe seizures. The seizure-induced PPARγ expression in brain may be part of an injury-damage response. The cellular localization of this effect and other ongoing studies aims to define if this gene induction is part of a neuroprotective or damaging response. (NIH/NS23002).

343.7

SEQUENCES REQUIRED FOR NEUROTENSIN RECEPTOR GENE ACTIVATION IN A NEUROBLASTOMA CELL LINE. Daniel J. Tavares, Keith Tully, and Paul R. Dobner*. Dept. of Mol. Genetics and Micro., Univ. Mass. Med. Center, Worcester, MA 01655.

N1E-115 neuroblastoma cells differentiate neuronally in response to treatment with DMSO and express the high affinity neurotensin receptor (NTR), providing a model for understanding the factors controlling NTR expression in catecholaminergic neurons. To examine NTR gene expression, RNA was isolated from N1E-115 cells at various times after treatment with 1.5% DMSO and NTR mRNA was quantitated using an RNAse protection assay. Treatment with DMSO resulted in a 4- to 5-fold increase in NTR mRNA levels after 72 hr. To identify promoter sequences required for induction, mouse NTR promoter-luciferase reporter constructs were transfected into N1E-115 cells (+/- DMSO). The starting construct (-1423 to -185 relative to the AUG codon) was DMSO-inducible and displayed low basal expression. Deletion of 5' sequences to -638 resulted in a large increase in basal activity, indicating that a silencer element is located in the deleted region. Further deletion to -443 abolished DMSO induction and greatly diminished basal activity. DNase I footprint analysis identified six protected regions (footprints 1-6). These footprints are located within the silencer region (1), the region that confers high basal and DMSO-inducible expression (2-5), and a promoter proximal region (6). Footprints 2 and 4 are detected only when nuclear extracts from DMSO-induced cells are used. The characterization of proteins that bind to these novel DMSO response elements should provide insights into the signaling mechanisms controlling NTR gene expression during neuronal differentiation (This work was supported by NIH grant RO1 HL33307).

343.8

CO-LOCALIZATION OF THE NEUROKININ 1 RECEPTOR (NK1-R) WITH β-ARRESTINS, G-PROTEIN RECEPTOR KINASES (GRKs) AND G PROTEINS IN THE RAT ENTERIC NERVOUS SYSTEM. K. McConalogue, E.F. Grady*, N.W. Bunnett, Depts Surg. & Physiol. UCSF, San Francisco, CA 94143-0660.

After activation, the neurokinin 1 receptor (NK1-R) is phosphorylated by G protein receptor kinases (GRKs). The receptor may then bind β-arrestins, which disrupt interaction with G proteins and thus mediate desensitization. Little is known about the tissue distribution of GRKs, β-arrestins and G proteins in the enteric nervous system. We have previously shown that in rat kidney epithelial cells transfected with NK1-R there is an altered subcellular distribution of GRKs and β-arrestins after exposure to substance P. Alterations in the subcellular distribution of these proteins suggest a role of the proteins in regulating the NK1-R. We used immunocytochemistry to localize NK1-R with GRK 2 and 3, β-arrestin 1 and 2 or Gq/11 in the rat ileum. Ileum was removed from rats perfused with fixative and postfixed overnight. Frozen serial sections of 5µm were prepared. Immunoreactivities for GRK 2 and 3, β-arrestin 1 and 2, and Gq/11 were detected at the plasma membrane of muscle cells. There was weak cytosolic GRK 2 and 3 immunoreactivity in the soma and in fibers of a subpopulation of myenteric and submucosal neurons. Antisera to β-arrestin 1 and 2 strongly stained superficial vesicles in the soma and fibers of many myenteric and submucosal neurons. The Gq/11 antiserum strongly stained the plasma membrane but not cell bodies of a population of submucous and myenteric neurons. By examining serial sections we determined that β-arrestin 1 and 2 were localized in cell bodies of NK1-R containing neurons. Few cell bodies were positive for GRKs, but those which were also had NK1-R immunoreactivity. All ganglia appeared to have Gq/11 staining, however, only a few ganglia had fibers which were NK1-R positive. Since NK1-R cells contain GRKs and β-arrestins and occur in ganglia where Gq/11 fibers are found, GRKs, β-arrestins and Gq/11 are appropriately distributed to regulate the activity of the NK1-R in the gastrointestinal tract. *β-arrestin 1 and 2 antibody was a generous gift of Dr. R. Lefkowitz. Supported by DK 43207.*

DEVELOPMENTAL GENETICS I

344.1

GENERATION OF NF1 CONDITIONAL KNOCK-OUT MICE. Y. ZHU and L. F. PARADA*, Center for Developmental Biology, Univ. of Texas, Southwestern Medical Center at Dallas, Texas 75235.

Neurofibromatosis type 1 is among the most common human autosomal dominant diseases, affecting 1 in 3500 humans. To understand the role of NF1 during normal development and to create an animal model for human NF1 disease, we have previously generated NF1 null mutant mice by gene targeting techniques. Unfortunately, the homozygous NF1 mice die in utero. Our lab has showed that sensory neurons from NF1 mutant mice no longer require neurotrophins for survival unlike their wild type counterparts (See Klesse and Parada, Abs. Soc. Neuro.). We are not able to extend our studies to the neurons from later developmental stages and into adulthood. We are also unable to assay the developmental consequences and potential tumorgenesis related to this phenotypic change observed in neurons.

To circumvent early lethality of NF1 null mutants, I am attempting to utilize the bacteriophage Cre-loxP system to disrupt the NF1 gene in a tissue- and time-specific manner. I have constructed two versions of targeting vectors. One of the vectors will leave a neo marker within an intron. It is possible that this insertion produces a hypomorphic allele rather than a null allele. In the second construct, the neo gene can be removed by expression of Cre recombinase which minimizes the risk that genetic modifications may affect normal NF1 gene function. The two targeting vectors have been successfully introduced into embryonic stem cells, and used to generate chimeric mice. High percentage chimeric mice for both targeting vectors have been produced.

Upon obtaining NF1 "flox" (flanked by loxPs) mice, I am going to use both viral and transgenic Cre-mediated approaches to disrupt the NF1 gene in a tissue- and time- specific manner. We believe that this system will allow us to define the role of the NF1 gene during neuronal development and tumorgenesis more precisely. This work is supported by NIH-NS34296-02 and National Neurofibromatosis Foundation.

344.2

GENDER DIFFERENCES IN BRAIN VOLUME AND SIZE OF CORPUS CALLOSUM AND AMYGDALA OF RHESUS MONKEY MEASURED FROM *MRI* IMAGES. H. Uno*, M. Franklin, G. Kraemer, S. Shelton, and N. Kalin, Primate Research Ctr., Harlow Primate Lab., and Depts. of Pathology and Lab. Med., and Psychiatry, Sch. of Med., Univ. of Wisconsin, Madison, WI 53715.

Sexual dimorphic structures in the rodent brain are well documented. Although the brain weight of the female rhesus monkey is lighter than that of the male, regional sexual dimorphism is not well known in the brains of nonhuman primates (Cupp and Uemura, 1981). Using a method of MRI image analysis, we measured the whole brain volume and the size of the corpus callosum (mid-sagittal) and amygdala (coronal section) in 41 MRI images of juvenile to adult rhesus monkeys from 8 months to 7.2 years of age. For the brain volume, 14 MRI images (T-1 weighted, 1.3 mm thick, 60 serial coronal images) of 5 male and 3 female monkeys,1.5 to 5.1 years of age, were used. The sizes of the corpus callosum and amygdala were measured in 27 MRI images (T-1 w., 3 mm thick, sagittal and coronal images) of 12 male and 15 female monkeys, 8 months to 7.2 years of age. The results revealed that the brain volume of male monkeys slightly increased with age; 80.5 (cm^3) at 1.5 years and 94.9 at 5.1 years. The brain volume of female monkeys was unchanged from the age of 1.5 to 4 years; the range was 70.9 to 74.8. By the age of 4 years, the average volume of the male brain was 88.2 ± 1.9 (SE) and that of the female brain 72.2 ± 0.7 cm^3. The average area of the corpus callosum increases from 8 months to 3 years; 0.56 (cm^2) to 0.93 in males and 0.45 to 0.66 in females. The average area of the amygdala after the age of 8 months in both genders was unchanged; 1.08 ± 0.03 cm^2. These data suggest that the whole brain volume and the size of the corpus callosum of young adult female rhesus monkeys are approximately 15% smaller than those of young adult males. (Supported by NIH grant RR00167.)

44.1

EFFECT OF DI TOCHROME OXIDASE GENE EXPRESSION ONAL CULTURE OF RAT CORTEX. C. Z... Dept. of Cellular Biol. and Ana., Medical College of Wisconsin, Milwaukee, WI 53226.

Our goal was to determine if depolarization caused any changes in subunit gene expression of cytochrome oxidase (C.O.) in cultured neurons from postnatal rat cortex. We also wished to know if the level of transcription factor (GA-binding protein) for C.O. would be altered by changes in neuronal activity. We analyzed C.O. activity, C.O. subunit mRNAs, and the distribution of GA-binding protein by C.O. histochemistry, in situ hybridization, and immunocytochemistry, respectively. Depolarization was induced in vitro by 20 mM KCl. Under normal conditions, C.O. activity in neurons increased with time in culture. Likewise, mRNA levels of C.O. subunit II (mitochondrial-encoded) and subunit VIa (nuclear-encoded) increased with time in untreated cultures. Moreover, β subunit of GA-binding proteins was found in both cytoplasm and nuclei of cultured neurons. In cultures treated with KCl for two days, there was a significant increase ($p<0.01$) in C.O. activity of neurons. Immunoreactivity of β subunit of GA-binding protein was increased, and was more concentrated in neuronal nuclei in comparison to untreated sister cultures. Furthermore, the levels of C.O. subunit mRNAs was upregulated. Our data indicate that increased depolarizing activity induces transcriptional regulation of cytochrome oxidase in response to heightened energy demand. The β subunit of GA-binding protein may play a role in probing changes in neuronal activity and in adjusting the level of transcription of C.O. subunit mRNAs.

(Supported by NIH grant EY05439).

44.2

APOLIPOPROTEIN D INCREASES IN RAT HIPPOCAMPUS FOLLOWING ENTORHINAL CORTEX LESIONING. M. Danik[1], L. Terrisse[2], D. Dea[1], J. Poirier[1] and E. Rassart[2]. [1]Douglas Hospital Research Centre, McGill University, Montréal, Québec, Canada, H4H 1R3; [2]Département des Sciences Biologiques, Université du Québec à Montréal, Montréal, Québec, Canada, H3C 3P8.

Apolipoproteins E, D, and J are components of plasma lipoproteins. In contrast to other known apolipoproteins (apos), they are synthesized in most tissues, the brain representing a major and seemingly privileged site of expression. These observations suggest that apoE, -D, and -J play an important role locally, particularly in the central nervous system (CNS). Local hippocampal upregulation of apoE and apoJ was previously shown to occur following experimental deafferentation of the dentate gyrus in the rat by entorhinal cortex lesioning (ECL). The increase in mRNA levels for both apos followed similar time courses which correlated with terminal proliferation and early reactive synaptogenesis.

Here, we report that hippocampal apoD transcript and protein levels increase ipsilaterally after ECL showing a time course that is also similar to those of apoE and apoJ. We observed a 54% increase in apoD mRNA levels 4 days post-lesion (DPL) which dropped to 42% after a week (6-8 DPL) and returned to baseline by the end of the second week (14 DPL). These apoD mRNA changes were paralleled by changes in corresponding protein and support the hypothesis of complementary trophic and coordinated roles between the apos following injury to the CNS. In order to gain more insight into the physiological role of these three apos in the CNS, we have investigated apoJ and apoD protein and mRNA levels in several brain regions from apoE-deficient mice. Differences in levels observed in some brain structures will be discussed in relation to local lipid homeostasis.

(Supported by the Fonds de la Recherche en Santé du Québec, the Canadian Medical Research Council and the Alzheimer Society of Canada.)

44.3

IN VITRO BIOSYNTHESIS AND METABOLIC STUDY OF DENTATO-RUBRAL-PALLIDOLUYSIAN ATROPHY (DRPLA) GENE PRODUCT: A PHOSPHORYLATED PROTEIN *IN VIVO*. K. Nakamura*, N. Nukina, M. Yamada, and I. Kanazawa. Dep. of Neurology, Div. of Neurosci., Graduate Sch. of Med. Univ. of Tokyo, Tokyo 113, Japan.

DRPLA is one of the diseases caused by an unstable expansion of a CAG repeat. We previously reported that the apparent molecular weight of DRPLA protein estimated by SDS-PAGE is much larger than that predicted from the amino acid sequences. To resolve this problem, we carried out an *in vitro* translation studies of human DRPLA cDNA and established the stable cell line expressing a mutant DRPLA protein. The molecular weight of expressed gene (64 repeats)product in HeLa cells is 205 kDa and is similar to that of endogenous DRPLA protein. The molecular weight of the primary translation product revealed 178 kDa (10 repeat) and 187 kDa (64 repeat) in SDS-PAGE, which is slightly smaller than the endogenous gene product (190 kDa) expressed in HeLa cells and DRPLA protein in affected brain (190 kDa and 205 kDa). However, they are almost one and a half times larger than the estimated molecular weight (124 and 131 kDa). These data strongly suggested that aberrant electrophoretic mobility of DRPLA protein is mainly caused by its unique amino acid sequence. We also demonstrate that DRPLA protein is a phosphorylated protein and has no N-linked glycosylation in three possible N-glycosylation site by the metabolic labeling and *in vitro* translation study with or without canine pancreas microsome. In addition, we could not detect any significant difference of phosphorylation between mutated DRPLA protein and normal one, suggesting that the phosphorylation is related only to the normal function of this protein.

44.4

ISOLATING RNAS THAT BIND TO THE FRAGILE X FMR1 PROTEIN USING DIFFERENTIAL DISPLAY. R. Denman, W. Ted Brown, and J. R. Currie*. NYS Institute for Basic Research, 1050 Forest Hill Road, Staten Island, NY 10314.

The Fragile X protein, FMR1, is an RNA binding protein known to associate with 60S ribosomal RNA, its own mRNA and approximately 4% of fetal brain mRNAs *via* KH and RGG binding domains. To isolate and characterize the brain RNAs that FMR1 binds, we have employed a novel strategy in which biotinylated FMR1, produced by a coupled transcription-translation system and bound to an avidin solid support, is used to capture FMR1-specific RNAs. The FMR1-bound RNAs are then eluted from the solid support and amplified by differential display (DDRT-PCR). Under ionic conditions where FMR1 binds polyribosomes (150 mM NaCl), normal human parietal cortex RNA bound specifically to the FMR1 solid support. Using five unique primer-pairs, four candidate FMR1-binding RNAs were isolated from an initial screening of the bound RNA. The identities of these RNAs are currently being determined, and the results will be placed in context with the localization and function of other KH-domain and RGG-domain containing proteins.

This work was supported, in part, by NYS Office of Mental Retardation and Developmental Disabilities grant 914-4353A and NIH grant 1146A.

44.5

PHAGOCYTOSIS OF ROD OUTER SEGMENTS (ROS) IS A SELECTIVE TRANSCRIPTIONAL ACTIVATOR OF PEROXISOME PROLIFERATOR-ACTIVATED RECEPTOR GAMMA (PPARγ) IN RETINAL PIGMENT EPITHELIUM (RPE) CELLS. A.V. Ershov, D.M. Linn* and N.G. Bazan. LSUMC Neuroscience Center, New Orleans, LA.

Phagocytosis of used tips of rod outer segments (ROS) by RPE cells is vitally important for maintaining structural and functional integrity of the retina. We found that receptor-mediated specific phagocytosis of ROS induces expression of certain early response genes encoded for transcription factors (Ershov, Lukiw, Bazan, *J. Biol Chem. 271:28458-28462, 1996*). This early gene response can be differentially and specifically modulated by prostaglandins including PGD_2 and its metabolites PGJ_2 and 15d-PGJ_2 which have recently been shown to be natural ligands for PPARγ. We studied the expression of peroxisome proliferator-activated receptors α, β and γ during the phagocytosis of ROS by rat RPE cells in primary cell culture, using competitive quantitative RT-PCR. During phagocytosis of ROS by RPE cells RT-PCR revealed a transient increase in mRNA expression of PPARγ with a peak at 4-6 hr. PPARα and PPARβ mRNA expression was also detected in RPE cells, but no change in the level of expression was observed during ROS phagocytosis. Selective activation of PPARγ may play an important part in regulation of expression of target genes modulated by photoreceptor renewal process (e.g., docosahexaenoic acid and/or prostaglandins) in RPE cells and may comprise a signal transduction mechanism associated with a putative ROS-phagocytosis-receptor of RPE cells. (EY05121).

44.6

HEAT SHOCK PROTEIN 70 IMMUNOREACTIVITY IN THE NORMAL, UNSTRESSED, RAT EYE: A COMPARISON OF CONSTITUTIVE AND INDUCIBLE FORMS. D.O. Dean*, C.R. Kent & M. Tytell. Department of Neurobiology & Anatomy, Bowman Gray School of Medicine, Wake Forest University, Winston-Salem, NC 27157.

Heat shock proteins, or stress proteins, are a group of highly conserved proteins expressed by virtually all organisms. In the eye, many of these proteins are constitutively expressed throughout normal ocular development and aging and/or can be induced by a variety of metabolic stresses, including heat shock and exposure to bright light. In this study, we have examined expression of the constitutive (Hsc70) and inducible (Hsp70) isoforms of the 70Kd heat shock protein in normal, unstressed, rat eyes. While this lab has published previously, studies with the Hsp70 antibody, a new improved fixation procedure has increased sensitivity and permitted visualization of hitherto undetectable staining.

Eyes from male Sprague-Dawley rats (200-300g) were fixed in methacarn and embedded in paraffin. Ten micron thick sagittal sections through the optic nerve were stained with haemotoxylin and eosin, or incubated with the appropriate heat shock protein, or control IgG. Bound antibody was visualized via an avidin-biotin-horseradish peroxidase detection system.

Our results show that both isoforms are present in the eye. Hsc70 immunoreactivity was observed in all layers of the retina, except the outer segments. In retinal pigment epithelium, staining was restricted to cells by the optic nerve-retina junction. Intense staining was also observed in glial nuclei of the optic nerve, while very weak staining was observed in basal and wing cells of the limbal and corneal epithelium. In contrast, Hsp70 immunoreactivity was intense only in the outer nuclear layer and inner segments of the retina. There was also strong Hsp70 staining in basal and wing cells of limbal cornea and a similar, but weaker, pattern in corneal epithelium. No such immunoreactivity was observed in the optic nerve.

In sum, our results indicate that Hsc70 is the predominant isoform in the optic nerve and retina of unstressed rats, while Hsp70 predominates in limbal and corneal epithelium. Supported by NEI grant EY07616.

2950

ANISOMYCIN INCREASES THE SENSITIVITY OF HL-60 CELLS TO ARA-C AND MITOXANTRONE INDUCED APOPTOSIS T.A. Stadheim and G.L. Kucera. Comprehensive Cancer Center of Wake Forest University, Bowman Gray School of Medicine

The fungal toxin, anisomycin, is a potent activator of the c-Jun N-terminal kinases (JNKs) whose activation has been shown to parallel the onset of apoptosis. In this study we used HL-60 human leukemia cells and anisomycin to investigate the role of JNKs in drug-induced apoptosis. While having different mechanisms of action, the anticancer drugs ara-C and mitoxantrone induce HL-60 cells to undergo apoptosis in a dose and time dependent manner. Maximum induction of apoptosis, as assayed by an agarose DNA fragmentation assay, occurred at 6 hours with 10 μM ara-C and 1 μM mitoxantrone. Anisomycin also caused a dose dependent increase in apoptosis over a range of 0.1 to 1000 ng/ml. A submaximal dose and schedule of ara-C or mitoxantrone (0.1 μM for 4 hours) incubated in the presence of 25 ng/ml anisomycin resulted in increased intranucleosomal DNA fragmentation compared to ara-C or mitoxantrone alone. These results suggest that the observed additive increase in apoptosis is the result of JNK activation. Furthermore, the JNK signalling pathway may be a target for the pharmacologic initiation of apoptosis in HL-60 cells.

2951

AGP-1, A NOVEL MEMBER OF THE TUMOR NECROSIS FACTOR FAMILY, INDUCES HEPATIC NECROSIS AND INFLAMMATION IN TRANSGENIC MICE. D.M. Danilenko,* T.M. Hughes,† H.Q. Nguyen,† J. Giles,§ D. Hill,* G.Y. Van,* J.E. Tarpley,* K. Klopchin,¶ the Amgen EST Program, M.J. Johnson§ and W.S. Simonet.† Departments of *Pathology, †Molecular Genetics, §Experimental Hematology and ¶Laboratory Animal Resources, Amgen Inc., Thousand Oaks, CA 91320-1789.

The tumor necrosis factor (TNF) family is a growing group of cytokines which function as mediators of immune regulation, acute and chronic inflammatory responses, and apoptosis. We have identified a novel gene from a murine cDNA library which encodes a polypeptide, termed AGP-1, which has significant homology to the TNF family member Fas ligand. Transgenic mice expressing murine AGP-1 in the liver via an apolipoprotein E promoter had increased hepatocellular apoptosis, as well as multifocal hepatic necrosis and marked chronic cholangiohepatitis with bile duct hyperplasia. Transgenic mice also had evidence of hepatic dysfunction, with marked and significant increases in total serum bilirubin and alkaline phosphatase levels, and moderate but significant increases in hepatic transaminase levels. AGP-1 transgenic mice also exhibited a circulating neutrophilia and lymphocytosis, marked splenomegaly with increased splenic myelopoiesis and lymphoid hyperplasia, increased numbers of osteoclasts, and uterine atrophy or hypoplasia in female transgenic mice, all findings which supported direct or indirect systemic effects of AGP-1. The nucleotide and amino acid sequence of AGP-1 was found to be identical to the sequence reported for TNF-related apoptosis-inducing ligand (TRAIL), a factor which induced apoptosis in a wide variety of transformed cell lines (Wiley, *et. al.* (1995) *Immunity* 3:673-682).

2952

Recombinant platelet-activating factor acetylhydrolase (rPAFAH) decreases NMDA-induced apoptosis in primary hippocampal neurons. Field Ogden, Mark A. DeCoster, and Nicolas G. Bazan. Neuroscience Center and Dept. Ophthalmology, LSU Medical Center, New Orleans, LA. 70112.

The bioactive lipid platelet-activating factor (PAF) is generated in brain during seizures and ischemia. We have used exogenous (plasma-type) rPAFAH (ICOS Corp., Inc. Bothell, WA) to test the hypothesis that PAF is involved in early events leading to apoptosis in neurons during injury to the brain. The cultures were labeled with TUNEL-Fluorescein and Propidium Iodide, digitized using fluorescence microscopy and a 3CCD color camera, with 2D graphics analysis software. At agonist concentrations of 50μM and treatment time of two hours, the greatest degree of apoptosis was observed in NMDA (5.5-fold increase over vehicle-treated control) followed by kainate (3.5-fold) and glutamate (2.7-fold). Preliminary data show that excitotoxicity (lactate dehydrogenase release) due to each agonist correlates with apoptosis. rPAFAH (20 μg/ml) was added to the cultures up to two hours at 37° C prior to treatment with NMDA. NMDA (50μM) was then added for two hours at 37° C. The media was then changed to remove any exogenous NMDA and rPAFAH, and the cells were incubated in media containing rPAFAH (10 μg/ml) for 22 hours. The time-dependent neuroprotective effect of rPAFAH was: 21% neuroprotection at 30 minutes, 42% at one hour, and 45% at two hours. Neuroprotection provided by rPAFAH suggests the involvement of PAF as an injury mediator in excitotoxicity. Further studies will focus on the effect that rPAFAH has on apoptosis as a result of kainate or glutamate stimulation. (NIH/NS23002)

2953

OXIDATIVE STRESS DEVELOPED DURING THE REPERFUSION OF ISCHEMIC HEART INDUCES APOPTOSIS AND DNA LADDERING. *Nilanjana Maulik, Richard M. Engelman and Dipak K. Das* University of Connecticut School of Medicine, Farmington, CT 06030

Inducers of apoptosis include oxygen free radicals and Ca^{2+} which are also implicated in the pathogenesis of myocardial ischemic reperfusion injury. To examine whether ischemic injury is mediated by apoptotic cell death, isolated perfused rat hearts were subjected to 15, 30 or 60 min of ischemia as well as 15 min of ischemia followed by 30, 60 or 120 min of reperfusion. At the end of each experiment, hearts were processed for the evaluation of apoptosis, DNA laddering and gene expression. Apoptosis was studied by visualizing the apoptotic cardiomyocytes by direct fluorescence detection of digoxigenin-labeled genomic DNA using APOPTAG *in situ* apoptosis detection kit. DNA laddering was evaluated by subjecting the DNA obtained from the hearts to 1.8% agarose gel electrophoresis and photographed under UV illumination. The results of our study revealed apoptotic cells only in the 60 and 120 min reperfused hearts as demonstrated by the intense fluorescence of the immunostained digoxigenin-labeled genomic DNA when observed under fluorescence microscopy. None of the ischemic hearts showed any evidence of apoptosis. These results corroborated with the findings of DNA fragmentation which showed increased ladders of DNA bands in the same reperfused hearts representing integer multiples of the internucleosomal DNA length (about 180 bp). The presence of apoptotic cells and DNA fragmentation in the myocardium were abolished by preperfusing the hearts in the presence of superoxide dismutase and catalase, which also removed the oxidative stress developed in the heart. Taken together, these results clearly demonstrate that oxidative stress developed in the ischemic reperfused myocardium induces apoptosis.

2954

APOPTOSIS AND RELATED GENE EXPRESSION IN A SWINE MODEL OF MYOCARDIAL ISCHEMIA-REPERFUSION INJURY Z.G. Li, L.Williams, S.Snow, G.Turi, C.Whyzmuzis, S.Horowitz and W.Scott (SPON: F.Homeidan) Winthrop-University Hospital, SUNY Stony Brook, Mineola, NY11501

To investigate whether apoptosis (programmed cell death) is a feature of myocardial ischemia/reperfusion injury (I-R injury) in a swine model, 20 pigs were subjected to 50 minutes of ischemia (by clamping the left anterior descending coronary artery), followed by 60 minutes of reperfusion. Apoptotic myocytes were evident in the injured myocardium as detected by the TUNEL (Terminal deoxynucleotidyl transferase-dUTP-Nick-End Labeling) assay. Apoptosis was also confirmed by the presence of nucleosomal ladders when myocardial DNA was analyzed by agarose gel electrophoresis. The extent of apoptosis was quantified by computer-aided image analysis. In the regions of frank I-R injury, the apoptotic index (per cent of TUNEL positive cells per field) was 39.2 +/- 11.1% (Mean +/- SE); whereas in the unaffected areas the apoptotic index was 0.9 +/- 0.5%, P<0.01. We have further studied regulation of apoptosis in myocardial I-R injury. The proteins Fas/APO-1 and interleukin-1 β converting enzyme (ICE) act as regulators of apoptosis. Western blot analysis showed that Fas/APO-1 and ICE were 2.5-fold and 3.6-fold higher, respectively, in the injured myocardium relative to the control areas. These observations provide evidence that apoptosis occurs in the swine model of myocardial I-R injury and suggest that Fas/APO-1 and ICE pathways are involved in regulation of myocardial apoptosis. Perhaps therapies targeted to steps along the pathway to apoptosis could mitigate myocardial I-R injury. Support: American Heart Association and Winthrop-University Hospital.

2955

INFLAMMATORY CYTOKINES INDUCE APOPTOSIS IN QUIESCENT LUNG PERICYTES (PC) IN VITRO. J. Khoury and D. Langleben. Lady Davis Institute, SMBD Jewish General Hospital, Montreal, Québec, Canada H3T 1E2.

Pulmonary hypertension (PH) often develops during sepsis-induced Adult Respiratory Distress Syndrome (ARDS). Remodelling and narrowing of the microvasculature, in part from proliferation of vascular pericytes, contibutes to the PH. Sepsis causes release of lipopolysaccharide endotoxin (LPS) and inflammatory cytokines. We have previously shown that LPS can directly stimulate PC growth in vitro, but that the cytokines interleukin-1ß (IL-1), tumor necrosis factor-α (TNF), and interferon-Γ (IFN), or a mixture of them (MIX, 5U/ml IL-1, 100U/ml IFN, and 500U/ml TNF), do not. Moreover, cytokines have been reported to induce apoptosis in smooth muscle-like cells, and we have shown that MIX reduces LPS-induced growth in previously quiescent PC. Therefore, we asked whether MIX or individual cytokines could induce apoptosis in PC. Rat lung PC were either grown in MCDB-131 medium + 10% FBS, or growth arrested in MCDB-131 + 0.3% BSA for 72h, and then exposed to LPS, MIX or cytokines for 3 to 7 days. DNA was then extracted and electrophoresed to look for DNA laddering as a sign of apoptosis. In proliferating PC, there was no DNA laddering with MIX or cytokines. However, in quiescent PC, LPS itself did not induce laddering, but MIX induced laddering in the presence or absence of LPS. Thus, a MIX of inflammatory cytokines, as might be found in sepsis, might alter the effects of LPS on PC in vivo.
Support: Fonds de la Recherche en Sante du Quebec.

894.11

RELATIONSHIP BETWEEN GLUTAMATE-INDUCED $[Mg^{2+}]_i$ CHANGES AND EXCITOTOXICITY IN CULTURED FOREBRAIN NEURONS. C. Cheng*, A.K. Stout and I.J. Reynolds. Dept. of Pharmacology, University of Pittsburgh School of Medicine, Pittsburgh, PA 15261.

It has been previously shown in our laboratory that the same glutamate stimuli that are normally considered excitotoxic in our neuronal cell cultures are also capable of producing millimolar increases in intracellular free magnesium ($[Mg^{2+}]_i$) (Brocard *et al.*, Neuron **11**: 751-757, 1992). However, there is cell to cell variability in the magnitude of the glutamate-induced $[Mg^{2+}]_i$ changes; therefore in this study, the correlation between glutamate-stimulated increases in $[Mg^{2+}]_i$ and neuronal toxicity is directly tested. Our working hypothesis is that the magnitude of glutamate-induced $[Mg^{2+}]_i$ changes determines cell survival. Cultured forebrain neurons from embryonic rats were stimulated with glutamate while $[Mg^{2+}]_i$ was simultaneously monitored using magfura-2. Subsequently, cell viability of the same individual cells was then monitored for up to 24 hrs post stimulation using propidium iodide. Preliminary results indicate that the neurons that survive a 5 min stimulation with 100μM glutamate/10μM glycine have a significantly lower change in the magfura-2 ratio than cells that do not. This suggests that agonist-induced $[Mg^{2+}]_i$ changes may be an indicator of the excitotoxic potential of a stimulation. Currently, we are investigating possible mechanisms underlying the variability in glutamate-induced $[Mg^{2+}]_i$ changes

Supported by NS 34138, GM 08424, and the American Heart Association.

894.12

MODULATION OF NEURONAL SENSITIVITY TO GLUTAMATE BY SECRETORY PHOSPHOLIPASES A_2($sPLA_2$s). M. A. DeCoster* and N. G. Bazan. LSU Medical Center, Neuroscience Center, New Orleans, LA 70112.

We have previously described the neurotoxic effects of purified $sPLA_2$s from snake and bee venom on cortical neurons *in vitro* (Kolko et al., JBC, 1996). We reported that the toxicity of $sPLA_2$s (10-25 ng/ml) and glutamate (GLU) (80 μM)demonstrated a synergistic action. Here we show that at non-toxic concentrations of GLU (1 μM), the presence of $sPLA_2$ (10-50 ng/ml) expresses synergistic toxicity. Furthermore, we have investigated intracellular calcium concentration ($[Ca^{2+}]_i$) dynamics as a possible mechanism of action for $sPLA_2$s and GLU. We have found that $sPLA_2$ alone (10-50 ng/ml), does not cause calcium flux into neurons, though these concentrations were slightly toxic. In fact, these concentrations of $sPLA_2$s (50 ng/ml) often obliterated the spontaneous calcium oscillations we observed in the neurons. When cortical neurons were treated with 1 μM GLU, calcium influx measured by confocal microscopy showed that $[Ca^{2+}]_i$ returned 90% to baseline in 80 secs. In contrast, when $sPLA_2$ (25 ng/ml) was added 3 minutes before addition of 1 μM GLU to neurons, the calcium influx was sustained, with $[Ca^{2+}]_i$ returning only 10% to baseline. These results indicate that $sPLA_2$ and GLU act synergistically, by modulating $[Ca^{2+}]_i$ dynamics, to alter neuronal sensitivity to excitation and excitotoxicity. (NS 23002).

EXCITATORY AMINO ACIDS: EXCITOTOXICITY III

895.1

EXCITOTOXICITY, CELLULAR CALCIUM SIGNALING AND MITOCHONDRIAL (DYS)FUNCTION IN CULTURED HIPPOCAMPAL CELLS

J. Keelan, O. Vergun, L. Patterson and M. R. Duchen*. Department of Physiology, University College London, London. WC1E 6BT. U.K.

Glutamate toxicity in the brain is believed to reflect cellular Ca^{2+} overload, in particular as a consequence of Ca^{2+} influx through NMDA channels. The specific mechanisms which couple activation of the NMDA channel to glutamate excitotoxicity remain incompletely defined Studies suggest that the underlying pathophysiology involves impaired mitochondrial function in response to increased cellular $[Ca^{2+}]$ possibly combined with the increased production of reactive oxygen species (ROS) from the mitochondrial respiratory chain.

We have used fluorescence imaging techniques to probe the consequences of glutamate receptor activation for changes in cellular $[Ca^{2+}]$ (using the Ca^{2+} sensitive fluorescent dyes fura-2 and rhod-2) and for mitochondrial potential (using the potentiometric probe rhodamine 123)

Hippocampal neurons exposed to toxic concentrations of glutamate (100 μM) under conditions that promote opening of the NMDA channel (Mg^{2+}-free, 10μM glycine) exhibited an increased cytosolic $[Ca^{2+}]$ and mitochondrial depolarization. The degree of mitochondrial depolarization for a given Ca^{2+} load varied significantly amongst the neuronal population Comparison of the mitochondrial responses to glutamate and to depolarization by 50 mM potassium suggest that a given $[Ca^{2+}]$ load is more likely to cause significant mitochondrial depolarization in response to NMDA receptor activation than to influx through voltage-gated calcium channels. Both forms of excitation appear to be associated with mitochondrial calcium uptake, as collapse of the mitochondrial membrane potential using the uncoupler FCCP altered the shape of the Ca^{2+} transients to both stimuli. It is also notable that comparable changes in calcium in the underlying glial cells, probably driven by activation of metabotropic glutamate receptors were far less likely to be associated with mitochondrial depolarization.

These data suggest that while a rise in mitochondrial $[Ca^{2+}]$ uptake is likely to be involved in glutamate toxicity, other features of the response to NMDA receptor activation are likely to contribute to the precipitation of mitochondrial dysfunction. We will examine further the basis for these responses and for the NMDA-induced mitochondrial dysfunction

(We thank The Wellcome Trust and the Royal Society for support).

895.2

EFFECTS OF OXIDATIVE STRESS AND GLUTAMATE RECEPTOR ACTIVATION ON MITOCHONDRIAL MEMBRANE POTENTIAL IN RAT FOREBRAIN NEURONS

J. Scanlon* and I.J. Reynolds. Dept. of Pharmacology, University of Pittsburgh School of Medicine, Pittsburgh, PA 15261.

Mitochondria may mediate neuronal injury via the activation of a large, non-selective pore which spans the mitochondrial inner membrane. Opening of this permeability transition pore (PTP) is sensitive to changes in $[Ca^{2+}]_i$ and oxidation of critical dithiols associated with the pore. We examined whether glutamate-receptor stimulation and oxidative stress interact to affect activation of the PTP. Mitochondrial membrane potential ($\Delta\Psi$) was measured in intact rat forebrain neurons with the ratiometric fluorescent dye JC-1 using a laser scanning confocal imaging system. Depolarization induced by 100 μM glutamate was Ca^{2+}-dependent and was inhibited by cyclosporin-A, a known PTP antagonist. Application of hydrogen peroxide (0.3-3mM) decreased $\Delta\Psi$ in a manner that was independent of the presence of extracellular Ca^{2+} and was not affected by the addition of cyclosporin-A. Our results also show that oxidative stress and NMDA-receptor activation interact to produce decreases in $\Delta\Psi$ that are greater than the response to either stimulant alone. The combined effect of peroxide and glutamate was Ca^{2+}-dependent and was partially inhibited by cyclosporin-A. Since activation of the PTP can occur as a result of dithiol cross-linking, the sulfhydryl reducing agent dithiothreitol (DTT) was examined for its effects on $\Delta\Psi$. 5 mM DTT both prevented and reversed the loss of $\Delta\Psi$ induced by hydrogen peroxide. In contrast, DTT enhanced the loss of $\Delta\Psi$ when coapplied with glutamate, consistent with an effect at the NMDA-receptor redox modulatory site. Our results suggest that oxidants can increase the sensitivity of mitochondrial depolarization to an excitotoxic stimulus.

Support Provided By: American Heart Association (IJR) and its Western Pennsylvanian Affiliate (JMS).

895.3

UNDER GLUCOSE DEPRIVATION GLUTAMATE PROTECTS RETINAL NEURONS A. C. Rego, M. S. Santos and C. R. Oliveira#, Center for Neurosciences of Coimbra, Department of Zoology and Faculty of Medicine, University of Coimbra, 3000 Coimbra, Portugal

Excitotoxic degeneration is a well established phenomenon that occurs during acute or chronic neurodegenerative diseases. The activation of ionotropic excitatory amino acid receptors induces intracellular Ca^{2+} rises and subsequent free radical formation. Moreover, retina lesioning caused by glycolysis inhibition is prevented in the presence of NMDA antagonists. The aim of our study was to analyze the response of retinal neurons when submitted to glutamate exposure under glucose free conditions and further recovered in glucose medium. Neuronal viability was analyzed by following the reduction of MTT. Neuronal toxicity was higher in cells submitted to low glutamate concentrations (10-100 uM) than to high glutamate concentrations (10 mM) in glucose free medium. Similar results were observed in the presence of 2 mM AOAA (aminooxy acetic acid), an inhibitor of GABA deamination, suggesting that protective effects of high glutamate doses depend upon its metabolic utilization. Analysis of endogenous amino acids showed that the extra cellular increase in glutamate concentration was followed by an increment in intracellular glutamate and a significant decrease in GABA. However, extracellular GABA levels increased. This increment in GABA release seemed to be of major importance in regulating the excitotoxicity of glutamate. ATP/ADP significantly decreased in cells submitted to 10 mM glutamate in glucose free medium. Under these conditions, glutamate inhibited the O_2 consumption and decreased the mitochondrial membrane potential. These data indicate that glutamate, when present in high concentrations, can be used as a metabolic substrate, protecting retinal neurons from excitotoxicity. This effect may be of a major relevance during cell recovering from metabolic dysfunctions.

This work was supported by JNICT (Portuguese Research Council) and the Human Capital Mobility Program (EU) Proposal nº ERB 4050 PL 932039

895.4

INHIBITION OF EXCITOTOXICITY IN THE PRESENCE OF HIGH EXTRACELLULAR POTASSIUM CONCENTRATIONS DEPENDS ON MITOCHONDRIAL FUNCTION. L. Kiedrowski*. The Psychiatric Institute, University of Illinois at Chicago, IL 60612.

During brain ischemia, glutamate (GLU) acts on neurons at high extracellular K^+ concentrations ($[K^+]_e$), which can reach 60-80 mM. To determine in primary cultures of rat cerebellar granule cells (CGCs) whether an increase in $[K^+]_e$ during excitotoxic exposure to GLU affects Ca^{2+} homeostasis, and neuronal survival following GLU withdrawal, CGCs were exposed for 15 - 90 min at 37 °C to GLU (100 μM) and glycine (10 μM) applied in Mg-free Locke's buffer containing 5 mM glucose and various K^+ concentrations (balanced with Na^+). Following the exposure, CGCs were returned to the conditioned medium and their viability was monitored for up to 4 days. Increasing $[K^+]_e$ from 5.6 to 60 mM: (1) reduced the GLU-mediated $^{45}Ca^{2+}$ accumulation, (2) prevented overload of mitochondria with Ca^{2+}, (3) completely antagonized the GLU-elicited neuronal death. If, however, during the exposure to 60 mM K^+ the CGCs were deprived of glucose, mitochondrial Ca^{2+} overload and neuronal death promptly occurred. The glucose deprivation-elicited neurotoxicity observed at 60 mM $[K^+]_e$ was inhibited by CNQX (10 μM) or MK-801 (10 μM), indicating that the activation of both AMPA/kainate and NMDA receptors was involved. The GLU-mediated $^{45}Ca^{2+}$ accumulation was enhanced either by inhibition of the plasma membrane Ca^{2+} pump with eosin (300 μM), or by glucose deprivation combined with inhibition of mitochondrial ATP synthase with oligomycin (3 μg/ml). These results suggest that, at 60 mM K^+, GLU is not neurotoxic as long as cellular energy reserves are sufficient to fuel the plasma membrane Ca^{2+} pump, which by extruding Ca^{2+} prevents mitochondrial Ca^{2+} overload. When there is a decline in the activity of the pump due to an energy deficit, Ca^{2+} starts to overload mitochondria, which leads to neuronal death. This sequence of events may be relevant to the mechanism of neuronal death in ischemia in vivo.

1891

A SH3 Binding Site Is Required for Activation of c-Jun N-terminal Kinase Kinase-1 (JNKK-1) N. Purcell, and A. Lin (SPON: T. Lincoln). University of Alabama at Birmingham. Birmingham, AL 35294

c-Jun N-terminal kinase-activating kinase (JNKK-1), a dual specificity tyrosine and threonine protein kinase, is a distant member of the MEK family. JNKK-1 is phosphorylated and activated by MEKK-1 and in turn phosphorylates and activates JNK. Activated JNK stimulates transcriptional activity of c-Jun by phosphorylating Ser63 and Ser73 residues located within c-Jun N-terminal transactivation domain. The MEKK-1->JNKK-1->JNK cascade mediates cell's responses to various oncogenes and extracellular stimuli including growth factors, cytokines, UV-irradiation, and protein synthesis inhibitors. Therefore, the JNK cascade may play a critical role in cell physiological and pathological events. Activation of JNKK-1 by oncogenes and various extracellular stimuli most likely occurs through protein phosphorylation. Yet, other mechanisms may also be involved in regulating JNKK-1 activity. Here we show that JNKK-1 activation by MEKK-1 depends on a potential src homology domain 3 (SH3) binding site located in its carboxyl (C) terminal. Mutation of the SH3 binding site, PATPSSP to AATASSA, completely abolished the activation of JNKK-1 by MEKK-1. These findings suggest there may be a SH3-domain containing protein which regulates JNKK-1 through interacting with its C-terminal SH3 binding site. Therefore, protein-protein interaction may play a role in regulation of JNKK-1 activity by extracellular stimuli.

1892

IDENTIFICATION AND CHARACTERIZATION OF HYPOXIA-REGULATED PHOSPHOPROTEINS (HRPPs) IN PC12 CELLS. Dana Beitner-Johnson and David E. Millhorn, University of Cincinnati, Department of Molecular and Cellular Physiology, Cincinnati, OH 45267-0576.

Hypoxic/ischemic trauma is a primary factor in the pathology of various cardiovascular, cerebral, and pulmonary disease states. Yet, very little is known about the intracellular signaling pathways involved in cellular responses and adaptations to hypoxia. Protein phosphorylation and dephosphorylation regulate the function of a multitude of substrate proteins. Given the universal role of protein phosphorylation in signal transduction, we hypothesized that O_2-related signals are also mediated, at least in part, by protein phosphorylation. Oxygen-sensitive PC12 cells were exposed to hypoxia (5% O_2) for various times. Cells were then harvested and subjected to endogenous phosphorylation. That is, broken cell preparations were incubated with γ-[^{32}P]-ATP in the absence or presence of various activators of protein kinases. Reactions were terminated and subjected to SDS-polyacrylamide gel electrophoresis followed by autoradiography. After a 3 hour exposure to hypoxia, the majority of phosphoproteins detected did not display alterations in phosphorylation levels compared to control (normoxic) cells. However, seven hypoxia-regulated phosphoproteins (HRPPs) were identified, with estimated M_r of 114, 90, 84, 60, 51, 42, and 28 kD. In cells exposed to hypoxia, HRPPs -114, -60, and -42 incorporated increased levels of ^{32}P compared to control cells, whereas hypoxia decreased levels of ^{32}P incorporation into HRPPs -90, -84, -51, and -28. Further studies are currently underway to identify these proteins and to determine whether hypoxic regulation of HRPPs occurs at the level of phosphorylation state, total amount, or both (supported by R37 HL 33831).

1893

HYPOXIA INDUCES DEPHOSPHORYLATION AND INACTIVATION OF MAP KINASE IN PC-12 CELLS.

P. William Conrad, David E. Millhorn, and Dana Beitner-Johnson. University of Cincinnati. Department of Molecular and Cellular Physiology, Cincinnati, Ohio 45267-0576

Oxygen is a strict requirement for normal mammalian cell function. PC-12 cells are an oxygen sensitive cell line that responds to hypoxia with alterations in ionic conductances and gene expression. The intracellular mechanisms by which organisms detect and respond to alterations in oxygen tension remain largely unknown. However, the pathways by which extracellular signals mediate biological effects almost invariably involve protein phosphorylation. As a first step towards identifying intracellular signaling pathways that are regulated by hypoxia, we examined the effect of hypoxia on MAP kinase. MAP kinase is a critical element in growth factor receptor signaling and requires both tyrosyl and threonyl phosphorylation for activation. A three hour exposure to hypoxia (5% O_2) decreased nerve growth factor (NGF)-induced tyrosine phosphorylation of p42 and p44 MAP kinase by 50%, without a change in the total amounts of p42 and p44 MAP kinase. Hypoxia also induced an 80% decrease in MAP kinase enzyme activity. The hypoxia-induced dephosphorylation of MAP kinase was first observed after 1 hour exposure to hypoxia, and persisted for up to 72 hours of hypoxia. Thus, hypoxia appears to oppose the effects of NGF, by diminishing MAP kinase activity. Current studies are underway to determine whether the upstream activators of MAP kinase (Ras, Raf, MEK) are also regulated by hypoxia. (R37HL33831)

1894

The B' γ subunit of Protein Phosphatase 2A is phosphorylated by cGMP-dependent protein kinase.

P. Komalavilas, A. A. DePaoli-Roach, and T. M. Lincoln. Department of Pathology, University of Alabama at Birmingham, Birmingham, AL 35294 and Department of Biochemistry and Molecular Biology, Indiana Univ. School of Medicine, Indianapolis, IN 46202.

Nitric oxide regulates vascular tone by elevating smooth muscle cell cGMP levels. Activation of cGMP-dependent protein kinase (PKG) results in the lowering of intracellular Ca^{2+} levels producing relaxation. Previous studies have shown that PKG stimulates the calcium- activated K^+ channel by dephosphorylation. To further understand the mechanism of the effects of PKG on cell function, we examined the phosphorylation of the B' γ subunit of protein phosphatase 2A (PP2A) by PKG. The B' γ subunit was expressed in E.coli and purified on a Ni-NTA resin column. The eluted protein was phosphorylated using PKG and the catalytic subunit of cAMP-dependent protein kinase (PKA) *in vitro*. The results demonstrated that the B' γ subunit is phosphorylated in a time-dependent fashion by both PKG and PKA upto a stoichiometry of 1.8 mol of phosphate/mol of the protein. Using comparable amounts of PKG and PKA kinase activity, PKG catalyzed maximal phosphorylation within 2 min, whereas PKA catalyzed maximal phosphorylation in 10 min. These results suggest that the regulation of PP2A activity may occur through the phosphorylation of the B' γ subunit.

1895

Kainic Acid (KA) activates JNK, p38 and the p42 mitogen-activated protein kinases (MAPK) in hippocampal neurons but not in hippocampal aastrocyte cultures.

Mark A. DeCoster[1], Pranab K. Mukherjee[1], Brandon S. Black[1], Roger J. Davis[2] and Nicolas G. Bazan[1]. [1]LSU Medical Center, Neuroscience Center and Department of Ophthalmology, New Orleans, LA 70112 and [2]Howard Hughes Medical Institute Research Laboratories, Univ. Mass. Medical Center, Worcester, MA 01605

Neuronal stimulation by excitatory amino acids (EAAs) is known to activate MAPKs. However, many previous studies have used embryonic tissue or immortalized cell lines and the role of glial cells has not been addressed. Here we have used primary cultures of hippocampal neurons and hippocampal astrocytes, to investigate activation of JNK, p38, and MAPKs (p42 and 44) after transient exposure to KA. After 10 minutes of exposure to 50 uM KA, activation of JNK, p38, and p42 MAPK was significantly elevated in hippocampal neurons compared to controls. This activation was blocked by the KA receptor antagonist CNQX (5 uM). These treatments were also neurotoxic and were protected by CNQX (5 μM). No significant activation of JNK, p38, or p42 MAPK was detected in hippocampal astrocyte cultures exposed to KA under the same conditions. While basal levels of JNK and p38 were significantly lower in hippocampal astrocyte cultures than in neuronal cultures, basal p42 MAPK levels were comparable. These results indicate that while astrocytes may have similar basal levels of p42 MAPK compared with hippocampal neurons, MAPK, as well as JNK and p38 are not activated in astrocytes after transient exposure to KA. In contrast, the activation of p42 MAPK, JNK, and p38 by KA exposure to hippocampal neurons is significant and correlates with subsequent neurotoxicity. (NIH/NS 23002)

1896

Differential activation of p38, JNK, and mitogen-activated protein kinases (MAPKs) by platelet activating factor (PAF), glutamate(GLU), and kainate (KA) in primary hippocampal neurons. Pranab Mukherjee[1], Mark A. DeCoster[1], Roger J. Davis[2] and Nicolas G. Bazan[1]. [1]Neuroscience Center and Dept. of Ophthalmology, LSU Medical Center, New Orleans, LA 70112 and [2]Howard Hughes Medical Institute Research Laboratories, Univ. Mass. Medical Center, Worcester, MA 01605.

The short-lived bioactive lipid PAF modulates neuronal responses to excitatory amino acids (EAAs). Protein kinases are part of signaling cascades transmitting extracellular receptor-mediated events to the cell interior. PAF (100 nM), KA (50 μM), or GLU (50 μM) all significantly activated p38, JNK, and MAPKs. Activation of these kinases by PAF was achieved by treatment for 60 minutes at 37° C, while activation by KA and GLU was significant after treatment for 15 minutes at room temperature. Activation by PAF, KA, or GLU was blocked by BN 50730 (1 μM), CNQX (5 μM), or MK-801 (300 nM), respectively. The PAF receptor antagonist BN 50730 blocked KA, but not GLU activation of the kinases. When neurons were activated with PAF plus KA or GLU, PAF plus KA showed no additive activation, while PAF plus GLU demonstrated an additive activation of p38, JNK, and MAPK. These results support the idea that PAF and KA stimulate common signaling cascades involving protein kinases, while PAF and GLU may use independent routes. This work raises the possibility that differential activation of protein kinase signaling cascades in neurons by GLU receptor subtypes may be modulated by the bioactive lipid, PAF. (NIH/NS 23002).

647

INVOLVEMENT OF CALCIUM/CALMODULIN KINASE II (CaMKII), MITOGEN-ACTIVATED PROTEIN KINASE (MAPK), AND PROTEIN KINASE C (PKC) IN THE RELEASE OF ARACHIDONIC ACID (AA) ELICITED BY PHENYLEPHRINE (PE) VIA SELECTIVE ACTIVATION OF PHOSPHOLIPASE D IN RAT-1 FIBROBLASTS TRANSFECTED WITH ALPHA 1a/c ADRENERGIC RECEPTOR (AR)

Y. Ruan, J. H. Parmentier, A. Ahmed, L. F. Allen and K. U. Malik
Dept. of Pharmacology, University of Tennessee, Memphis, TN 38163

PE, an α1 AR agonist, stimulates AA release in rat-1 fibroblasts transfected with α1a/c AR (FASEB J., 10: A146, 1996). The present study was conducted to determine the type of phospholipase (PL) involved in AA release and the underlying mechanism of its activation by PE in these cells. PE (2 μM) increased AA release and PLD activity but not PLA_2 activity. Inhibitors of PLD (C2-ceramide, 10 μM), phosphatidate phosphohydrolase (propanolol, 50 μM) and diacylglycerol lipase (RHC80867, 10 μM) attenuated PE-induced AA release. Removal of calcium from the medium abolished the PE-induced AA release and PLD activity. The inhibitors of calmodulin (E6-brebamine, 10 μM), CaMKII (KN-93, 10 μM), and MAPK kinase (MEK) (PD-98059, 50 μM), attenuated both AA release and PLD activity. A PKC activator, phorbol-12-myristate-13-acetate (PMA), also increased AA release and PLD activity. The effect of PMA (5 μM) as well as of PE on AA release and PLD activity was attenuated by PKC the inhibitor bisindolylmaleimide I (0.5 μM). These data suggest that PE stimulates the release of AA in rat-1 fibroblasts transfected with α1a/c AR by selective activation of PLD via stimulation of PKC, CaMKII, and MEK. Supported by USPHS Grant-19134 from NIH-HLBI.

648

THE ROLE OF PROTEIN KINASE C IN THROMBOXANE A_2 - INDUCED PULMONARY ARTERY CONTRACTION. Y.M. Murtha, B.M. Allen, and J.A. Orr. Dept. of Physiology and Cell Biology, University of Kansas, Lawrence, KS 66045

Although the signal transduction mechanism for thromboxane A_2 (TxA_2) is thought to involve activation of protein kinase C (PKC), the role of this intracellular enzyme in the contraction of pulmonary vascular smooth muscle is uncertain. These experiments were therefore designed to determine if inhibition of PKC would attenuate the pulmonary vasoconstriction elicited by TxA_2. Rabbits were sacrificed and 4mm segments of the main trunk of the pulmonary artery removed. Isolated vessels were placed within a temperature controlled organ bath and contractile responses evoked by addition of U46,619 (0.5 μM), a known TxA_2 mimetic, to the organ bath. Contractile responses were measured under baseline conditions and following incubation of the vessel with known inhibitors of PKC (staurosporine: 200 nM or calphostin C: 2 μM). Contractile responses to the TxA_2 mimetic were reduced by 35% and 22% following pretreatment with staurosporine and calphostin C, respectively. Control experiments demonstrated that the attenuation elicited by these inhibitors of PKC was not due to either a time dependent decrease in the contractile response or an effect of the organic solvent used to dissolve the inhibitors. We therefore conclude that PKC plays a modest role in TxA_2-induced pulmonary arterial vasoconstriction. (Supported by a grant from the Amer. Heart Assoc. - KS Affiliate)

649

NOREPINEPHRINE STIMULATES ARACHIDONIC ACID RELEASE FROM VASCULAR SMOOTH MUSCLE VIA ACTIVATION OF $cPLA_2$. E.F. LaBelle and E.Polyak Graduate Hospital, Philadelphia, PA 19146

The metabolism of arachidonic acid (AA) was studied in segments of rat tail artery in order to determine if this compound was important in mediating the effects of adrenergic agonists on force generation. The segments of tail artery were prelabeled with [^{3}H] AA and then stimulated with norepinephrine (NE) and the radioactivity of the extracellular medium determined. Thin layer chromatography was used to prove that nearly 100% of the radioactivity excreted from the tissue was free AA. AA release from the tail artery was directly proportional to time for 20 min, and the NE concentration required for half-maximal stimulation of AA release was between 0.5 and 1μM. Inhibitors of phospholipase C (U73122) and diacylglycerol lipase (RHC 80267) failed to block NE-stimulated AA release, which indicated that neither of these enzymes were required during AA release. Inhibitors of both $sPLA_2$ (manoalide) and calcium-independent $iPLA_2$ (haloenol lactone suicide substrate, HELSS) also failed to block NE-stimulated AA release, again suggesting that the process did not depend on either enzyme. NE-stimulated AA release was almost completely blocked by the specific inhibitor of $cPLA_2$, arachidonyl trifluoromethylketone ($AACOCF_3$), which indicated that $cPLA_2$ most likely was activated by adrenergic agonists in vascular smooth muscle in order to permit AA release from the tissue. (Supported by Grant HL 37413 from NHLBI).

650

EXPRESSION OF PROSTGLANDIN E_2 RECEPTOR SUBTYPES IN THE DEVELOPING SHEEP BRAINSTEM. T.C. Tai, S.J. Lye and S.L. Adamson. Inst. of Medical Science and Dept.of Ob/Gyn., University of Toronto, and Program in Dev. and Fetal Health, Samuel Lunenfeld Res. Inst., Mount Sinai Hospital, Toronto, Ontario, Canada, M5G 1X5.

Prostaglandin E_2 (PGE_2) has diverse brainstem-mediated physiological effects (respiratory, cardiovascular and sensory). We hypothesized that developmental changes in the physiological effects of PGE_2 may be due to changes in PGE_2 receptor subtypes in the brainstem. PGE_2 receptor subtypes (EP1, EP2, EP3 and EP4) differ in their structure, ligand binding specificity and coupling to signal transduction pathways. We examined the ontogeny of PGE_2 receptor subtypes using RT-PCR conducted for each subtype and β-actin (normalization control) at 3 cycle lengths in the linear range for each message. Specificity of the PCR was confirmed by sequencing of amplified products. The cloned fragments of the sheep EP subtypes show high homology (>90%) with known sequences from other species. Results show that all four subtypes were expressed in the medulla and pons of the fetal (120 and 140d gestation), newborn (5 and 15d) and adult sheep brainstems (n=3 at each age). Gene expression of all four subtypes increased (~2 fold) post-natally in the pons (15d; $p<0.05$) then decreased to fetal levels by adulthood. Similar changes were also observed in the medulla, showing peak gene expression at 5d (EP1, $p<0.05$). Since the post-natal increase in expression was transient, we speculate it may be caused by the >10 fold decrease in plasma PGE_2 levels observed after birth. The observation that all four subtypes followed a similar developmental pattern suggests that these genes may have a similar regulatory mechanism. In conclusion, we have shown that all four PGE_2 receptor subtypes are expressed in the sheep brainstem and their expression is developmentally regulated. *(Supported by MRC Canada and a studentship from the Genesis Research Foundation)*

651

Increased upregulation of the inducible prostaglandin synthase (COX-2) gene precedes light-induced photoreceptor apoptosis

NG Bazan, VL Marcheselli, WC Gordon, T Harris and D Zhang. LSU Medical Center, Neuroscience Center and Department of Ophthalmology, New Orleans, LA

Photoreceptor cell apoptosis takes place in retinitis pigmentosa. The upstream cellular signaling involved in cell death in this retinal degenerative disease are not well understood. We have studied COX-2, the enzyme that converts arachidonic acid to prostaglandin H2, which is the precursor of eicosanoids. COX-2 transcriptional activation is an early hippocampal event preceding neuronal cell death (VL Marcheselli and NG Bazan, J Biol Chem 271:24794-9, 1996). Rats were light-damaged. Inferior-temporal retinal quadrants (region of greatest light-induced apoptosis) were compared to superior-nasal quadrants (region of least damage). Western and Northern blots of COX-2, COX-1, and PGDS (lipocalin-type prostaglandin D synthase) were studied and tissue monitored histologically to localize COX-2 by TUNEL analysis and to quantify apoptosis and determine cell loss. By 4 hrs post-light treatment, neither apoptosis nor levels of PGDS demonstrated any difference between control and light-damaged retinas in either quadrant.There was no change in COX-2 levels in superior-nasal quadrants; however, COX-2 was increased several-fold in light-damaged retinal regions. The early induction of COX-2 preceded apoptosis, suggesting that COX-2 is involved in apoptotic photoreceptor loss. COX-2 localizes within inner segments of photoreceptors. Light-induced COX-2 may be involved in the events leading to apoptosis, as part of repair/rescue responses when photoreceptors are confronted with adverse, survival-threatening environmental conditions. (NIH/EY05121)

652

Platelet-activating factor (PAF), kainic or glutamate increase expression of the inducible prostaglandin H synthase-2 (COX-2) in primary hippocampal neurons. Victor L. Marcheselli, Foster Z. Campbell, Mark A. DeCoster, and Nicolas G. Bazan. LSU Medical Center, Neuroscience Center and Department of Ophthalmology, New Orleans, LA 70112

Kainate treatment in vivo (IP injections in rat) increases the expression of COX-2 but not COX-1 in hippocampus. RNA levels of COX-2 peaked 3 hrs after injection, while protein levels peaked at 8 hrs. These effects were significantly inhibited by the PAF receptor antagonist BN 50730 (J Biol Chem 271:24794-9, 1996). To determine the relative importance of glutamate receptors and PAF in excitotoxicity, we have used primary hippocampal neurons and the excitatory amino acid (EAA) receptor agonists glutamate and kainate, as well as PAF, to measure induction of COX-2 in vitro. Treatment with agonists was carried out for 1 hour at 37°C, followed by 5 hrs in the absence of agonists; thus expression of COX-2 protein was measured 6 hrs after treatment. Glutamate, kainate and PAF each induced COX-2 but not COX-1. Expression of COX-2 was induced at 50 uM glutamate or kainate (toxic concentrations as determined by lactate dehydrogenase release), while a dose-dependent response to PAF was measured, peaking at 1 nM PAF. The induction of COX-2 expression by glutamate, kainate or PAF treatments were all partially inhibited by pretreatment with the PAF antagonist BN 50730. These results indicate that the bioactive lipid PAF and the EAAs kainate and glutamate may share common mechanisms in excitatory synaptic transmission and in neuronal excitotoxicity. (NIH/NS 23002)

1215

A secretory phospholipase A_2 ($sPLA_2$) receptor agonist induces expression of prostaglandin endoperoxide synthase-2 (COX-2) and of inducible nitric oxide synthase in hippocampal neurons but not glia. Michael Serou, Victor Marcheselli, Mark A. DeCoster, and Nicolas G. Bazan. *Neuroscience Center and Dept. of Ophthalmology, LSU Medical Center, New Orleans, LA 70112.*

The $sPLA_2$ receptor agonist $sPLA_2$ from bee venom (BV), as well as the excitatory amino acid (EAA) agonists glutamate and kainate cause significant cell death to primary cortical neuronal cultures. Coadministration of glutamate and BV synergistically activates cell death and arachidonic acid turnover (M Kolko et al., J Biol Chem 271:32722-8, 1996). Kainate causes a platelet activating factor (PAF)-dependent induction of prostaglandin (COX-2) in hippocampus (VL Marcheselli et al., J Biol Chem 271:24794-9, 1996). Here we studied the effects of BV (10 or 25 ng/ml) added to primary cortical neuronal and astrocyte cultures, either alone or in combination with 50μM glutamate. We followed the induction of COX-2 and/or inducible nitric oxide synthase (iNOS) protein. Chemiluminescent protein detection showed that iNOS, neural specific NOS (nNOS), and COX-1 were expressed at comparable levels in neurons and astrocytes, while COX-2 was detectable in neurons only. iNOS and COX-2 proteins were both induced in neurons 6 hrs after treatment with either glutamate or BV, while no changes were seen in nNOS and COX-1. Combination of glutamate and BV produced an enhanced induction of iNOS and COX-2 protein levels. We conclude iNOS and its enzymatic product nitric oxide may mediate part of the glutamate and/or $sPLA_2$ agonist effects, and may represent a locus of synergy between the two. Supported by NIH NS23002.

1216

CYCLIC A.C. SWEEP VOLTAMMETRY PROVIDES INCREASED SENSITIVITY FOR DETECTING CATECHOLAMINES A. Strickholm. Medical Sciences Program, Indiana University, Bloomington, Indiana 47405

A.C. sweep voltammetry was examined to determine if improved sensitivity over cyclic voltammetry could be obtained to measure low levels of catecholamines utilizing carbon fiber electrodes. In a.c. sweep voltammetry a small a.c. signal is superimposed on the linear sweep voltage utilized for oxidation and reduction. The instrumentation and theory for the current obtained is complex and has been described. In the experiments here the current signal was separated into the real and imaginary components and additionally, the a.c. current component was nulled with a phase opposite signal to improve signal resolution. The standard three electrode voltammetry arrangement was used with the working electrode a carbon fiber a few hundred microns long or embedded in epoxy with the end polished. To determine if improved sensitivity was obtainable, the catecholamine (dopamine, etc.) concentration was reduced to where it was no longer detectable by standard cyclic voltammetry. The a.c. current component was then introduced onto the sweep potential and an a.c. current response was obtained. The results showed an increased detection sensitivity for oxidation and reduction in all the three signal modes described above when compared to cyclic voltammetry alone. Support for this research has been by NIH grant 2RO1 NS20784-07.

1217

REGULATION OF M4 MUSCARINIC RECEPTOR BINDING BY PROTEIN KINASE C IN GH_3 PITUITARY CELLS. P.-H. Kuo and J.C. Fong (SPON: S. Chan). Inst. Biochem., Natl. Yang-Ming University, Taipei, Taiwan, R.O.C.

The regulation of M4 muscarinic receptor down-regulation and desensitization by protein kinase C was studied in GH_3 pituitary cells that endogenously express M4 muscarinic receptor. Receptor number on the cell surface was measured by binding of the hydrophilic antagonist [^{3}H]N-methylscopolamine (^{3}H-NMS). Exposure to 4β-phorbol 12β-myristate 13 α-acetate (PMA), an activator of protein kinase C (PKC), caused a dose- and time-dependent biphasic change on ^{3}H-NMS binding. The binding was decreased by approximately 55% following 4 h-pretreatment with PMA. Thereafter the binding gradually returned to the control level after another 20 h. The effect of PMA on the receptor number was not influenced by the presence of cycloheximide. The change of potency of carbachol to inhibit forskolin-stimulated cAMP production was closely correlated to the change in the receptor number. Although TRH was known to activate PKC, it had no effect on ^{3}H-NMS binding. Thus stimulation of a PKC isoform different from that activated by TRH seemed to induce a transient M4 muscarinic receptor sequestration in GH_3 cells. (Supported by a NSC grant NSC85-2331-B010-113-M10, R.O.C.)

1218

DYNAMIC ALTERATIONS IN FIRING CHARACTERISTICS OF DORSAL HORN INTERNEURONS. S.P. Schneider. Department of Anatomy, Michigan State University, E. Lansing, MI 48824-1316.

Integrative function of neural networks is influenced by temporal patterning of impulse activity of constituent elements. In whole-cell recordings from spinal slices, dynamic alterations in firing patterns of dorsal horn interneurons have now been observed that are associated with periods of repeated or sustained activity.

Neurons responded to depolarizing current pulses injected through the recording pipette (20-200pA, 500-700ms) with one of three discharge patterns based on timing and spike-frequency adaptation: tonic, phasic, and delay. For a majority of neurons (39/56; 70%) repeated activation (20-30 pulses, 0.2-0.5Hz) induced rate- and intensity-dependent changes in firing, accompanied by shifts in V_m. For 41% of such cells (16/39) resting V_m hyperpolarized (2-5mV), discharge frequency decreased and/or adaptation increased, reversing 30-120s after terminating stimulation. Hyperpolarization and altered spike-firing were associated with decreased R_N, but not with observable changes in synaptic activity, and could not be blocked by the Na-K ATPase inhibitor strophanthidin or the $GABA_A$ antagonist bicuculline. In other cells (23/39; 59%) repetitive activation or injection of depolarizing current (5s) induced persistent (up to 15min) depolarizing shifts in V_m (2-6mV), complex changes in R_N, and increased excitability that were not associated with changes in synaptic activity. Increased firing could be reversed by hyperpolarizing V_m but not by application of the excitatory amino acid antagonists D-AP5 and CNQX. Intracellular staining revealed that neurons capable of firing plasticity were interneurons with dense terminations in spinal laminae III-V.

These findings demonstrate that dorsal horn interneurons can undergo dynamic alterations in firing pattern which may alter integrative properties of local spinal networks. Such phenomena may contribute to sensory habituation, secondary hyperalgesia, and alterations in reflex function. *Supported by NINDS grant NS25771.*

1219

DETECTION OF GABA TRANSPORTER CURRENT IN BIPOLAR CELLS OF TIGER SALAMANDER RETINA. C.Y. Yang (SPON:S.F.Fan). Dept. Neurobiol. & Behavior, SUNY, Stony Brook, NY 11794.

Purpose: Bipolar cells (BCs) in vertebrate retina transfer excitatory signals from photoreceptors in the distal retina to amacrine and ganglion cells in the proximal retina. However, we found that in tiger salamander (TS) retina, a subpopulation of Type IB and IIB BCs were GABA- and L-glutamic acid decarboxylase-immunoreactive (IR) (Yang & Yazulla, Vis. Neurosci. 11:1193 '94), and GABA-IR BCs colocalized with GABA transporter (GAT)-IR as well (Yang *et al.*, submitted). These results indicate that a subset of BCs use GABA as inhibitory transmitter and re-uptake GABA via GAT. Detection of GABA transporter current in BCs will provide further evidence for the existence of GABAergic BCs. **Methods**: Whole-cell current was recorded from soma of BCs in retinal slices with conventional patch clamp method. Patch pipettes were filled with Lucifer Yellow to identify the BCs. GABA (30-500 μM) was puffed through another pipette with a picospritzer. **Results**: (1) In 2 out of 18 BCs with current elicited by GABA puffed at the terminal, the GABA transporter blocker, NO-711, suppressed up to 30% of the current. (2) In 1 out of 10 BCs without descending process, NO-711 suppressed ≈ 80% of the current elicited by GABA puffed close to the soma. **Conclusion**: The results obtained in this study support the notion that there is a subset of GABAergic BCs in TS retina which transport GABA likely via GAT. (Supported by NIH grant EY10322).

1220

THE ADENOSINE A_1 RECEPTOR AGONIST 2-CHLORO-N^6-CYCLOPENTYLADENOSINE (CCPA) BLOCKS THE ADENOSINE TRANSPORTER IN RAT BRAIN SYNAPTOSOMES. H. Zhong, C. Clough Helfman, J.C. Dunbar and G.F. Anderson. Depts. of Physiology and Pharmacology, Wayne State Univ. Sch. of Med., Detroit, MI 48201.

Both cyclopentyladenosine (CPA) and CCPA are selective adenosine (Ado) A_1 receptor agonists in the low nM range, while CPA but not CCPA has inhibitory actions on evoked release of norepinephrine (NE) from brain slices in the 1.0 and 10 μM range.

Freshly prepared rat brain cortical or striatal synaptosomes incubated with 1.0 μM [^{3}H]Ado for 1 or 5 min actively accumulate [^{3}H]Ado and this transport is partially blocked by dilazep, nitrobenzylthioinosine (NBTI) or dipyridamole. [^{3}H]CCPA was not accumulated by synaptosomes. Both CPA and CCPA displace [^{3}H]NBTI from crude membranes K_i 0.5 and 3.2 μM respectively. [^{3}H]CCPA binds to cortex and striatal crude membranes with K_d of 5.1 and 6.9 nM and B_{max} of 357 and 326 fmol/mg respectively. [^{3}H]CCPA was displaced from membranes by the Ado A_1 antagonist cyclopentyl-dimethylxanthine (DPCPX) K_i 171.2 nM. CPA and CCPA blocked [^{3}H]Ado uptake in synaptosomes with an EC_{50} of 9.1 and 5.1 μM respectively. The inhibitory effects of CPA may be more closely associated with the inhibition of Ado transport than with it's A_1 receptor binding. While CCPA had similar binding to the Ado transporter and receptor, but no effect on NE release even at 50 μM concentrations. Supported by: NIH MH 47181 and MH 17153.